The clinical relevance of visualising the peripheral retina

Quinn, N., Csincsik, L., Flynn, E., Curcio, C., Kiss, S., Sadda, S. V. R., ... Lengyel, I. (2018). The clinical relevance of visualising the peripheral retina. Progress in Retinal and Eye Research. DOI: 10.1016/j.preteyeres.2018.10.001

Published in:
Progress in Retinal and Eye Research

Document Version:
Publisher's PDF, also known as Version of record

Queen's University Belfast - Research Portal:
Link to publication record in Queen's University Belfast Research Portal

Progress in Retinal and Eye Research xxx (xxxx) xxx–xxx

Contents lists available at ScienceDirect

Progress in Retinal and Eye Research

journal homepage: www.elsevier.com/locate/preteyeres

The clinical relevance of visualising the peripheral retina

Nicola Quinn[a,1], Lajos Csincsik[b,1], Erin Flynn[c,1], Christine Curcio[d,1], Szilard Kiss[e,1], SriniVas R. Sadda[f,1], Ruth Hogg[a,1], Tunde Peto[a,1], Imre Lengyel[b,*,1]

[a] Centre for Public Health, Queen's University, Belfast, United Kingdom
[b] Centre for Experimental Medicine, Queen's University, Belfast, United Kingdom
[c] School of Medicine and Health Sciences, The George Washington University, Washington, D.C., United States
[d] School of Medicine, University of Alabama at Birmingham, AL, United States
[e] Department of Ophthalmology, Weill Cornell Medical College, New York, United States
[f] Doheny Eye Institute, University of California, Los Angeles, CA, United States

ARTICLE INFO

Keywords:
Retinal imaging
Ultra-widefield
Peripheral retina
Image grading
UWFI
Grading grid

ABSTRACT

Recent developments in imaging technologies now allow the documentation, qualitative and quantitative evaluation of peripheral retinal lesions. As wide field retinal imaging, capturing both the central and peripheral retina up to 200° eccentricity, is becoming readily available the question is: what is it that we gain by imaging the periphery? Based on accumulating evidence it is clear that findings in the periphery do not always associate to those observed in the posterior pole. However, the newly acquired information may provide useful clues to previously unrecognised disease features and may facilitate more accurate disease prognostication. In this review, we explore the anatomy and physiology of the peripheral retina, focusing on how it differs from the posterior pole, recount the history of peripheral retinal imaging, describe various peripheral retinal lesions and evaluate the overall relevance of peripheral retinal findings to different diseases.

1. Introduction

Since the invention of the first ophthalmoscope in 1851 by Hermann von Helmholtz, imaging the retina has undergone dramatic improvements, not only arousing interest in previously undescribed abnormalities but changing our understanding of numerous retinal and choroidal diseases (Keeler, 2002). The continuous advances in imaging technologies enabled the capture of retinal areas beyond the posterior pole, which were not previously routinely documented digitally. The introduction of ultra-widefield imaging (UWFI) led to a renewed interest in lesions in the peripheral retina and a better understanding of their relevance to the diagnosis and prognosis of different retinal conditions. To develop appropriate understanding of the images generated by novel technologies, several principles need to be considered. An understanding of the anatomy of the entire neurosensory retina and choroid/retinal pigment epithelium (RPE) interface and the differences and similarities between the different geographic retinal locations must be developed. These can help to establish appropriate descriptive terminologies to describe and interpret the different UWFI modalities such as colour imaging, fundus auto fluorescence (FAF), fundus fluorescein angiography (FFA) and indocyanine green (ICG) angiography.

2. The structure and function of the peripheral retina

2.1. Definition of the peripheral retina

Based on ophthalmoscopic examination a readily recognizable feature of the neurosensory retina is the optic disc, the exit point for the ganglion cell nerve fibres and central veins, and entry point for arteries supplying the inner layers of the neurosensory retina. The arteries form the so called “arcade” encompassing the macula, including the foveola (Yamada, 1969), fovea, parafovea and perifovea, definitions that are essential for image analysis of fundus photographs and define the widening areas around the foveola (Bringmann et al., 2018; Provis et al., 2005). The fovea containing the foveola is the place of the highest visual acuity (Hirsch and Curcio, 1989). Other landmarks of the macula are the foveal avascular zone and the visually recognizable yellow macular pigment.

* Corresponding author. The Wellcome-Wolfson Institute for Experimental Medicine School of Medicine, Dentistry and Biomedical Science, Queen's University Belfast, 97 Lisburn Road, Belfast, BT9 7BL, United Kingdom.
E-mail address: i.lengyel@qub.ac.uk (I. Lengyel).

[1] Percentage of work contributed by each author in the production of the manuscript is as follows: Nicola Quinn 25%; Lajos Csincsik: 20%; Erin Flynn 5%; Christine Curcio10%; Szilard Kiss 5%; SriniVas R. Sadda 5%; Ruth Hogg 5% ; Tunde Peto10%; Imre Lengyel 15%.

https://doi.org/10.1016/j.preteyeres.2018.10.001
Received 24 June 2018; Received in revised form 1 October 2018; Accepted 7 October 2018

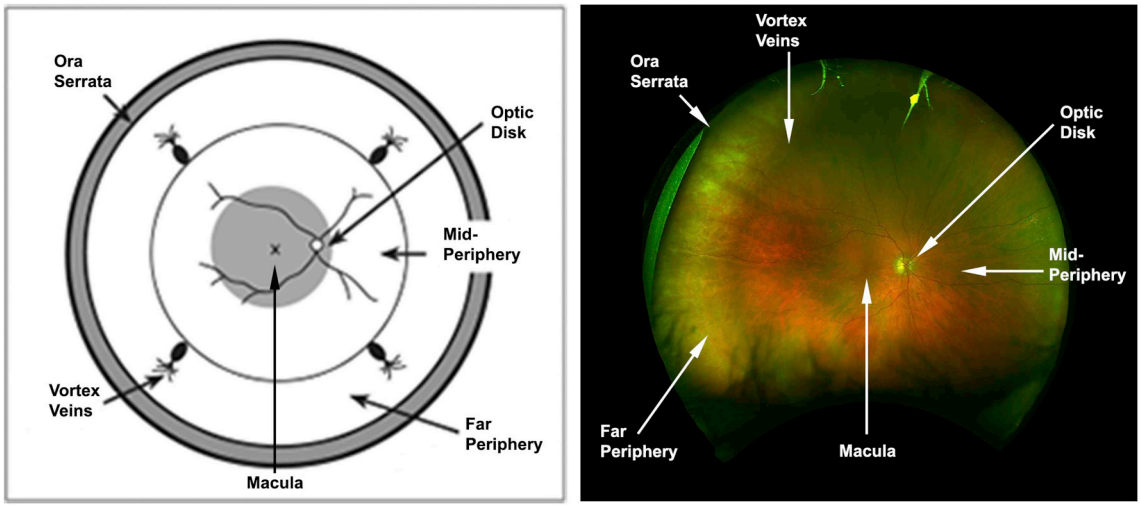

Fig. 1. Illustration of the major landmarks in the retina.
The left image illustrates the different structures of the retina and their position (Modified from Cybersight, Interpretation of Stereo Ocular Angiography: Retinal and Choroidal Anatomy (Santini, 2017). The right image is an Optomap image taken from the Reykjavik Study and adapted to display the location of the various structures on the retina. (MP = Mid-periphery and FP = Far-periphery).

Retinal regions based on gross anatomy including vessels was defined in 1961 by Duke-Elder who categorised the peripheral retina into four zones (Duke-Elder, 1961). These zones are: 1) the near periphery, a 1.5 mm ring adjacent to the 6 mm diameter macula (centred on the foveola and often defined as the posterior fundus); 2) the middle periphery, the next 1.5 mm ring; 3) the far-periphery, measuring the next 9–10 mm on the temporal and 16 mm on the nasal side; 4) the *ora serrata* or extreme periphery, measuring the additional 2.1 mm in the temporal and 0.7 mm on the nasal side. In 1967 Rutnin divided the back of the eye into 3 regions: 1) posterior fundus, a circle centred on the foveola and including the optic disc; 2) equatorial zone, a ring shaped area about 5.83 mm wide adjacent to the posterior fundus and bordered by an imaginary circle through the posterior extremities of the vortex veins; 3) and the *ora serrata*, the area outside of the equatorial zone (Fig. 1) (Rutnin and Schepens, 1967).

Human retinal regions based on the cellular content of the neurosensory retina were defined by Polyak (1941), which we will examine in detail in 2.3.3. For the purpose of this review, the peripheral retina will be considered as area peripheral to the macula, a retinal region that can itself be subdivided (see section 2.3).

Grading for retinal abnormalities in clinical studies still use different definitions, evidenced by the use of different grading grids summarized in Section 4. It is important to recall that grading grids, like all metrics, were developed to investigate specific diseases, for specific purposes, by investigators following then-current models of pathogenesis. Thus, it is prudent to periodically ask whether these grids still make sense in the light of new knowledge.

2.2. Embryological differences between the central and peripheral retina

The embryological development of the retina is a complex process (Oyster, 1999; Provis, 2001; Venters et al., 2013, 2015). At birth, the retinal neuronal cytoarchitecture and physiology is still immature and continues to undergo changes for several years (Hildebrand and Fielder, 2011). Retinal development is known to begin centrally before extending peripherally, further expansion of the peripheral retina continues and matures before the posterior pole (Hendrickson and Drucker, 1992). The initial stage of growth involves the neural tube. As development proceeds, optic vesicles evaginate, producing a bi-layered optic cup with an inner and outer layer subsequently differentiating into the sensory neural retina and the RPE, respectively (Hendrickson, 2016). Following this initial differentiation, the most central portion of the neural retina is thought to differentiate early with cells at the peripheral retina margins remaining proliferative and thus differentiating last. In fact the proliferating capacity of the peripheral retina appears to be retained in adults, at least in animal models (Al-Hussaini et al., 2016).

Previous work by Venters et al. (2013) has provided useful insights into the derivation of mature eye tissues by a vital labelling strategy of chick embryos. They demonstrated that significant portions of the peripheral retina is made up of cells that resided at the optic cup lip and these same cells did not make up any of the central retina, providing the first evidence that two distinct sub-domains arise during embryogenesis, namely the central and peripheral retina (Venters et al., 2013). The central retina has previously been shown to be derived from distal optic vesicles, where upon invagination they displace to the back of the eye and form the central retina (Shin and O'Brien, 2009). In 2015, Venters et al. further described the subdivision in the neural retina between the central and peripheral retina. There is notably a variety of characteristics that distinguish between the central and peripheral retina, with an obvious distinction being the different photoreceptor densities found within the central and peripheral retina, with cones predominantly found in the central and rods in the peripheral retina (Venters et al., 2015). In this review we will use the terminology of Polyak (1941) for the human retinal regions (see later).

2.3. Anatomical differences between the central and peripheral retina: cells, layers, and regions

2.3.1. Cells

The human retina, like all mammalian retinae, is made up of five major cell classes of neurons: photoreceptors, bipolar cells, ganglion cells, horizontal cells and amacrine cells, which are subdivided into approximately 60 molecularly and morphologically distinct types. The simplest circuit begins with the photoreceptors, which transduce light into electrochemical signal and connect to the bipolar interneurons. These in turn contact ganglion cells, which transmit signal to the brain. Human retina has ~100 million rods (active in dim light) and 4.6–6 million cone photoreceptors (active in bright light) and 1.0 to 1.5 million ganglion cells, implying a tremendous level of signal compression. At the same time, there are at least 13 bipolar cell types that split signals at the photoreceptor synapse into multiple parallel pathways, each with distinct functions, for transmission to the brain. Horizontal cells and amacrine cells are interneurons that establish lateral interactions at the first (photoreceptor → bipolar) and second (bipolar →

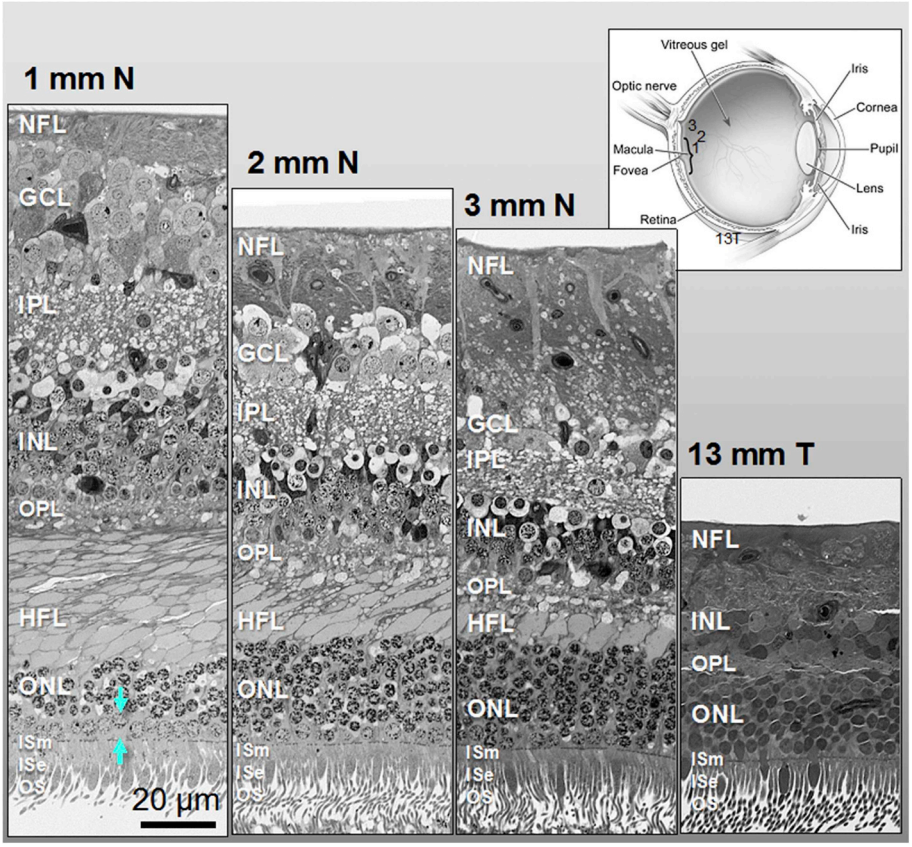

Fig. 2. Thickness of human neurosensory retina varies by region.
N, nasal fovea; T, temporal to fovea. 1, 2, and 3 mm N pertain to parafovea, perifovea, and near periphery, and 13 mm T is extreme periphery, in the terminology of Polyak (1941). 88-year-old female donor with normal retina, < 6 h death-to-preservation, post-fixed with osmium tannic acid paraphenylenediamine, 0.8 µm epoxy sections, stained with toluidine blue; original at http://projectmacula.cis.uab.edu/. NFL, nerve fibre layer; GCL, ganglion cell layer; IPL, inner plexiform layer; INL, inner nuclear layer; OPL, outer plexiform layer; HFL, Henle fibre layer; ONL, outer nuclear layer; ISm, inner segment myoid of photoreceptors; ISe, inner segment ellipsoid of photoreceptors; OS, outer segments of photoreceptors. The abundance of ganglion cells and cone photoreceptors in addition to the Henle fibre layer distinguish the macula from the periphery. Arrows indicate a single continuous row of cone nuclei in the parafovea. Some cell bodies in GCL and INL are edematous (vacuolated).

ganglion cell) synapse. In addition to neurons are glial cells, specifically the Müller cells that span the retina from the inner surface to external limiting membrane (a series of junctional complexes), astrocytes in the nerve fibre layer, and microglia that reside in inner retina for surveillance. The RPE is simple cuboidal epithelium that provides essential support services to the photoreceptors on its apical aspect and the choriocapillary (ChC) endothelium on its basal aspect. The retina has a dual vasculature, with the attendant vascular endothelium and pericytes – the intrinsic retinal circulation supplying the inner retina including the internal part of the Müller cells, and the choroidal circulation supplying the RPE, photoreceptors, and external portion of the Müller cells. Between RPE and ChC is a laminated sub-endothelial extracellular matrix called Bruch's membrane (BrM), which functions as a vessel wall laid out flat, in parallel to vascular lumens, rather than circumferentially around them.

2.3.2. Layers

Retinal layers have been named by several schemes; the nomenclature of Polyak is widely accepted (Fig. 2) (Polyak, 1941). Retinal layers vary markedly by region. Fig. 2 shows the neurosensory retina at three locations in the central retina and one in the peripheral retina. The macula, a 6-mm-diameter area centred on the fovea, comprises numerous clinically relevant layers, sublayers, and potential spaces. As classically described (B. B. Boycott, 1969; Hogan et al., 1971; Polyak, 1941), these include (from inner to outer) the RNFL, ganglion cell layer (GCL), inner plexiform (synaptic) layer (IPL), inner nuclear layer (INL with bipolar, horizontal, amacrine and Müller cell bodies), outer plexiform (synaptic) layer (OPL), outer nuclear layer (ONL, with photoreceptor cell bodies), photoreceptor inner and outer segments (IS, OS; Polyak's bacillary layer), and RPE. The macular OPL has sublayers of bipolar and horizontal cell neurites, cone pedicles and rod spherules, and Henle fibres (photoreceptor axons and Müller cells). Photoreceptor IS have myoid and ellipsoid compartments. Choroidal layers include the inner and outer BrM, the ChC, and the choroid, delimited from the sclera by the lamina suprachoroidea. Stereotypic extracellular deposits accumulate with aging and age-related macular degeneration in the subretinal space (subretinal drusenoid deposit), between the RPE and its basal lamina (basal laminar deposit), and between the RPE basal lamina and the inner collagenous layer of BrM (drusen).

2.3.3. Regions

According to the terrain theory of vision (Hughes, 1977), the sampling of visual space by neurons in each species' retina is influenced by the species' normal habitat. Mammalian retinae have an area of high neuronal density specialised for visual acuity, onto which images are registered by coordinated head and eye movements (Wassle and Boycott, 1991). A well-known example of this principle is the visual streak of rabbits (Vaney, 1980), in which numerous ganglion cells align horizontally for optimal surveillance of predators. Conversely, neuronal density and spatial resolution is low in peripheral retina, because the peripheral retina has other important functions, i.e., specialization for movement detection and sensitivity, and the part of the visual brain processing this information can be limited in size. Further, the level of convergence from photoreceptors to ganglion cells is high in the periphery, which contributes to lesser acuity and enhances movement detection.

Polyak (1941) defined the human retinal regions as concentrically organized around the visual axis in the fovea and based it on retinal neurobiology in humans and macaques, especially the topography of retinal ganglion cells and the local rod: cone ratio. The Henle fibre layer (fibres of cones, rods, and Müller cells) is present in para- and perifovea. The given diameter is for the region in humans (of unspecified ages). The radius of the outer boundary is distance from the fovea:

- foveola, 350 µm (175 µm radius), absent ganglion cells;
- foveal floor, 400 µm (200 µm radius), absent ganglion cells;

- parafovea, 2500 μm (1250 μm radius), 5–8 rows of ganglion cells; 1 rod between cones
- perifovea, 5500 μm (2750 μm), 4 rows of ganglion cells diminishing to 1 row; 2 rods between cones;

In addition to these macular regions, which are still used today, Polyak also defined regions of peripheral retina on the basis of ganglion cell density. These are not clinically detectable with current technology but are described here for completeness:

- near periphery, 8500 μm (4250 μm radius); single continuous row of ganglion cells; 2–3 rods between cones; mid-periphery, 14,500 μm (7250 μm radius); discontinuous row of ganglion cells; 3 rods between cones;
- far periphery, 26,000 μm (10,000 μm temporal, 16,000 μm nasal); widely separated ganglion cells; extreme periphery, to the *ora serrata.*

The entire expanse of human retina is ~43 mm from *ora serrata* to *ora serrata*. The human macula, 6 mm in diameter, is thus defined as an area with a continuous layer of ganglion cells (Polyak, 1957) and in epidemiology as the area included in the Early Treatment of Diabetic Retinopathy Study grid for grading colour fundus photographs (Early Treatment Diabetic Retinopathy Study Research Group, 1991b). The macula constitutes ~3% of the total retina area (of ~1000 mm^2), leaving 97% of retina considered extramacular. Indeed, human peripheral retina can be described as a generic mammalian retina that lacks features that are specific to the macula.

In 1990, comprehensive 2-dimensional maps of cone and rod density in short post-mortem retinae prepared as unstained whole mounts (Curcio et al., 1990) visualized the topography and morphologic detail of inner segments. With accurately localized centres and computerized microscopy, it was possible to determine photoreceptor density over the entire retina (Fig. 3). The human macula was shown to be overall numerically rod-dominant, including a rod-dominant perifovea surrounding a cone-only foveola (0.8 mm in diameter). The foveola had a high peak density of cones (> 150,000 mm^2) and a sharp decline with eccentricity. Rods were also numerous (peak > 150,000 mm^2) in an elliptical crest at 2–5 mm eccentricity (i.e., along the macular perimeter) that encircled the optic nerve head nasally, with a hot-spot in superior retina (Curcio et al., 1990) (Fig. 3). Outside the macula, cones were 40% more numerous nasally than at corresponding eccentricities in temporal retina. The highest ratio of rods to cones was 25–30 at 6–14 mm eccentricity, because cones continued to decrease across the retina more rapidly than did rods, except for nasal quadrant, where this ratio was ~20 due to a less step decline. Cone density is increased at the nasal *ora serrata*, as previously seen (Osterberg, 1935).

Similar tissue, microscopy, and computational approaches were recently applied to cell density and autofluorescence of human macular RPE (Ach et al., 2014). A demonstrated peak cell density of ~7200 RPE cells/mm^2 and a shallow eccentricity-dependent decline was consistent with previous literature (Gao and Hollyfield, 1992; Snodderly et al., 2002). With photoreceptor and RPE maps represented in a unified coordinate system, it is possible to represent the phagocytic load on RPE by a ratio of photoreceptors (cones + rods)/mm^2 to RPE/mm^2. This ratio is high (≥28) at the foveal cone peak and lower in the parafovea (13), rising to 29 at the edge of the macula, in human and non-human primate (Curcio, 2018; Snodderly et al., 2002). These quantitative data do not support a widely-held belief that higher phagocytic load on RPE renders the macula uniquely vulnerable to age-related disease. In the macula, RPE cell bodies, excluding the apical processes, are ~14 μm tall and the centre-to-centre spacing of these hexagonal cells is 13, 15, and 16 μm in fovea, perifovea, and near-periphery, respectively (Ach et al., 2014; Curcio et al., 2011). At the periphery, cells are flatter and can be as wide as 60 μm (Harman et al., 1997).

The RPE cells are supported by BrM, an extracellular matrix that can be defined as penta-laminar (if both basal membranes of the RPE and ChC are considered), or trilaminar (if only the inner and outer collagenous layer and the elastic layer are considered). Histological examination of BrM of older eyes at the peripheral and central retina showed that the basal membranes of ChC are similar in the macula and periphery (Johnson et al., 2007). Both geographic locations showed significantly increased collagen fibril density and accumulations of extracellular lipoprotein-like material and proteins eventually with age (Booij et al., 2010) leading to impaired nutrient flow and clearance of remnants of the phagocytosed photoreceptor outer segment debris.

Neurons of the inner nuclear and ganglion cell layers are numerous and are displaced from the foveal centre to create the foveal pit (Fig. 3) (Provis et al., 2013). Approximately 95% of macular ganglion cells are midget cells, i.e., compact neurons responsible for transmitting signal for high acuity and colour vision to the brain (Dacey, 2000). Mapping studies using the same methods used for photoreceptors described above have shown at least 2 ganglion cells for each foveal cone within the central several degrees of vision (Curcio and Allen, 1990; Dacey, 1993; Watson, 2014). Each foveal cone contacts two midget bipolar cells, splitting the output signal along "private lines" signifying light ON and light OFF to corresponding midget ganglion cells (Calkins et al., 1994). This unique circuitry means that 40% of human retinal ganglion cells are laterally offset from their corresponding photoreceptors in the centres of their receptive fields in visual space (Curcio et al., 1990). The Henle fibre layer thus comprises 14% of retinal thickness in the macula and contains inner fibres of rod and cone photoreceptors (interleaved with Müller glia and up to 600 μm long) extending centrifugally to contact bipolar neurons (Drasdo et al., 2007; Perry and Cowey, 1988; Polyak, 1941). Outside the macula, ganglion cells are reduced in density (by a 40:1 gradient) but are 3 times more numerous in nasal quadrant than in temporal quadrant, resembling a visual streak. High concentration of macular ganglion cells is responsible for the high proportion of visual cortex (primary and secondary areas) devoted to central vision. Müller glia span the retina between external and internal limiting membranes. In the macula Müller cells equal or exceed the number of foveal cones (Burris et al., 2002) and are Z-shaped due to the Henle fibre layer. Extra-macular Müller cells are vertical and outnumbered by photoreceptors.

In the periphery, the retina is thinner and less elaborate in structure, and neurons increase in size and become scarcer (see Fig. 2). Greater convergence of photoreceptor signal into interneurons allow summation of signal from more photoreceptors and thus permit a response to weak visual stimuli. The emergence in the late 1980's of cell-type specific markers and techniques for dye-filling with electrodes meant that retinal neurons could be studied as entire populations, where new properties emerged such as cooperative tiling of visual space (i.e., fitting dendritic fields together for efficient coverage) (Wassle and Boycott, 1991). These studies showed eccentricity-dependencies that had implications for spatial vision, e.g., ganglion cells increased in dendritic field area with distance from the fovea (Dacey, 1993; Dacey and Petersen, 1992), maintaining the tiling so that spatial density decreased (cells/mm^2). Other studies in macaque retina, which are similar to human in many ways, have shown eccentricity-dependent density declines specific for each cell type as identified with molecular markers (e.g., displaced amacrine cells (Wassle et al., 1989), midget bipolar cells (Wassle et al., 1994), AII amacrine cells (Wassle et al., 1995), and horizontal cells) (Wassle et al., 2000). Thus the peripheral retina is exemplified by divergence of cone signal to multiple bipolar classes (Chun et al., 1996) whereas the macula includes this level of divergence plus the private lines of the midget system. Thus, in the fovea centre, there are 3.5 bipolar cells per cone. This ratio is at least 2 out to 5 mm eccentricity (10° in a monkey) (Martin and Grunert, 1992).

2.4. Molecular differences between the central and peripheral retina

Alongside the morphological differences, there is an increasing

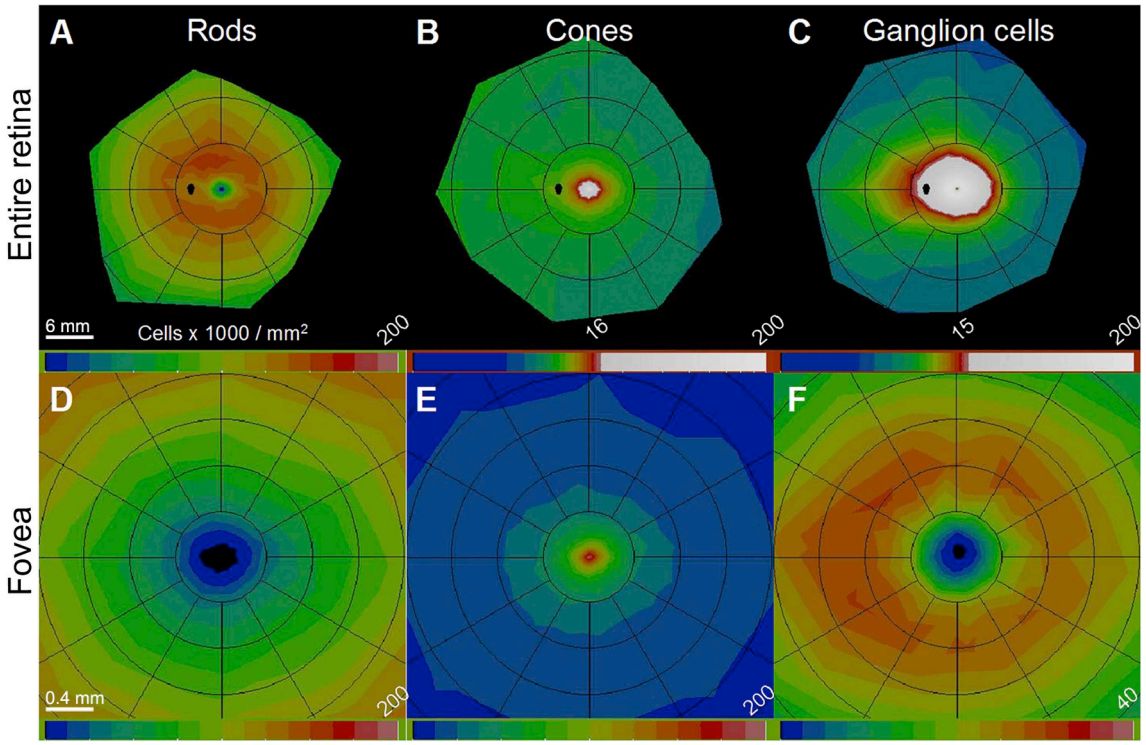

Fig. 3. *Photoreceptor and ganglion cell topography in adult human retina.* (Modified from Curcio et al. (Curcio and Allen, 1990; Curcio et al., 1990) Maps of cells/mm^2 represent a composite of at least 5 donor eyes. Colour bars show cells (x1000) per mm^2 in linear scales for A, D, E, and F and in non-linear scales to show peripheral retinal contours in B, C. Increments of colour bars are (A) 12,500; (B) 1000; (C) 500 cells/mm^2, then 1000 cells/mm; (D, E) 12,500; (F) 2500.
A. Rods are most numerous superior to the macula and in a nasally-extending, horizontally-oriented elliptical ring (rod ring) that extends around the optic nerve head. Rods outnumber cones 20:1 overall. The small map relative to cones and to rods is due to the difficulty of mapping rods in far peripheral retina. B. Cones are 40% more numerous in the nasal periphery than at corresponding eccentricities in the temporal periphery. There is a nasal rim of higher cone density. C. Ganglion cells are 3-fold more numerous in the nasal periphery than in corresponding areas of the temporal periphery. D. Rods are absent from the rod-free foveola, (0.350 mm diameter). E. Cones are predominant in an area 0.8 mm in diameter. The point of highest density is in a < 50 μm-diameter area corresponding to the central bouquet. F. Ganglion cells are most numerous in a horizontally oriented elliptical ring, cresting at 0.8 mm eccentricity. They are largely absent from the foveal floor.

knowledge base about the molecular differences between the central and peripheral retina (see for reviews (Li et al., 2017; Tian et al., 2015)). Comparison of gene expression between the macula and periphery has been investigated by several studies both in human and in animal models which lack maculae but do have centre-to-peripheral gradients of neuronal densities (Al-Hussaini et al., 2016; Cai et al., 2012; Ishibashi et al., 2004; Kociok and Joussen, 2007; Li et al., 2014).

Li et al. showed that 2000 differentially expressed genes between macular and peripheral retina, using human post-mortem tissues with less than 6 h' post-mortem time (Li et al., 2014). Genes expressed at significantly higher levels in the macular area include genes involved in lipid metabolism, ion transport, neuronal differentiation, regulation of transcription, cell adhesion, cell motility and differentiation. Conversely genes expressed at significantly higher levels in the peripheral retina were those involved in the Wingless-type MMTV integration site family (Wnt) receptor signalling pathway. Wnt signalling controls many events during embryogenesis, exerts significant regulation of cell morphology, proliferation, motility and cell fate (Cai et al., 2012). Inhibition of the Wnt pathway is correlated with preventing cells from moving into a regenerative state, and Wnt signalling is crucial in transdifferentiation of ciliary margin stem cells into neural retina at the ciliary marginal zone (Cai et al., 2012). Alongside the transcriptomic changes, differences in protein levels have also been investigated. Proteomic studies have highlighted the differential protein distribution and the differential change with disease progression (Ethen et al., 2006; Okamoto et al., 2010). A comparison of protein expression between the macula and peripheral retina has concluded that arrestin-C and 3′(2′),5′-bisphosphate nucleotidase 1 are highly expressed in the macular region compared to the periphery. This is thought to be due to the fact arrestin-C is located in photoreceptor outer segments and the outer plexiform layer, while 3′(2′),5′-bisphosphate nucleotidase 1 is highly expressed in cone photoreceptors which are most dense in the macular area (Okamoto et al., 2010). The proteome of the human eye, especially the retina, is now under intense investigation and promises to be hot topic for the years to come (Zhang et al., 2015). This is due to the increasing sensitivity of mass spectrometric approaches, which in turn will allow a more precise definition of the proteomic landscape of the retinal layers and in fact the whole eye (Zhang et al., 2016).

There are difficulties as well when one wants to compare gene expression with protein expression. For example, when epidermal fatty acid binding protein (E-FABP) gene expression was compared between peripheral and macular RPE in humans using a comparative transcription study, E-FABP was found to be 6.3 fold higher in the peripheral RPE (Umeda et al., 2003). This, however, differs from the investigation of the proteomics of the macular and peripheral retina (Zhang et al., 2015). In addition, immunohistochemical labelling of E-FABP showed that the protein is in the neurosensory retina, but not in the photoreceptors, while the gene expression change was associated with the RPE (Umeda et al., 2003). With improving methodologies and with the availability of better preserved tissues, analysis is now being carried out for lipids (Anderson et al., 2014; Thompson et al., 2015; Zemski Berry et al., 2014), small molecules (Ablonczy et al., 2013), molecular ions (Thomson et al., 2015) and trace elements (Flinn et al., 2014) which will refine the molecular understanding of differences between central and peripheral retina in both health and disease at these geographic locations.

A key molecular difference between the macula and peripheral human retina is the distribution of specialised macular pigments. The

Table 1
Illustrates the key differences between the central and peripheral retina.

	Central Retina	Peripheral Retina
Bruch's membrane	Thin (2–4 μm), acellular, five-layered extracellular matrix located between the retina and choroid (Christine and Curcio, 2012; Hildebrand and Fielder, 2011)	Half as much accumulation of lipoprotein-like material than central. It is approximately 1-2μm in thickness nearing the ora serrata (Hildebrand and Fielder, 2011).
Retinal Pigment Epithelium (RPE)	RPE cells have a peak density of 7500 cells/mm^2 at the fovea (Ach et al., 2014)	They have a density of 2000 cells/mm^2. (Boulton and Dayhaw-Barker, 2001)
Photoreceptors	Measures approximately 6 mm in diameter centred on the fovea. Rods are absent in the fovea and are only present in the central retina in an elliptical ring that passes through the optic nerve. Around 50% of the retinas cone photoreceptors are present in the central 30° of the retina (Curcio et al., 1990; Kolb, 1995).	Stretching to the ora serrata the peripheral retina is approximately 21 mm measured from the centre of the fovea. It accounts for around 92 million rods. The cone-to-rod ratio in human retinas is approximately 1:20 (Curcio et al., 1990).
Outer nuclear layer (ONL)	Similar thickness in central and peripheral retina. In the central retina cones have oblique axons displacing their cell bodies (Kolb, 2005)	Similar thickness in central and peripheral retina. In the peripheral retina the rod cell bodies outnumber the cone cell bodies while reverse is true for the central retina (Kolb, 2005)
Outer plexiform layer (OPL) and Henle fibre layer	The OPL is thickest in the macula and associates with the Henle fibre layer (a pale staining fibrous like area present in the central retina due to fibres of cones and rods and accompanying Muller cell processes) (Kolb, 1995; Perry and Cowey, 1988; Polyak, 1941)	Thinner and no Henle fibre layer is present.
Inner nuclear layer (INL)	Thicker due to greater density of cone-connecting second-order neurons (cone bipolar cells, horizontal cells and amacrine cells) (Kolb, 2005)	Thinner due to the decreased density of cone photoreceptors (Kolb, 2005)
Inner plexiform layer (IPL)	Thicker due to high number of ganglion cells making connections in this layer.	Thinner due to the decreased density of the ganglion cells towards the periphery
Ganglion cell layer (GCL)	Densely packed and often numerous layers of ganglion cells. Density levels reach 32,000–38,000 cells/mm^2 in a horizontal elliptical ring 0.4–2 mm from the fovea (Curcio and Allen, 1990).	GCL density drops by 35,000 to 5,000 cells/mm^2 within 4 mm of the fovea with this dropping again from 4 mm to the ora serrata by 5000 to 200-300 cells/mm^2 (Curcio and Allen, 1990)
Nerve fibre layer (NFL)	Thicker in the central retina and continues to thicken towards the optic disc due to convergence of retinal ganglion axon fibres on the optic disc (Kolb, 2005).	Thinner and difficult to recognize. (Kolb, 2005)
Macular Pigment	Mass ratio of Lutein to Zeaxanthin is approximately 1:2.4 (0–0.25 mm) (Bernstein et al., 2010)	Mass ratio of Lutein to Zeaxanthin 2:1 (8.7–12.2 mm) (Bernstein et al., 2010).
Gene Expression	Neurofilament 3 (NEF3), Light neurofilament (NEFL), Brain-specific α-tubulin (TUBA3), α-tubulin (κ-α-1), B-tubulin (FKBP1A) (Sharon et al., 2002)	Rhodopsin(RHO), β and γ subunits of transduction (GNB1 and GNGT1), β and γ subunits of rod cGMP-phosphodiesterase (PDE6B and PDE6G), α subunit of the cGMP-gated cation channel (*CNGA1*), and recoverin (*RCV1*) (Sharon et al., 2002)

xanthophyll pigments lutein, zeaxanthin, and meso-zeaxanthin are highly concentrated in the fovea (Bernstein et al., 2016), decline by an order of magnitude within 2° of fixation, reach very low levels at the edge of the macula, and remain low throughout the retina (Bone et al., 2001; Hammond et al., 1997; Snodderly et al., 1984). The distribution can be envisioned as 3 concentric zones centred on the fovea: zeaxanthin is central-most (foveola, 350 μm diameter), overlapped by meso-zeaxanthin (foveal avascular zone, 500 μm diameter); these two surrounded by lutein (foveal-parafoveal annulus of outer diameter, 2.0 mm) (Nolan et al., 2016). The role of xanthophyll pigments in vision is investigated under several mechanistic hypotheses - anti-oxidant protection against blue light damage (Loane et al., 2008), enhanced visual performance and visual comfort by reducing chromatic aberration and light scatter (Nolan et al., 2011; Stringham et al., 2015), and enhanced neural efficiency hypothesis by direct interaction with neurons (Renzi and Hammond, 2010). Xanthophyll pigments are also found in the brain and studied in reference to cognition and aging (Erdman et al., 2015; Mohn et al., 2017). Dietary supplements containing lutein and zeaxanthin are recommended for patients with intermediate AMD (Age-Related Eye Disease Study 2 Research Group, 2013).

Recent evidence supports macular Müller cells as the principal cellular reservoir of xanthophylls. High concentration in the Henle fibre layer, foveal centre, and inner plexiform layer is well explained by the morphology of individual Müller glia (Bringmann et al., 2018; Curcio, 2018; Snodderly et al., 1984). The finding of rings and shoulders in addition to a strong central peak is consistent with Müller cell side branches in the synaptic layers (Delori et al., 2006; Dietzel et al., 2011). In 1984 Snodderly et al. attributed strong xanthophyll signal in the Henle fibre layer to cone axons, a description which overlooks the numerous rod and Müller processes also in this layer (Curcio et al., 1990; Perry and Cowey, 1988; Snodderly et al., 1984) and is often mistakenly taken to mean that these pigments localize to only cone axons. In macular telangiectasia type 2, xanthophyll absence is associated with histologically confirmed degeneration of foveal Müller cells (Powner et al., 2010, 2013). Patients with Sjögren-Larsen syndrome exhibit loss of clinically detectable xanthophyll and presence of inner retinal cysts suggestive of Müller cell degeneration (Theelen et al., 2014; van der Veen et al., 2010). Surgically excised lamellar hole associated epiretinal membranes are enriched both in Müller cell markers and in xanthophylls (Obana et al., 2017; Pang et al., 2016). Clinical imaging suggests that xanthophylls persist in central geographic atrophy (Dysli et al., 2016; Sauer et al., 2018; Sunness et al., 1999), even after photoreceptor death, because Müller cells remain (Li et al., 2018). It has been suggested that HDL-mediated delivery of xanthophylls through the RPE is a physiologic activity that contributes lipids to the formation of soft drusen in advanced age (Curcio, 2018).

The ratio of lutein to zeaxanthin within 0.25 mm of the fovea is approximately 1:2.4 with this reversing in the retinal periphery where the ratio is 2:1 between 8.7 and 12.2 mm from the fovea (Bernstein et al., 2010). There is a 100 fold drop in the concentration of macular pigment in the peripheral retina compared to the macula, although levels vary considerably between individuals (Bartlett et al., 2010).

The principal signal source for clinical autofluorescence imaging is RPE lipofuscin and melanolipofuscin. These are numerous lysosome-related, long-lasting inclusion bodies that are detectable in human RPE starting in childhood (Feeney, 1978). Throughout adulthood, the RPE continues to accumulate lipofuscin both in the central and peripheral retina. The topography of histologic autofluorescence matches that of photoreceptors (Ach et al., 2014; Curcio et al., 1990; Wing et al., 1978), i.e., high in a rod-dominated crest at the edge of the macula and present but not absent in the fovea. RPE lipofuscin has been postulated as central to many deleterious events in AMD, including phototoxicity-mediated cell death and drusen formation (Sparrow et al., 2002; Wu et al., 2010), primarily through studies of cultured cells exposed to A2E, a bisretinoid derivative of vitamin A. A2E was originally isolated from whole human eye cups (Eldred and Lasky, 1993), from which it is

difficult to detect macula-specific signals. Recent data using assays with higher spatial precision have indicated that A2E is sparse in the macula and abundant in the periphery (Ablonczy et al., 2013; Adler et al., 2015; Anderson et al., 2017; Bhosale et al., 2009; Pallitto et al., 2015; Zemski Berry et al., 2014), in humans and in non-human primates, raising the question of what fluorophore(s) account for macular autofluorescence signal. Table 1 shows differences between the central and peripheral retina.

2.5. Functional differences between the central and peripheral retina

When referring to peripheral vision, we refer to the vision mediated by the photoreceptors within the "peripheral" retina. These special features of the fovea as outlined earlier (section 2.3) enable high spatial resolution, low spatial summation, poor scotopic vision but excellent photopic vision, whereas the peripheral retina, which is rod-dominant, enables excellent scotopic vision, high spatial summation but poor spatial resolution.

From a functional/psychophysical perspective, peripheral vision is usually considered to be any point outside the central 1.7° field of vision (i.e. rod-free fovea) (Rosenholtz, 2016). Far peripheral vision has been designated as beyond 60° as this is the approximate value for occlusion by the nose and eyebrow. (Simpson, 2017). Other regions such as 8°–30° for near peripheral vision and 30°–60° for mid-peripheral vision have been used in the literature (Simpson, 2017) though these designations are not solidly linked to anatomy (Section 2.3), but rather have developed through convention.

An often-overlooked feature of the retina in the far periphery is the existence of a cone-rich rim, a 1 mm strip adjacent to the *ora serrata* in which cones predominate rather than rods (Mollon et al., 1998; Østerberg, 1937). Mollon et al., postulated that it may be important for detecting sudden movements, measuring optic flow, contributing to colour constancy or involved in modulating circadian rhythms (Mollon et al., 1998). However, given that a similar cone-rich rim is also present around the optic disk it could be argued that it should not be assumed that there is a significant functional role of such anatomical features (Curcio et al., 1990).

Peripheral vision has a different role in visual perception than central vision. This is due to the peripheral retina's ability to detect movements via the wide dendritic trees of the peripheral ganglion cells, while the fovea is poor in movement detection but high in distinguishing details because of the small dendritic trees of the ganglion cells at this location (Walls, 1963). Contrast sensitivity beyond 70° has been shown to the higher to moving stimuli than stationary (To et al., 2011). Peripheral vision compensates for the lack of high acuity by the area it covers (Larson and Loschky, 2009). Patients more quickly understand and process low-detailed stimuli like a big shape with a uniform "bland" colour when using their peripheral vision than when they were limited to using their central vision only. Furthermore, blocking out peripheral vision in order to mimic vision loss in the peripheral retina correlated to a dramatic slowing of this "low-detail" processing (Larson and Loschky, 2009).

Peripheral vision also participates in a phenomenon termed "scene gist recognition" or perception without awareness (Larson and Loschky, 2009). Peripheral vision has been shown to be more important than central vision for an individual's awareness of their surroundings, even when the environment is highly detailed or has high spatial frequency (HSF) information that could not be fully resolved by the peripheral retina. This is extremely interesting, because perception of HSF stimuli is generally associated with central vision. (Musel et al., 2011). But experiments illustrate that even in highly detailed environments, individuals primarily rely on peripheral vision for awareness and recognition of their settings (Ramanoel et al., 2015). This principle applies both to perception of natural settings containing low spatial frequencies and urban settings containing higher spatial frequencies (Musel et al., 2013).

The more we understand about peripheral vision, the more we understand its importance in understanding an individual's engagement with their environment. Numerous studies illustrated the importance of peripheral vision in attention processing tasks (Desapriya et al., 2014; Ludwig et al., 2014). One study comparing children with normal vision with those with poor peripheral vision found that the latter group had slower visual scanning and impaired motion detection, concluding that reduced peripheral vision in children can have a large impact on normal development (Huurneman et al., 2014). Most importantly, children with peripheral visual deficits performed significantly worse on tasks that required visual attention than the normal vision peers and children with poor central vision (Tadin et al., 2012). This correlation between peripheral visual deficits and attention tasks isn't surprising. Most studies on elderly also find that peripheral vision is important in driving and postulate that peripheral visual health is a much better predictor of driving ability than visual acuity (Huestegge and Bockler, 2016; Peli et al., 2016). Furthermore, studies have implicated peripheral visual deficits as a larger cause of pedestrian accidents in dementia patients than cognitive impairment alone (Owsley and McGwin, 2010).

Peripheral visual health is vital in the aging population and not only for driving (Fisk and Mennemeier, 2006; Fisk et al., 2002; Wolfe et al., 2017). Peripheral visual function has a more pivotal role than central vision in mobility, locomotion, and postural stability (Black et al., 2008; Marigold, 2008; Nakayama, 1985; Vargas-Martin and Peli, 2006). Therefore, maintaining and monitoring peripheral vision is likely to become a crucial factor for determining if an individual can live independently. Lack of understanding and monitoring peripheral visual function both in clinical and in everyday settings can have deleterious consequences in a population where the majority is elderly. Despite growing evidence of its importance in daily living, very little research has been carried out to date to explore the effects of retinal pathologies on peripheral visual function and this should be given more attention. Further consideration of the role of far peripheral vision has been given in a review by (Simpson, 2017).

2.6. Pathological differences between the central and peripheral retina

A major contribution to the literature on peripheral retina are 17 publications of Foos, Lewis, Straatsma, and colleagues (1967–1986). These studies outlined a systematic and quantitative characterization in 1191 eyes recovered from 631 individuals at autopsy. Particular attention was paid to ex vivo macrophotography prior to paraffin histology, and the resulting imaging-histology correlations are valuable for elucidating today's wide-field imaging. Here we summarize findings on pigmentary change and drusen. An early demonstration of the fineness of histologic detail potentially available to clinical imaging, these data represent an informative comparison to macular changes associated with Age-related Macular Degeneration (AMD). Although AMD affects primarily central vision, it is important for understanding the underlying biology to appreciate the degree to which peripheral retina is also affected.

2.6.1. Pigmentary changes

At the ocular equator and anterior to it, 7 macroscopically defined patterns of pigmentary change were identified and characterised by topography and histology (Bastek et al., 1982).

All increased in prevalence across the lifespan. Virtually all older eyes had one or more of these morphologically distinct degenerations. By affected location, these patterns were divided into 3 groups. Reticular degeneration of RPE is shown in Fig. 4.

Affecting the retina: Linear, a sharply demarcated radial pattern of black pigment adjacent to the inner retinal surface at the *ora serrata*, corresponding to RPE of the pars plana extending along the inner aspect of the retina. Dusting, a coarse, sprinkled pattern of red-brown pigment in the retina, corresponding to intracellular pigment accumulations of varying size, throughout the retinal layers. Spicular, a bone spicule

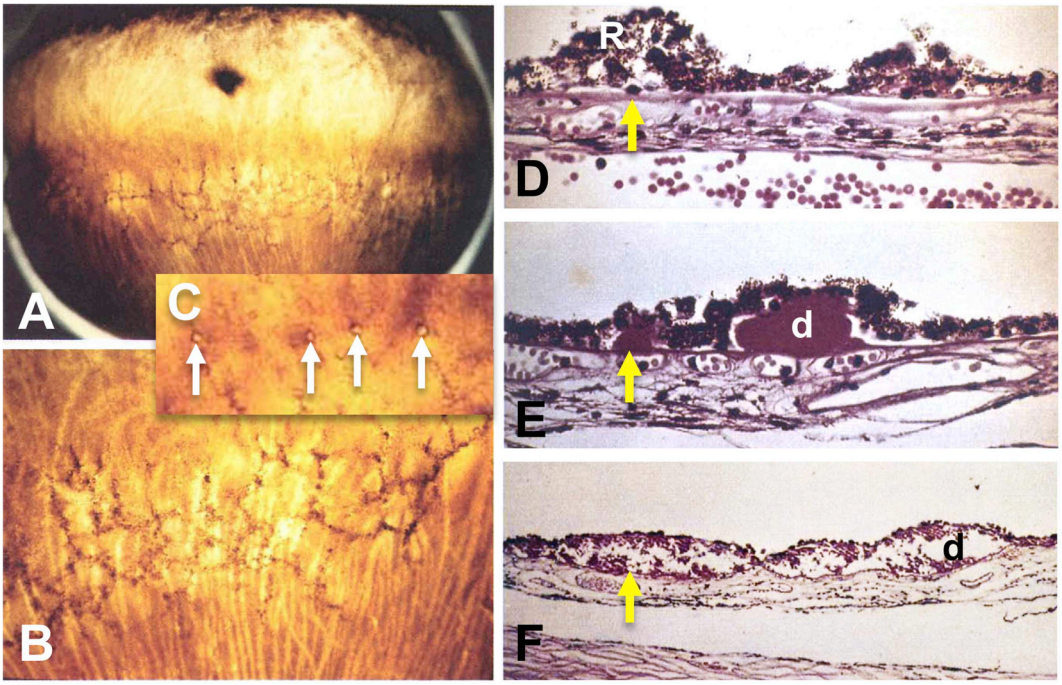

Fig. 4. Reticular degeneration of the retinal pigment epithelium (RDPE).
Panels A–C show the RPE layer after the neurosensory retina is removed, in caps sliced off the equator of human globes at autopsy. Panels D–F show 6-μm-thick paraffin sections (D, hematoxylin-eosin stain; E, F, periodic acid-Schiff stain); R, RPE; d, druse; yellow arrows, Bruch's membrane. Panels D, E are more highly magnified than panel E (compare the sizes of erythrocytes across panels). Adapted with permission from (Lewis et al., 1985)
A. Panoramic view. Hyperpigmented lines form a netlike pattern, delineating a region of hypopigmented polygons. Incomplete polygons and branching hyperpigmented lines contain hard drusen. **B.** Detailed view. Hyperpigmented lines form a fishnet-like pattern, delineating a region of hypopigmented polygons. **C.** Close-up view. Drusen (arrows) at the nodes of the fishnet of hyperpigmented lines are hypopigmented in the centre and hyperpigmented around the base. **D.** Histologic section through a hyperpigmented line. RPE cells are tall and thick, with numerous pigment granules. Bruch's membrane appears thickened. Choriocapillaries are intact. **E.** Dome-shaped hard drusen (d) in linear arrangement with hyperpigmentation and occasional heaping up of RPE cells surrounding them. Choriocapillaries are intact. **F.** A section through the centre of a hypopigmented polygon shows confluent drusen (called soft) with hypopigmented, flattened, and thinned RPE cells.

pattern of black pigment usually aggregated around blood vessels in middle and inner layers (like retinitis pigmentosa (Li et al., 1995)).

Affecting the RPE: Granular, a discrete pattern of small pigment aggregations, corresponding to variable cell size and pigmentation. Clumping, discrete large pigment aggregations, due to heterogeneity in cell size and pigmentation correlating with hyperpigmented and hypopigmented areas. Reticular, a fishnet-like pattern of linear pigment aggregations that branched and formed incomplete or complete 5 or 6 sided polygons, with internal hypopigmentation, and associated with lines of hard drusen (Fig. 4A–C). Hyperpigmented lines corresponded to RPE cells that were tall and relatively thick, increased in pigment content, and occasionally heaped up into multilayers. Effaced and hypopigmented RPE overlay drusen, and hyperpigmented and occasionally heaped RPE surrounded drusen bases (Fig. 4D–F).

RPE and choroid: Tapetochoroidal hypopigmentation, a distinct band of decreased pigmentation of RPE and choroid, located circumferentially at the equator, corresponding to a diffuse diminution in size and pigmentation of RPE cells.

Reticular degeneration of RPE (RDPE) was first described clinically by Haab in 1901 (Lewis et al., 1985), and due to its associations with genetics and macular pathology, this entity merits re-visiting today. Gass described and illustrated RDPE in a series of 200 older persons, noting that 1/3 of eyes with AMD also had RDPE (Gass, 1972). This association with AMD was confirmed (Humphrey et al., 1984) and further shown to be significantly higher in AMD eyes than in age-matched control eyes. Lewis et al. (1985) showed in a large autopsy study and a parallel clinical series (n = 50) that RDPE was present in all quadrants, involving the full circumference of the eye, with less involvement in temporal retina. The age-increase (4.3% prevalence in eyes < 50 years; 60% in eyes > 90 years), high degree of bilaterality, and association with AMD changes in the same and fellow eyes were notable features of RDPE. Lewis et al. speculated that RDPE was a "zonal degeneration related to relative ischemia in the watershed area of the antero-posterior choroidal circulation and the gradual decline with aging in the metabolic activities of the RPE."

Several studies showed that RDPE might signify genetic susceptibility for AMD, perhaps even before AMD is visible in the macula. Postel et al. (2005) found that in 411 singletons and 125 multiplex probands stratified using standardized colour fundus photography, RDPE was almost as common (50.6%, 41.0%, respectively) as RPE hyperpigmentation (59.5%, 58.5%) and large drusen in the macula (49.4%, 47.3%), two well-known ocular risk factors for progression. These same authors (Shuler et al., 2008a) found that the proportion of eyes with RDPE was significantly higher in carriers of the risk-conferring Y402H allele of complement factor H (CFH, n = 796) than in non-carriers (n = 160). RDPE was the only one of 34 characteristics that associated with this variant. In a sample of 2103 AMD patients, Seddon et al. found that 25% of eyes had RDPE and that this percentage increased with AMD severity by standardized colour fundus photography (Seddon et al., 2009). There was a two-fold greater risk of maculopathy in eyes with RDPE, even in those eyes at low AMD grades. Other tested genes did not exhibit this association, and interestingly the risk allele of ARMS2 was inversely related to RDPE.

2.6.2. Drusen

S.H. and J.P. Sarks, with M.C. Killingsworth, contributed foundational AMD pathology, including drusen heterogeneity, in studies utilizing transmission electron microscopy of affected maculae from

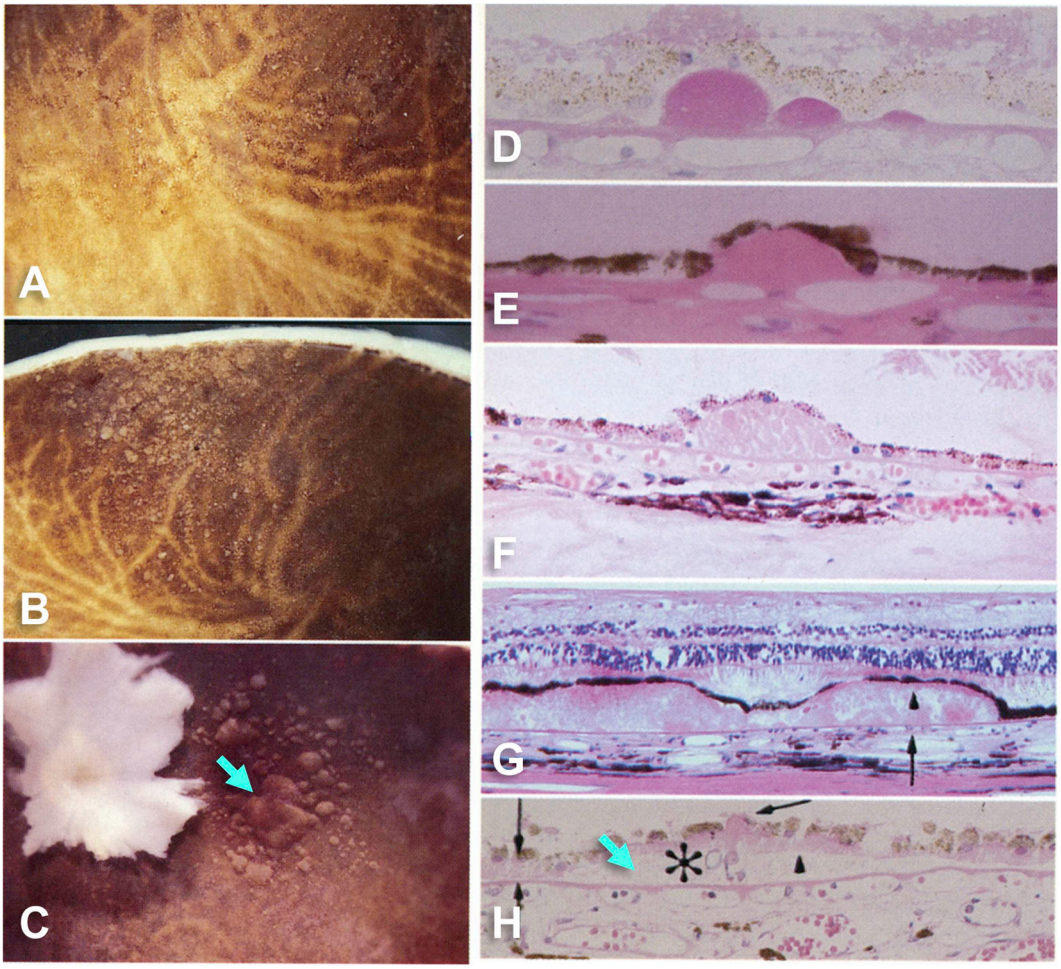

Fig. 5. Drusen in peripheral retina, in comparison to macula.
Retina is completely removed from retinal pigment epithelium (RPE) in A-B and partially in C. **A.** Temporal equatorial region in an eye with multiple extramacular drusen, all hard. Soft drusen were not present. The macula also had multiple hard drusen. **B.** Temporal equator in an eye with multiple extramacular drusen. Numerous hard, discrete soft and confluent soft drusen are present. **C.** Macular region of the same eye showing discrete and confluent soft drusen (teal arrow). A remnant of retina remains and is attached at the optic nerve head. **D.** Contiguous hard drusen with a globular configuration (periodic acid-Schiff). **E.** Hard druse in the peripheral fundus with minimal thinning of the overlying RPE and mild hyperpigmented borders (hematoxylin-eosin). **F.** Discrete soft druse with a dome-shaped configuration and lightly staining material (hematoxylin-eosin). **G.** Confluent soft drusen, with vacuolated granular material between basal laminar deposit (arrowhead) and the inner collagenous layer Bruch's membrane (arrow) (hematoxylin-eosin). **H.** A soft druse with apparent membranous debris (by the Sarks' definition, teal arrow) in the macula. Thick basal laminar deposits are adjacent to the druse (between arrows) and also attached to the inner aspect of Bruch's membrane (arrowhead). A nodular excrescence is noted on the inner side of Bruch's membrane (arrow). Calcification within the druse is also seen (asterisk; hematoxylin-eosin). Adapted with permission from (Lewis et al., 1986b).

clinically documented eyes of S.H. Sarks' patients. Studies definitively localized drusen in the sub-RPE-basal laminar space and demonstrated that risk-conferring soft drusen are dome- or mound-shaped with sloping sides and filled with ‘membranous debris’ implying abundant lipids (Sarks et al., 1980, 1994). However, drusen are numerous in peripheral retina (Friedman et al., 1971; Lengyel et al., 2004), which is large, and thus the majority of drusen are extramacular. Yet the macula is more vulnerable to AMD.

This conundrum might be resolved if macular and extramacular drusen had different molecular composition. The Sarks stated that soft drusen localized exclusively to central macula (Sarks et al., 1996) but did not provide supporting data. In particular, data indicating scarcity or absence of soft drusen in the periphery could definitively establish a relationship of these deposits with foveal biology, as postulated (Curcio et al., 2013). Few published studies were designed to test this possibility. Lewis et al. using ex vivo imaging of RPE with retina removed, paraffin histology, and evaluation in 14 defined regions (Lewis et al., 1986a; b) illustrated macular and peripheral drusen in one figure. Fig. 5 panel C, H (modified from their papers) shows mound-like, confluent “serogranular drusen” (a Sarks term) in macula. These were contrasted to globular (‘hard’) drusen (Fig. 5D and E) and other drusen from the periphery, also called soft (Fig. 5F and G). Although they are low mounds, it is arguable whether these latter drusen are soft in the Sarks' sense. Rather, the druse bases are not as circular as macular drusen (compare panel C to B), paraffin histology and light microscopy are suboptimal for assessing lipid, and the druse interior of panel H appears mostly empty as though it was extracted. In a much smaller comparison of macula and periphery (Rudolf et al., 2008b), drusen from 9 eyes of 7 AMD donors were micro-dissected and pelleted for high resolution histology. This study found soft drusen only in the macula, where they were also more likely to have overlying BLamD, continuous coverage by RPE, and interiors dominated by a friable and homogeneous membranous material consistent with the Sarks' descriptions. These suggestions of regional differences in druse composition should be revisited and tested with new histology and clinical imaging of the entire retina.

The genetic associations of peripheral drusen have been studied, although with variable definitions for the regions, AMD stages, and druse types. Peripheral drusen, defined as those anterior to the ocular

equator, were more significantly common in multiplex than singleton probands (22.8% vs 7.5%) (Postel et al., 2005). Neither variants in CFH nor ARMS2/HTRA1 were associated with peripheral drusen or extra macular drusen in a clinic-based study of 755 AMD patients; how periphery and extra-macula were differentiated, however, was not defined (Shuler et al., 2008a, 2008b). In contrast, a study of 2103 AMD patients found a positive association of two CFH variants with peripheral drusen (i.e., located near the equator) with all severity levels of AMD but not if only eyes early AMD were analysed (Seddon et al., 2009). In a cohort of adults ≤67 years, the presence of drusen peripheral to the vascular arcades was associated with the Y402H variant of CFH, with a fourfold increase in the odds of drusen among subjects homozygotic for Y402H compared with those in subjects without this polymorphism. This association also held for macular drusen ≥63 μm but not for numerous drusen ≤63 μm (Munch et al., 2010).

3. Historical development of peripheral retinal imaging

While imaging the fundus has been a standard for screening, detecting and monitoring the presence of ocular diseases including the systemic diseases that manifest in the retina, obtaining peripheral views of the retina remained challenging due to the limitations imposed by the physical properties of the eye. Since the production of the first reliable fundus camera by Carl Zeiss in 1926, imaging of the retina has undergone several significant technical advances. Before the introduction of UWFI, traditional techniques provided adequate imaging of the optic nerve and posterior pole, but a limited view of the retinal periphery. With the introduction of modalities fit to capture the peripheral retina, evaluation and documentation of the retinal periphery has become more practical in a clinical environment. Below is a summary of the methodologies used to examine and/or record peripheral retinal pathology.

3.1. Retinal drawings

The first known method of wide-angle retinal illustration is thought to be retinal drawings. The well-known ophthalmic artist Terry Tarrant sketched retinal maps from 1958 to 1988, producing drawings of the ocular fundus (Fig. 6). Drawings took from 30 min to 3 h to map pathologies on the retina, which included tears and retinal detachments (Dvorak and Russell, 2011). He continued retinal drawings, even though imaging techniques had been made available, to educate the examiner in ocular anatomy and the use of imaging.

3.2. Indirect ophthalmoscopy

In 1900s Trantas (1900), used the indirect ophthalmoscope to view the peripheral retina by indenting the sclera, through the upper lid over the limbus, using the nail of his thumb to apply firm pressure. This allowed him to visualize wider angle of the eye including examination of the anterior part of the retina; the view was imperfect and the procedure was highly uncomfortable for the patient. An improvement introduced by Schepens 50 years later refined the use of scleral indentation while using his newly manufactured binocular indirect ophthalmoscope, allowing visualization of the retina to the *ora serrata* and into the pars plana (Schepens and Bahn, 1950).

3.3. Fundus imaging technique

Advancements in retinal imaging included Jackman and Webster producing the first published human fundus photographs in the late 1800's (Jackman WT, 1886). The first known wide-angle camera, the Equator-Plus camera was developed by Pomerantzeff in the 1970s. This method used scleral trans-illumination coupled with a contact lens to produce a field of view of approximately 148° (Pomerantzeff, 1975). The introduction of fundus cameras in 1926 revolutionalised imaging of

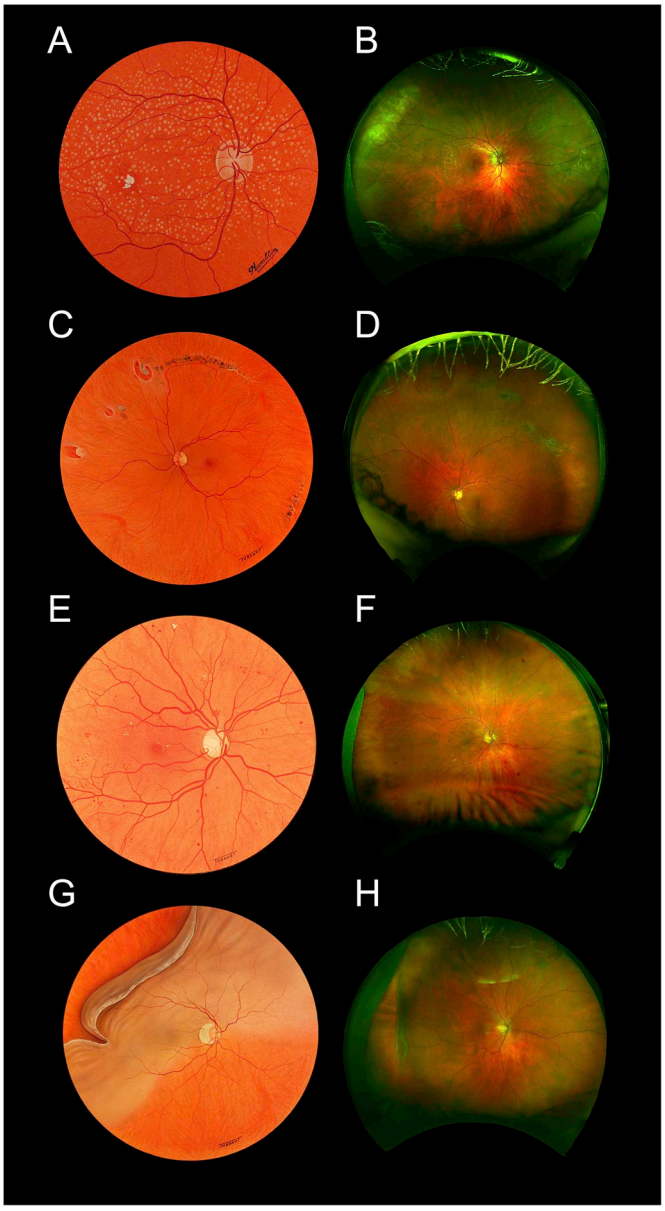

Fig. 6. Pathology detected on the ocular fundus.
A: example of retinal drusen on a retinal drawing; B: Optomap image showing drusen on the retina; C: retinal drawing showing retinal tears and lattice degeneration; D: Optomap image showing a lattice degeneration; E: retinal drawing showing retinal haemorrhages and exudates; F: Optomap image showing retinal haemorrhages; G: retinal drawing showing a retinal detachment; H: Optomap image showing a retinal detachment.

the eye. Traditional fundus cameras can provide images of the peripheral retina covering around 75° field of view by directing the objective lens to the periphery and at the same time asking the patient to fixate eccentrically. Multiple photographs of the posterior pole from different angles can be taken and subsequently montaged together. This has been refined for the purpose of diabetic retinopathy (DR) clinical trials in which a seven standard field (7SF) images are captured covering a field of view of approximately 100° (Lotmar, 1977). Montaging images has several limitations including distortions in alignment, magnification, or brightness between the retinal images. The ability to accurately register images for longitudinal monitoring is technically challenging when using montaged images. This capability is particularly important for lesions such as choroidal nevi and tumours, where careful longitudinal monitoring and measurements are required.

3.4. Retcam

The year 1997 saw the introduction of another wide field fundus camera known as the RetCam II retinal imaging system (Clarity Medical Systems, Inc, Pleasanton, CA). This portable camera requires the use of a contact lens and allows for several different lens attachments. The Retcam can produce retinal images up to 130° field of view. This camera is primarily used for retinal imaging in children, such as screening for retinopathy of prematurity, retinoblastoma evaluation, shaken baby syndrome screening and many other paediatric conditions (Dhaliwal et al., 2009). Although this technique was originally regarded as relatively simple and easy, challenges such as media opacities resulted in poor image quality. In addition to the Retcam, another system known as the Panoret-1000 (CMT Medical Technologies, Inc, Valley Stream, NY), also produces approximately 130° field of view of the retina by using a contact lens system; however, the Panoret uses scleral transillumination resulting in less difficulty with lens opacities.

3.5. Optomap

In 2000, the Optomap (Optos PLC, Dunfermline, Fife, Scotland, UK) noncontact camera was launched for imaging the eye at an angle of 200° field of view, equating to 82.5% of the total retinal surface area. The Optomap allows detection of retinal pathologies at locations where otherwise these might be missed if indirect ophthalmoscope or standard fundus camera image were utilised. The wide-field view was achieved by employing a scanning laser ophthalmoscope while utilizing an ellipsoid mirror to obtain images of the retinal periphery. It uses a red (633 nm) and green (523 nm) laser to scan the retina and obtain UWFI. The red and green lasers used to capture an Optomap image produces a pseudocolour retinal image, which differs from the “true colour” image produced by a traditional fundus camera using a white-light source. Apart from obtaining fundus photographs, the Optomap is also capable of producing high-resolution fluorescein angiogram images of the retinal periphery (vascular structure of the retina) and FAF images. FAF imaging uses green laser and reveals defects in the retinal pigment epithelium which contains fluorophores in lipofuscin that emit light in a range of 540–700 nm range. Advantages of FAF imaging include an increased depth of the retina captured in a single image, thus overcoming the anatomical curve of the retina, and the capture of 200° including the posterior pole and periphery without requiring pupil dilation in approximately 0.25 s. Imaging the eye using this device not only reduces the number of images required to map the fundus, but also decreases patient exposure to light and patient imaging and waiting times, which is important in a busy clinic. Although these wide-field imaging modalities enhanced our understanding of peripheral retinal diseases and are now valuable research tools, there are still some limitations (Bonnay et al., 2011) (Fig. 7). One limitation is the variability of the total retinal surface captured between images or imaging sessions. Much of this variability can be attributed to the presence of image artefacts driven by patient factors such as small pupils, eyelashes, and eyelids; camera factors relating to illumination and physical set-up; and intraocular issues such as the brightness of the reflectance superior of the optic nerve. In addition, presence of small hard drusen-like “deposits” on the image appearing more frequently in the superior retina in red and green laser separation has been found to contribute to image analysis conundrums. These artefacts may be due to motion during image capture, the experience of the photographer, patient cooperation, and media opacity (e.g. dense cataract). Especially for novice users the pseudo-colour image may challenge the interpretation of certain structures (e.g. pigmented choroidal tumours).

Optomap images represent a compromise between area of retina imaged and resolution required to see relevant retinal changes and so there is a decreased image resolution(4000 × 4000) when compared to other colour fundus imaging modalities (3456 × 2304) (Witmer and Kiss, 2013). The conventional fundus image methods produce a narrower field of view with good central area resolution whereas the Optomap will produce a simultaneous view of the posterior pole and the periphery but with adequate resolution for each. In particular, on the Optomap image, the temporal and nasal peripheral retina have less resolution resulting in noticeably fewer details. Distortion and decreased resolution mainly occurs around the far temporal and nasal areas of the periphery. However, there are methods to correct for this (Spaide, 2011). Peripheral distortion occurs as a result of the Optomap using an ellipsoid mirror in order to produce wide-field image. The distortion is particularly apparent in the far temporal and nasal periphery. This means that lesions found in the periphery may look bigger than they truly are and therefore appropriate corrections must be applied when measuring peripheral retinal structures (Witmer et al., 2013).

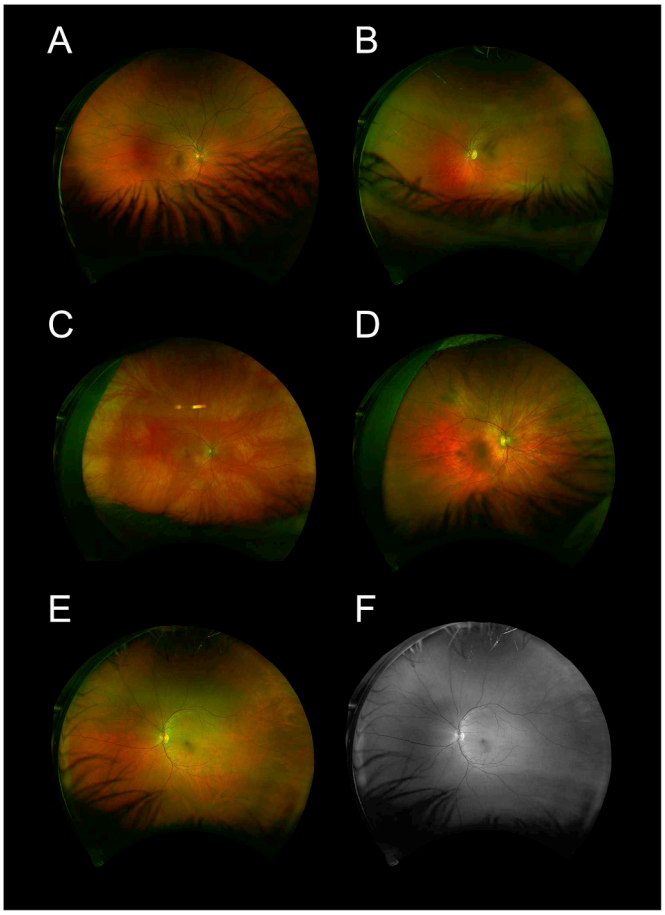

Fig. 7. Artefacts that can appear on Optomap images.
A: the presence of eyelids restricting the view of the retina inferiorly; B: presence of an eyelid and eyelashes that restricts the view of the inferior retina; C: camera reflectance on the image and appears a bright green, the image also has eyelid and camera pad present; D: camera pad present on the temporal retina restricting the view of the retina. E: pseudocolour Optomap image highlighting the reflectance that can appear above the optic nerve; F: green separation of image E: showing the reflectance above the optic nerve, the image also has eyelid present.

To address measurement issues, the manufacturer produced a tool that transform Optomap images into a stereographically projected image using assumptions based on a model eye with a diameter of 24 mm, and thus reducing the impact of peripheral distortion. This was achieved by ray-tracing every pixel in the Optomap image through a combined optical model of the Optos 200Tx SLO and the Navarro ultra-widefield model eye. This combined model represented the “projection” utilised by the Optos 200Tx platform to create the two-dimensional Optomap from scans of a respective eye. By reversing this device-

specific projection, a representation of the image data on a three-dimensional sphere was created (Croft et al., 2014).

Projection of Optomap images also enables image overlays using the Registration tool. Registration of images removes any minor shift or rotation between pairs of images taken of the same eye by automatically adjusting one or more follow-up image to best fit the layout of the baseline image. Appropriate registration is vital in longitudinal studies where baseline and follow-up images are captured at different times. In addition to these tools, the montaging capability serves the purpose of being able to stitch together images taken using eye-steering resulting in the widest field of images being generated.

In early 2014, Croft et al. investigated the quantification and montaging of the retinal surface area on UWFI (Croft et al., 2014). For accurate quantification of retinal surface and precise montaging of the steered images, UWFI warping, precision and accuracy were assessed as a function of different gaze angles. Precision was tested by a standard retinal surface area being quantified across 10 montages of the same eye. Once standard areas were measured across the image set, a mean of 408.97 mm^2 surface area with a standard deviation of 0.7% was found, this reflected a high degree of precision. No major outlier was found in any montages, regardless of gaze angles. Accuracy of measurements was then assessed by quantifying the mean disc area of 50 patients and comparing them to standard normative disc area measurements with a range of 1.60–2.63 mm^2 mean disc areas (El-Dairi et al., 2009). The authors concluded that precise montaging and accurate quantification of retinal surface area (mm^2) can be achieved in UWFI images (Croft et al., 2014). In addition, using an intraocular retinal prosthetic implant of known dimensions as a "ruler" inside the eye, Sagong and colleagues verified that after stereographic projection (and adjustment for axial length), retinal measurements could be obtained reliably within 1% of the ground truth (Sagong et al., 2015).

3.6. Other wide-field imaging technologies

Heidelberg Engineering's (Heidelberg, Germany) Spectralis® equipment produces a 25- and 35- degree retinal field of view with an option to expand to 55° by using a noncontact lens attachment to attain FAF, FFA and ICG images. Additionally, the Staurenghi contact lens could be used with the Spectralis® to provide a 150-degree view of the retina. In 2012, Heidelberg Engineering introduced a non-contact ultra-widefield angiography (UWFA) module for both the Spectralis® and Heidelberg Retina Angiograph II models, by using an interchangeable non-contact lens attached to the camera head (Fig. 8). It captures a single confocal scanning laser ophthalmoscopy image that is evenly illuminated and has high contrast across the periphery (Witmer et al., 2013). Fluorescein and ICG can be performed individually or simultaneously, revealing clinically relevant peripheral changes such as but not limited to; non-perfusion, microaneurysms or neovascularisation. In 2014, Espina et al. presented data from evaluating the non-contact UWFA and ICG using a modified Heidelberg Spectralis (Espina et al., 2014). They concluded from examining 35 eyes that a 105-degree retinal field of view was captured. This device has been utilised for autofluorescence, infrared, intravenous fluorescein angiography, oral fluorescein angiogram and ICG (Espina et al., 2014).

3.6.1. Zeiss CLARUS 500

In late 2017, Zeiss Medical Technology introduced a non-contact, high-definition UWFI system, the CLARUS 500. The CLARUS utilizes four LED light sources: Red at 585–640 nm; Green at 500–585 nm; Blue at 435–500 nm; and an infrared laser diode at 785 nm. The fundus image produced resembles conventional white-flash photography. Using the red, green and blue channels true colour images can be separated to help enhance the visual contrast of details in certain layers of the retina. In addition blue and green autofluorescence allows the visualization of lipofuscin in the RPE. It also has the capability of providing an external eye image. In the future Zeiss plans to incorporate fluorescein and ICG into CLARUS models. In the widefield single image mode, the CLARUS captures up to 133° of the retina with a 7.3 µm optical resolution. In the UWFI mode, which involves capturing two separate images, this device can capture up to 200° of the fundus. A third, montage mode automatically stitches up to six individual images, netting up to 267° of the retina in a single display (Appold, 2017). The manufacturer asserts that 'true colour' images produced by the CLARUS more closely mimic the colouration of the retina seen during dilated fundoscopy. This may ultimately assist in a more accurate diagnosis and documentation of retina disorders (e.g. choroidal nevi). However, to date, no peer-reviewed studies have substantiated advantages of 'true colour' images, nor to corroborate any deficiencies in accurate identification of retinal pathologies with technologies that blend the red, green and blue channels (e.g. devices from Optos and Heidelberg). Moreover, as with the EIDON (see below), direct comparisons among the available UWFI devices is also lacking.

3.6.2. CenterVue EIDON

The EIDON confocal scanner from CenterVue received FDA clearance in December 2014. This device was the first to combine the confocality of scanning laser ophthalmoscope (SLO) systems with 'true colour' fundus imaging. Unlike other SLO devices with monochromatic lasers, the EIDON utilizes white illumination (440–650 nm) to generate fundus images whose colouration is more similar to that seen on dilated fundoscopy. In addition to the colour fundus image, the EIDON is capable of capturing near infra-red (with an 825–870 nm source) as well as red-free fundus images. The EIDON's optical resolution is approximately 15 µm with an image sensor resolution of 14 megapixels. In

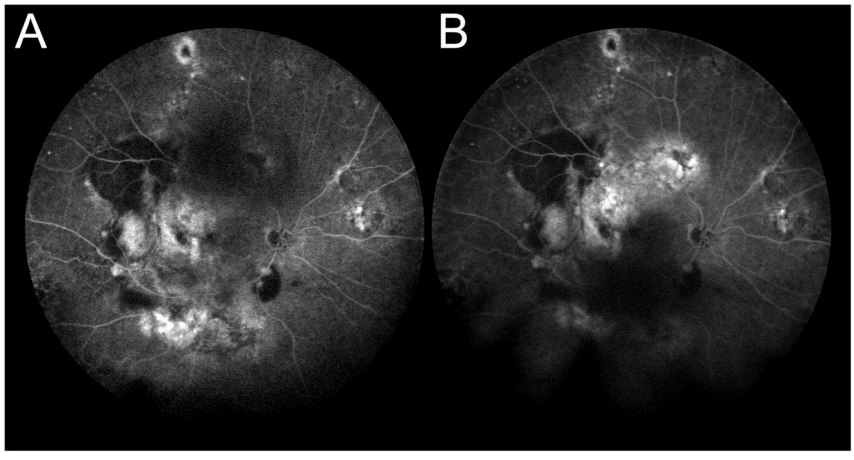

Fig. 8. Fluorescein Angiography images taken at 4 min (A) and at 5 min (B) using the Heidelberg non-contact lens.

a single image capture, the EIDON camera is capable to capture up to a 60° retinal field of view. Using a programmable internal fixation target, along with an auto montage software feature, up to 110° of the fundus may be imaged. This, however, requires four individual fundus photographs to be taken. Getting closer to the widefield imaging parameters requires an external fixation and six or more images to be captured, and even then, only approximately 150° can be montaged into a single picture. As is the case for the CLARUS 500, peer-reviewed studies comparing confocal 'true colour' images and blended single channel SLO images are absent, as are comparisons to other widefield imaging devices.

3.6.3. Wide-field OCT

In 1991, Optical Coherence Tomography (OCT) (Huang et al., 1991) was first introduced by researchers as a non-invasive, radiation-free diagnostic technique producing high-resolution *in vivo* imaging of retinal, choroidal, and optic nerve head structures (Sung et al., 2012). Following its introduction, OCT has undergone several improvements such as increased speed, resolution and depth of image. Recently peripheral retinal lesions were imaged with a widefield swept-source OCT (SSOCT) with a field of view of 4.62 ± 0.62 "optic nerve to fovea distance units, increasing the single steer field of view (McNabb et al., 2016). In the same year Choudhry et al. generated far-field OCT images through eye steering (Choudhry et al., 2016). The field of view of OCT images are increasing (Shinohara et al., 2018) and it is possible that in the near future we will be able to capture full-filed OCT without steering. Overall, it is now possible to image the far periphery with OCT and this will deepen our understanding of the lesions identified on UWFI (Choudhry et al., 2016).

4. Comparison of UWFI grading methods

Conventional retinal imaging is well established, and it is imperative that new imaging modalities are scrutinized for validity, reliability and clinical utility. As early as 2013, the utility of UWFI image-assisted assessment compared to traditional fundus examination consisting of slit-lamp biomicroscopy and binocular indirect ophthalmoscopy was carried out (Brown et al., 2013). Altogether 170 subjects (339 eyes) were investigated within this study, with image-assisted examination being superior to examination carried out without imaging. Specifically, image-assisted examination detected 90.6% of drusen in the posterior pole area compared with 43.8% using no image-assistance. The same was true for the 128 vitreoretinal interface abnormalities detected, where out of the 122 white without pressure 92.2% was detected using assistance versus 54.7% without. In cases where both techniques disagreed, a retinal specialist performed an adjudication using slit-lamp biomicroscopy, binocular indirect ophthalmoscopy, scleral indentation and a review of UWFI concluded that the image-assisted examination was correct in 75% of cases. The conclusion of the study was that non-mydriatic UWFI is useful in detecting and managing ocular disease in conjunction with traditional examinations though further work was required to determine the value of UWFI alone (Brown et al., 2013).

In case of DR clinical studies and research, our understanding of UWFI is growing steadily as there are now several studies comparing UWFI to standard imaging. Comparing UWF Optomap images to the standard Early Treatment Diabetic Retinopathy Study (ETDRS) 7SF, resulted in a more severe DR grade in many due to the visibility of additional peripheral lesions in areas beyond the 7SF view (Silva et al., 2015; Talks et al., 2015; Wessel et al., 2012a). These studies highlight the importance of UWFI for more accurate diagnosis of severity of DR, but it requires longitudinal studies to understand the clinical importance of this difference. Standard fundus photography has been an integral part of ocular examination for well over 40 years, and so understanding how UWFI compared to such a well-established technique is paramount. It might be that taking UWFI in one disease will have less utility than in another, and its adoption for the diagnosis, treatment and monitoring of retinal diseases will develop on the underlying pathology.

Objective, valid, reliable and reproducible image analysis is the cornerstone of generating good quality results both for clinical and research studies. Grading grids existed since the advent of image analysis using conventional transparencies (film), but these have to be re-established and re-evaluated for the large area covered by UWFI. Given the extent of the area available for grading on such UWFI, a grid is usually used to divide up the area into relevant and manageable sections so grading of abnormalities can be carried out. Over the years, a number of grading grids have been developed and in the section below the advantages and disadvantages for these are to be discussed.

It is instructive to review the development and application of grading systems for macular disease. The ETDRS grid was first used for fine-grained documentation of vasculopathy and exudation in 7 overlapping 30° fundus photographs viewed stereoscopically (Early Treatment Diabetic Retinopathy Study Research Group, 1991a; b). Drusen were assessed, to differentiate them from hard exudates. The macula was subdivided into 9 zones, one central encompassing the fovea and foveal avascular zone, and inner (outer diameter at 3 mm radius) and outer rings (outer diameter at 6 mm radius) of 4 subfields each. This grid was used for major epidemiologic studies of AMD in European-derived populations (Klein et al., 1991, 1992; Mitchell et al., 1995; Vingerling et al., 1995). Originally designed for inner retinal pathology in diabetes, this grid captures the distribution of inner retinal neurons whose metabolic demands dictate the distribution of vessels of the intrinsic retinal circulation. However, the ETDRS grid has important limitations for mechanistic insight on outer retinal disease including AMD. It does capture the division of macula into *cone-dominant* and rod-dominant sub-regions (central subfield vs inner and outer subfield). However, the grid combines the *cone-only* foveola and mixed rod-cone parafovea in the central subfield, and it omits altogether a horizontally oriented elliptical ring of high rod density that localizes to the edge of the grid and extends nasally around the optic nerve head.

4.1. Moorfields grid

In 2008, the Moorfields grid was developed and was initially derived from the International Classification for AMD system of dividing the macular area into 3 central zones. The Moorfields grid is loaded onto an individual Optomap image once the user set the location of the optic disc and fovea manually and then allowed the system to set up the grid on the image, centred on the macula. The standard Wisconsin age-related maculopathy grading scheme (WARMGS) grid was modified with additional two grading zones added based on the distance between the centres of the optic nerve head and the foveola (defined to be 4500 μm). Zone 4 represents the mid periphery, which has a diameter of 11000 μm, and zone 5 consists of the far periphery representing all areas outside of zone 4. The Moorfields grid can only be loaded on unprojected Optomap images, without correcting peripheral distortion. Once the concentric rings were fitted, the zones were subdivided into four quadrants through the centre of the fovea, resulting in superior and inferior nasal quadrants and superior and inferior temporal quadrants (Lengyel et al., 2015). See Fig. 9A.

4.2. Manchester Grid

The Manchester Grid (MG) was initially developed for grading ischemia in fluorescein angiograms for Professor Paulo Stanga at the University of Manchester (Sala-Puigdollers et al., 2013). The grid initially utilised three ellipses that divided the retina into three different zones: posterior pole, mid-periphery and periphery, to facilitate grading of DR. This was replaced with x- and y-coordinates centred on the fovea (0, 0). The MG covers the retina with approximately 754 squares with each square being approximately one optic disc area in size (1.77 mm^2)

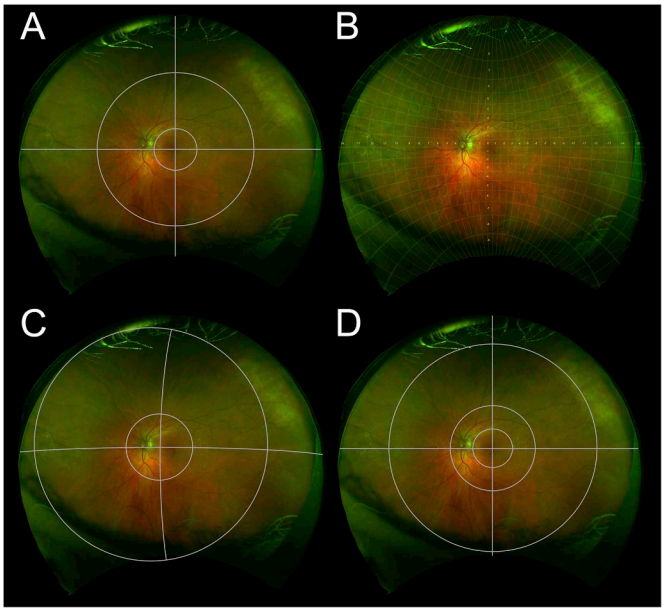

Fig. 9. Currently available grading grids.
Moorfield's grid (A), Manchester Grid (B), Opera Grid (C), Boston grid (D).

(Jayadev et al., 2016). See Fig. 9B. Each grid rectangle can be labelled with the numbers 1 to 5 with mouse clicks, depending on the pathology being graded. Once an image is graded and saved a spreadsheet is automatically generated displaying the co-ordinates of the pathology and its approximate size. The MG therefore maintains fine spatial location information about a lesion as well as quantitative information, in an unbiased manner.

4.3. Opera Grid

The Opera Grid was developed for grading AMD within a sub study of Age-related Eye Disease Study (AREDS) 2 called Optos Peripheral Retina AMD (OPERA) study (Domalpally et al., 2017; Friberg et al., 2014). The images can be graded on both un-projected and projected Optomap images. It displays the Studies of Ocular Complications of AIDS (SOCA) grid which is placed on the image based on the user providing the fovea and disc locations (AIDS Clinical Trials Group, 1992). The SOCA grid is divided into three zones: Zone 1, Zone 2 and Zone 3. Zone 1 was 6000 μm diameter area centred on the fovea and approximately the area enclosed by the vascular arcades, Zone 2 extending anteriorly from zone 2 to the anterior borders of the vortex vein ampullas (the furthest anterior that could be photographed easily) and Zone 3 extends from Zone 2 to the *ora serrata*. Zone 1 and Zone 2 are both divided into four quadrants, superonasal, superotemporal, inferotemporal and inferonasal. Zone 3 is divided into two hemispheres (superior, inferior) using a visual extension of the horizontal cross line. A properly aligned grid has the centre point of Zone 1 at the centre of the line that connects the disc to the macula. The outer circle dividing Zone 2 and 3 crosses the vortex veins. See Fig. 9C.

The OPERA grid was based on a grid developed for trials of ganciclovir treatment of cytomegalovirus retinitis (AIDS Clinical Trials Group, 1992; Holland et al., 1989) in order to assess progression of virus infection and permanent vision loss and the utility of antiviral treatment in clinical trials. Zone 1, the macula, was the portion of where this infection would have been immediately sight-threatening. This grid may be less useful for assessing diseases involving neurodegeneration, because the macula was not subdivided into fovea and perifovea, and the peripheral zones did not take into account radial asymmetries in distribution of retinal neurons, which were described and quantified after the grid was initially developed (Curcio and Allen, 1990; Curcio et al., 1990).

4.4. Boston grid

More recently Oellers et al. developed a novel grid to study peripheral retinal abnormalities of AMD on projected images (Oellers et al., 2017). This proposed grid is based on image size rather than dimensions of the human eye and consists of three concentric zones with crosshairs centred on the fovea. The first zone (radius of 29 mm) corresponds with the ETDRS grid. The second zone is the perimacular area (radius of 65 mm). This zone was defined based on clinical observations and, interestingly, corresponds to observations made in another UWFI study that defined this area as the arcade zone (Lengyel et al., 2015). The last zone separates the mid and far periphery and it is located on the vortex veins (radius of 160 mm). See Fig. 9D.

4.5. Comparison of different grids

Different grids subdivide the back of the eye in different ways. The Opera grid is centred half way between the fovea and the optic disc (Fig. 9C), whereas the Moorfields (Fig. 9A), Manchester (Fig. 9B) and Boston (Fig. 9D) grids are centred on the fovea, allowing comparison with standard fundus images of the past (Csutak et al., 2010). For detail, the |Manchester grid exceeds all others as it contains 754 zones (Sala-Puigdollers et al., 2013), which are useful especially in longitudinal studies (Quinn et al., 2017). However, grading takes significantly longer than that of the other three grids. The OPERA grid has 10 zones, the Moorfields grids has 12, and the Boston grid has 16; these allow faster, though less detailed grading.

To compare the information generated by using the different grids, we selected 114 UWF images that had been graded for hard drusen using the Manchester grid, then we interpolated a hard drusen grading with the other 3 grids (Fig. 10). Based on this, clinicians and researchers can draw their own conclusion about which one is better for a given application. As the images were selected from a general population, comparison of the outcome can only be made in relationship to the Moorfields grid that was designed for the population-based Reykjavik Eye Study (Lengyel et al., 2015). Similar to the finding of the Reykjavik Eye study, there is a higher prevalence of far peripheral hard drusen phenotype in this sample of the general population (Lengyel et al., 2015) as well. The detailed Manchester grid can define locations within the general zones of the other grids; whether this has clinical relevance will need further investigation. It might be also important to point out that none of the grids currently takes into account the distribution of neuronal cells in the retina (see section 2).

5. Peripheral retinal lesions

The evaluation of retinal periphery plays an ever-increasing role in screening, diagnosing, monitoring and treating retinal diseases. Indeed, several studies have suggested that wide-field imaging can be a useful adjunct to the standard clinical exam, improving the diagnosis of diabetic retinopathy and the extent of retinal detachments as two examples (Brown et al., 2013; Kornberg et al., 2016; Manjunath et al., 2015). These advantages of widefield imaging may be particularly apparent to the general clinical user in patients with poor pupillary dilation or media opacity where standard ophthalmoscopy may be challenging. One of the most striking findings from several studies are that virtually all eyes have what would be classified as an abnormality present within the peripheral region (Denniston and Murray, 2009). Covering all lesions in detail is beyond the scope of this paper, but we have produced a comprehensive list of lesions with relevant references in Table 2. Some common lesions are to be discussed in Section 7 below.

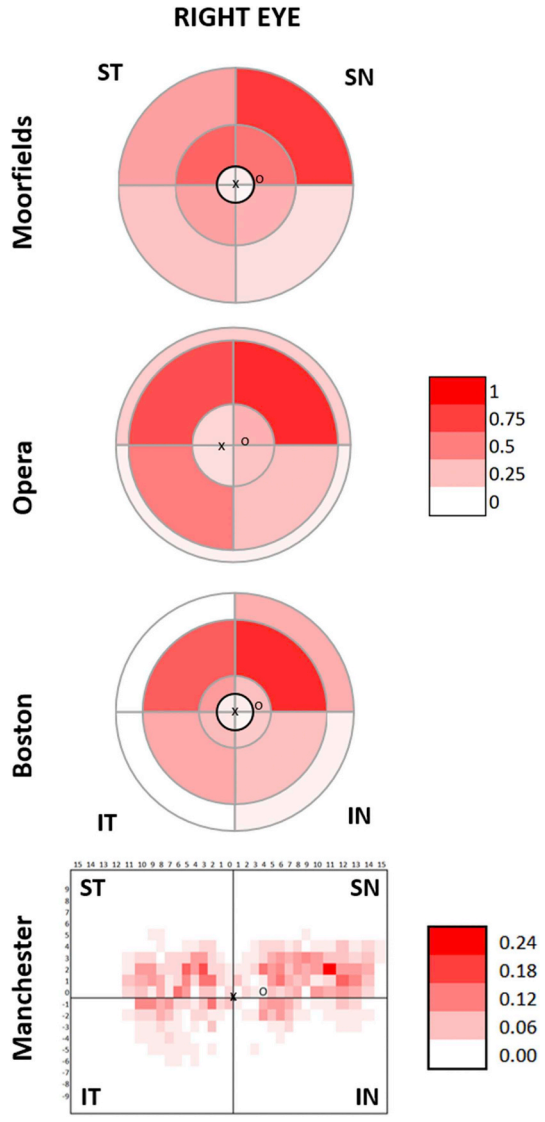

Fig. 10. Spatial distribution of hard drusen using the Moorfields, Opera grid, Boston and Manchester grid respectively.
Moorfield's grid: centre ring (black) represents zone 3 (ETDRS equivalent), middle ring represents zone 4 (mid-periphery) and outer represents zone 5 (far-periphery). Opera grid: centre ring represents zone 1, middle ring represents zone 2 and outer represents zone 3.
Boston grid: centre ring (black) represents zone 1 (ETDRS equivalent), the second ring represents zone 2 (perimacular area), the third ring represents zone 3(mid-periphery) and outer ring represents zone 5 (far-periphery). The location of the foveola labelled with "x" and the optic disc labelled with "o". Red: high prevalence of hard drusen; White: absence of hard drusen; ST-superotemporal; SN-superonasal; IN-inferonasal; IT-inferotemporal.

6. New insight into retinal disease from wide-field imaging

As wide-field imaging is increasingly integrated into standard practice, it has been noted that the presentation of disease in the posterior pole does not always mirror the severity of that seen in the retinal periphery and vice versa. Using UWFI new insights have been gained into a number of common retinal conditions:

6.1. Retinal vein occlusion (RVO)

RVO is a common retinal vascular disease; causing vision loss in many of those affected. RVO occurs more frequently in patients with ischaemic heart disease, hypertension and diabetes mellitus. Depending on the location of the occlusion it can be classified as either central (CRVO) or branch retinal vein occlusion (BRVO). RVO is characterised by retinal vascular tortuosity, retinal haemorrhages, cotton wool spots, optic disc swelling and macular oedema. In a CRVO retinal haemorrhages will be seen in all retinal quadrants whereas in a BRVO retinal haemorrhages will be seen in the area where the vein is occluded (Karia, 2010). Prasad et al. investigated whether peripheral angiographic features of BRVO and hemicentral retinal vein occlusion (HRVO) are associated with macular oedema and neovascularisation using UWFA imaging and concluded that areas of untreated retinal nonperfusion may encourage the production of biochemical mediators which in turn trigger macular oedema and neovascularisation (Prasad et al., 2010). Singer et al. (2014) examined the extent of peripheral retinal nonperfusion in RVO on the effect of macular oedema severity using UWFA and OCT and reported that people with a higher ischaemic index correlated with greater macular thickness and worse vision in RVO. Following treatment, OCT imaging showed that the more ischemic an eye was the greater the decrease in retinal thickness, and this was accompanied by improved visual acuity.

6.2. Age-related macular degeneration

AMD is the leading cause of irreversible central vision loss among the elderly population. To elucidate the prevalence and significance of AMD-like lesions in the periphery, several studies used UWFI in patients with AMD. In 2013, Tan et al. found that peripheral FAF abnormalities using UWFI (Optos 200Tx, Optos, Dunfermline, Scotland) occurred in 68.9% of patients with AMD. There were several distinct patterns of peripheral FAF, including granular (46.2%), mottled (34.0%) and nummular (18.1%). Significant risk factors for FAF abnormalities were AMD type (neovascular or non-neovascular), older age and female sex. Some colour photography features had a high correlation with specific FAF patterns: these included granular FAF with peripheral drusen and mottled FAF with RPE depigmentation (Tan et al., 2013). Another study investigated peripheral FAF in patients with AMD and found that wide-field FAF imaging revealed a significantly increased central and peripheral FAF signal as well as an increased peripheral FAF irregularity in patients with AMD with or without anti vascular endothelial growth factor (anti-VEGF) treatment compared with eyes in the control group (Reznicek et al., 2012). In 2015, Lengyel et al. investigated the relevance of peripheral retinal AMD-like within a population based cohort. Presence or absence of hard, crystalline, and soft drusen; retinal pigment epithelial changes; choroidal neovascularisation (CNV); atrophy; and hypoautofluorescence and hyperautofluorescence were graded in the peripheral retina. In 18.9% of eyes examined there was no pathology detected in the macula or periphery; however in 57.4% of eyes, AMD-like pathology was detected in both the macula and peripheral retina. In 13.6% of eyes, AMD like changes were found in the macula alone and in 10.1% of eyes, AMD like lesions were found in the peripheral retina only (Lengyel et al., 2015). More recently, Guduru et al. examined subjective grading of UWFA images in AMD patients and if there was an association between peripheral FAF abnormalities and AMD. They found that there was a moderate agreement in the interpretation of peripheral FAF abnormalities. FAF abnormalities appeared both in AMD patients and controls; however people with AMD were at a greater risk of FAF abnormalities (Guduru et al., 2017).

These studies provided interesting insights into the potential associations between macular and peripheral changes (See section 2.6). It is clear that further work is needed to determine if the development and progression of retinal pathology related to AMD in the peripheral retina is associated with the development and progression of changes found in the macula. This should provide both mechanistic insights into the pathophysiology of the condition as well as practical insights into whether imaging and assessing the peripheral retina should be a priority for clinicians treating AMD patients.

Table 2
Shows a description of retinal features and diseases and if UWF imaging was used on these retinal lesions and diseases.

Lesion/Disease	Description	Has it been investigated using UWF retinal imaging?
Chorioretinal Atrophy	A condition where both the choroid and retina are damaged. It can be classified as: diffuse or patchy. It is characterised by choroidal depigmentation and thinning of the retina. (Tokoro and SpringerLink, 1998)	Y (Salcedo-Villanueva et al., 2015)
Retinal detachment	It is characterised by the separation of the neurosensory retina (NSR) from the RPE. This causes a build-up of subretinal fluid between the NSR and RPE. The key types of detachment are; rhegmatogenous, tractional, exudative and combined tractional-rhegmatogenous (Bowling, 2015f)	Y (Bonnay et al., 2011; Bowling, 2015f)
Congenital Hypertrophy of the Retinal Pigment Epithelium (CHRPE)	CHRPE is a benign lesion that appears on the retina as a round usually well-defined lesion that typically is dark grey in colour. It may contain lacunae and a 'halo' like lining of hypopigmentation surrounding it. CHRPE can be classified into three entities (solitary, grouped or multiple pigmented fundus lesions) each with their own distinct features and implications (Youhnovska et al., 2013).	Y (Shneor et al., 2014; Turgut, 2015)
Bear Tracks	Known as grouped (multifocal) CHRPE. They appear a lot smaller than regular CHRPE and without the lacunae and 'haloes'. They appear in groups with a pattern resembling animal footprints hence the name 'Bear Tracks' (Bowling, 2015c).	Y (Ly et al., 2015)
Peripheral Drusen	It is characterised by the gathering of small/yellow deposits on the retina made up of waste products from degenerating RPE cells, lipids and some proteins. It is appears similar to the drusen found at the posterior pole only differing location (Rudolf et al., 2008a).	Y (Aslam et al., 2014)
Choroidal Melanoma	It appears as an irregular or oblong feature that has abrupt elevated edges. It can be pigmented or non-pigmented with overlying subretinal fluid and orange pigment (Bowling, 2015a).	Y (Bowling, 2015a; Kernt et al., 2010)
Vitreous Haemorrhage	This occurs due to the disruption of healthy or diseased retinal vessels that causes extravasation and/or leakage of blood into the vitreous of the eye. It may also be due to the growth of abnormal retinal vessels (Manuchehri and Kirkby, 2003). It may be diffusely spread throughout the vitreous cavity, or the blood may conform to the anatomy of the vitreous. For example, haemorrhage in the subhyaloid space may result in a scaphoid (boat-shaped) haemorrhage.	Y (Kim et al., 2014)
Asteroid Hyalosis (AH)	AH is a degenerative condition that affects the vitreous humour of the eye. It consists of spherical bodies in the vitreous cavity most commonly found inferiorly. (Kador and Wyman, 2008)	Y (Ogino et al., 2014)
Retinoschisis	This is a vitreo-retinal dystrophy characterised by the splitting of the sensory retina into two layers; inner and outer layer. It is most likely due to vitreous traction where the retina is pulled apart. It may appear either shallow or bullous and retinal vessels appear dark due to light being blocked (Selaru et al., 2000).	Y (Agarwal et al., 2015)
Sclerosed/Ghost Vessels	Vessels become sclerotic when retinal vessels pass through an area of degenerating retina. It is known as sheathing of the vessels. When the anterior surface becomes involved, the entire vessel appears opaque. When sheathing encircles the wall it produces a wire like vessel.	N
Snail Tracks	This is a vitreoretinal degeneration that is similar to lattice degeneration. It appears like shiny 'snowflakes' on the retina. It is usually well-defined and oblong in configuration (Bowling, 2015e).	Y (Kothari et al., 2012)
Pavingstone	Pavingstone degeneration is characterised by patches of chorioretinal atrophy that coalesce into groups. Pigmentation may surround the lesion. It is more commonly found in the inferior retina (Bowling, 2015c).	Y (Kothari et al., 2012)
Lattice	This is where there is a break of the internal limiting membrane with atrophy of the neurosensory retina apparent. It appears spindle shaped and often sclerosed vessels form. It is commonly bilateral found both superiorly and inferiorly (Bowling, 2015e).	Y (Kothari et al., 2012)
Peripheral Cystoid degeneration	This is characterised by the appearance of small vesicles with indistinct boundaries on a white/greyish background. It is thought to be present in all adult eyes, increasing in extent with age (Bowling, 2015c).	N
Diabetic Retinopathy	It is a microvascular disease that is characterised by the damage of small blood vessels due to high glucose levels. It is characterised by micoaneursym/macroaneursym, exudates, cotton wool spots, intraretinal microvascular abnormality, dot and blot haemorrhages and venous loops or beading (Bowling, 2015b).	Y (Liegl et al., 2014; Silva et al., 2014)
Gyrate Atrophy (GA)	GA is a chorioretinal dystrophy that is relatively rare. It is characterised by well-defined patches of chorioretinal atrophy in the peripheral retina. GA affects myopes and as people age these lesions tend to increase in size and number and coalesce throughout the retina (Kaiser-Kupfer Mi, 2002).	Y (Paciuc-Beja et al., 2014)
Choroideremia (CHM)	Choroideremia is an X-linked degeneration characterised by atrophy of photoreceptors, RPE and choroid. Areas of RPE atrophy are seen initially in the periphery and progress centrally.	Y (Morgan et al., 2014)
Retinitis pigmentosa (RP)	RP isn't a single disease but a group of hereditary disorders. It is characterised by the degeneration of both the RPE and photoreceptors. (Natarajan, 2011). On the fundus RPE degeneration can be seen throughout the retina, pale optic disc and thinner retinal vessels (Jones et al., 2016).	Y (Jones et al., 2016; Ogura et al., 2014)
Retinal Dialysis	This is an expression used when describing retinal holes that appear at the ora serrata. In around 5% of cases dialysis is bilateral most commonly found in the lower temporal area. Demarcation lines and cysts are also associated with retinal dialysis (Tasman, 1974).	N
Choroidal Rupture	Choroidal ruptures occur due to ocular trauma. It is characterised by a break in the choroid, Bruch's membrane and RPE. It may appear as a yellow or white sub-retinal streak, which may be linear or curved in shape. (Ament et al., 2006)	N
Metastasises of the Choroid	It appears as a yellow/orange subretinal mass, colour depending on where the primary tumour is. It is associated with the accumulation of subretinal fluid and its location again depends of the primary site (Arepalli et al., 2015).	Y (Coffee et al., 2009)
Retinoblastoma	This is a rare form of childhood cancer occurring in approximately 1:18000 live births. It is characterised by the cells of the retina growing rapidly and out of control (Bowling, 2015d). It classically presents with one or multiple nodular, white or cream coloured masses often associated with increased vascularisation.	N
Sickle Cell Retinopathy (SCR)	SCR can be classified as either proliferative or non-proliferative. In the non-proliferative stage the most common clinical finding is salmon patched haemorrhages in the peripheral retina. In the non-proliferative stage the most common clinical finding is retinal neovascularisation in the peripheral retina following vaso-occlusion (Melo, 2014; Mudvari et al., 2010).	Y (Cho et al., 2011)
Cytomegalovirus retinitis	It may appear asymptomatic, however if symptoms do arise they include floaters, vision problems and blind spots. It appears irregular in configuration and is characterised by retinal whitening which appears granular, haemorrhages may also be present (Heiden et al., 2007).	Y (Mudvari et al., 2010)
Giant Retinal Tear (GRT)	GRT is a full-thickness neurosensory retinal break measuring $> 90^{\circ}$ that extends circumferentially around the retina for three or more clock hours in the presence of a posteriorly detached vitreous (Shunmugam et al., 2014).	Y (Meyer and Saxena, 2010)

(*continued on next page*)

Table 2 (*continued*)

Lesion/Disease	Description	Has it been investigated using UWF retinal imaging?
Stargardt disease/Fundus Flavimaculatus	It is characterised by the presence of white to yellow dots that surround pigmentary maculopathy and can extend to the midperiphery (Armstrong et al., 1998).	Y (Zein and Brooks, 2012)
Familial Exudative Vitreoretinopathy (FEVR)	This is a rare disorder that can be inherited. It affects retinal angiogenesis thus the vascularisation of the peripheral retina remains incomplete and poor vascular differentiation is visible (Gilmour, 2015). In serious cases pre-retinal neovascularisation and fibrosis at the junction between vascular and avascular retina can occur that causes traction of the macula and retinal vessels.	Y (Trese et al., 2012)
Susac syndrome (SS)	This consists of a triad of symptoms; encephalopathy, branch retinal artery occlusion (BRAO) and hearing loss. It is a very rare disease and can be misdiagnosed due to this (Nazari et al., 2014).	Y (Kumar et al., 2013)
Marfan syndrome	This is a connective tissue disorder affecting the skeleton, eyes and cardiovascular system in particular. In relation to the eyes the signs and symptoms are myopia, early glaucoma and/or cataracts and detached retina (Dean, 2002).	Y (Rahmani et al., 2013)
Retinitis Punctata Albescens	This is a disorder of the sensory retina and retinal pigment epithelium. It is thought to be congenital and characterised by white dot like lesions that are found scattered deep to the retinal vessels (Smith et al., 1959).	N
Chorioretinal coloboma	It is often associated with other changes in the eye, these include microphthalmos, high myopia, glaucoma, cataract, and phthisis bulbi. A major risk of coloboma of the choroid is retinal detachment (Jesberg and Schepens, 1961).	Y (Barnard et al., 2012)
Retinal Haemorrhage	They can be RNFL haemorrhages arising from pre-capillary arterioles. They can also be intraretinal haemorrhages that occur at the venous end of the artery that result in a dot/blot appearance. Deeper darker round haemorrhages occur due to retinal infarcts that happen in the middle retinal layers (Bowling, 2015b).	Y (Nakagawa and Skrinska, 2001)
Retinal Hole	This is full thickness degeneration of the sensory retina. It appears round to oval in shape and may have a white collar representing localized detachment.	Y (Kothari et al., 2012)
Floaters	They appear as hairlike, dark grey or black in colour due to the shadow they form by blocking exiting laser light. They take a variation of sizes and appearances on the retina and hide underlying retinal detail. Floaters are thought to be due to an age-related process or due to ocular trauma, asteroid hyalosis, foreign bodies or retinal tears (Sebag et al., 2014).	N
Horseshoe Tear	This is due to vitreous traction of the retina. A tear is pulled from the sensory retina in the shape of a horseshoe. They are most commonly seen between the ora serrata and equator where the retina is thinner.	N
Choroidal Naevus	This is a benign lesion that is characterised by the accumulation of melanocytes. They are usually asymptomatic and appear black to slate grey in colour and can have pigmentary changes present. It has well defined edges and can be flat or slightly risen. Over time drusen may be present on the lesion. A nevus is closely followed as it may evolve into a malignant melanoma (Gordon-Shaag et al., 2014).	Y (Gordon-Shaag et al., 2014)
White without Pressure (WWOP)	WWOP is a retinal phenomenon that is described as an area of retinal whitening which blocks the view of the underlying choroid. It is thought to be due to vitreous traction. WWOP occurs in the far periphery and never takes the same configuration between eyes (Orlin et al., 2013).	Y (Orlin et al., 2013)
Exudates	Exudates appear as waxy yellow lesions that take a ring-like configuration with relatively distinct margins. They are caused by chronic localized retinal oedema (Bowling, 2015b).	N
Cotton Wool Spots	They appear as small fluffy whitish lesions that block the view of underlying blood vessels. They are made up of debris from the nerve fibre layer (Bowling, 2015b).	N
Cholesterol Embolus	They are small, yellow reflective lesions. Usually there are multiple present on the retina. They are seen at arteriolar bifurcations and can move or even disappear (Rousseau et al., 2013).	N
Acute posterior multifocal placoid pigment epitheliopathy (APMPPE)	APMPPE is a posterior uveitis. Clinically, it appears as grey-white lesions on the retina. There is usually multiple present and appears in both eyes. At the site of APMPPE there is usually pigment clumping (Mrejen et al., 2013).	Y (Mrejen et al., 2013)
Vogt-Koyanagi-Harada (VKH)	In most cases VKH is a bilateral disease affecting multiple organs of the body. In the eye it is characterised by panuveitis with iridocyclitis, serous retinal detachment, diffuse choroidal swelling and optic disc hyperaemia (Agrawal and Biswas, 2011).	Y (Heussen et al., 2011)
Birdshot Retinopathy (BSRC)	BSRC is an uncommon chronic posterior uveitis. It is characterised by multiple ovoid spots primarily in the posterior pole/mid-periphery. It usually appears bilateral with a distinctive presentation and a strong genetic association (Gasch et al., 1999).	Y (Piffer et al., 2014)
Central Serous –Chorioretinopathy (CSCR)	CSCR is an acquired chorioretinal disorder. It is due to a serous detachment of the retina that appears like a clear blister. Pigment epithelial detachment and subretinal fluid may also be present (Daruich et al., 2015).	Y (Nam et al., 2015)
Retinopathy of Prematurity (ROP)	ROP is a proliferative disorder that affects the developing vessels of the retina in premature infants. The main cause of ROP is thought to be the abnormal growth of blood vessels. The growth of these vessels can lead to retinal detachments and ultimately blindness (Casteels et al., 2012).	Y (Fung et al., 2014; Theodoropoulou et al., 2013)
Microaneurysms	This appears as a tiny area of blood protruding from the retinal capillary wall. They form either by focal dilation or by fusion of two arms of a capillary loop (Bowling, 2015b).	Y (Leicht et al., 2014)
Coats' Disease	Coat's disease is characterised by a defect in retinal vascular development which ultimately leads to leaky vessels, subretinal exudation and detachment of the retina. It is thought to be more frequent in men and appears unilateral (Black et al., 1999).	Y (Bass et al., 2011)
Pathological Myopia	Myopia is characterised by the extreme increase in axial length of the eye and the formation of posterior staphyloma(s). Lesions also may appear in the posterior pole including, myopic choroidal neovascularisation, myopic tractional maculopathy, myopic optic neuropathy and myopic chorioretinal atrophy (Kaneko et al., 2014).	Y (Kaneko et al., 2014)
Acute zonal occult outer retinopathy (AZOOR)	It is an idiopathic syndrome which involves loss of function in one or more zones of the outer retina. It is characterised by photopsias and/or scotoma. Some cases present with a grey/white ring surrounding the involved part of the retina i.e. acute annular outer retinopathy (AAOR). Chronic stages have signs of atrophy of the RPE and/or intraretinal pigment migration.	Y (Shifera et al., 2017)

6.3. Retinopathy of prematurity

Retinopathy of Prematurity (ROP) affects the vasculature of prematurely born babies' eyes. This disease is biphasic: first causing delayed retinal vascular growth, followed by hypoxia-induced pathological vessel growth (Chen and Smith, 2007). It may be mild with no visual defects, however it may also be aggressive with the formation of new vessels, possibly progressing to a retinal detachment. The Optomap has become increasingly popular with studies reporting its capability of capturing clinically useful images documenting retinal features known to define ROP (Patel et al., 2013), using the "flying baby" technique to facilitate image acquisition. Historically, Retcam has been the standard imaging modality for monitoring ROP. However, the comparison of Retcam and Optomap for their ability to capture high quality ROP images in ROP showed that Retcam takes significantly longer to capture an image and is particularly difficult to use in older babies due to the excessive head movements. They reported reduced distress response and found that Optomap could potentially help monitor ROP progression and document regression following treatment more reliably (Patel et al., 2013). Dai et al. evaluated the efficacy of wide field retinal imaging utilizing the Retcam 2 wide field digital camera for screening of ROP and found a sensitivity and specificity of 100% and 97.9% respectively when compared to the gold standard binocular indirect ophthalmoscopy in detection of treatment requiring cases. Their conclusion supported that wide field imaging of ROP infants is accurate, reliable and efficient in detecting treatment requirements. This could potentially improve cost, detection rate and accessibility of ROP care (Dai et al., 2011).

6.4. Retinitis pigmentosa

Retinitis pigmentosa refers to a diverse family of inherited eye disorders characterised by degeneration and dysfunction of rod and cone photoreceptors. Rod photoreceptors are more commonly affected than cones; thus retinitis pigmentosa often affects the peripheral retina first due to the high density of rod photoreceptors present there compared to cones (Hamel, 2006). Most subtypes of retinitis pigmentosa are characterised by pigment deposits (bone spicule pigmentation) initially in the peripheral retina (Hamel, 2006). There is limited data in the literature regarding the use of UWFI in retinitis pigmentosa. In 2013 Kaufman et al. used the Optomap UWFI and UWFA to report the presence of vascular leakage in the peripheral retina of 15 of 25 patients, suggesting not only vascular dysfunction but also an inflammatory component may play a role in the pathogenesis of this disease (Kaufman et al., 2013). In 2016 a study used UWFA on a patient with retinitis pigmentosa and intermediate uveitis. They picked up peripheral preretinal exudates, clinical features of retinitis pigmentosa, disc leakage and cystoid macular oedema identifying both pathologies in a single investigation using UWFI (Tripathy et al., 2016). This further stresses the advantages of using UWFI techniques for its ability to simultaneously capture pathology in the central and peripheral retina.

6.5. Uveitis

Patients with uveitis can be challenging to image and manage and accurate diagnosis of peripheral affection can be vital for diagnosis and management. In the peripheral retina uveitis is characterised by vascular leakage, non-perfusion and neovascularisation to name a few (Hamel, 2006). The use of UWFA allowed for more complete evaluation of patients with uveitis showing more excessive disease activity than apparent from fundus examination, leading to more aggressive and potentially more efficacious treatment (Kitchens et al., 2009). Campbell et al. investigated whether the use of UWFI influenced the management of disease in patients with non-infectious posterior uveitis. Management of disease in clinical judgement alone as well as both clinical judgement and FAF traditional fundus imaging led to an alteration of management for a total of 17 patients out of 43. However, with the addition of UWFI analysis, treatment was modified in those 17 patients as well as an extra 14 patients out of the 43. This led to a 33% increase in treatment modification even in such a small study sample. The study concluded the use of UWFI can aid in management of non-infectious posterior uveitis; however, further studies are required to determine if these findings would improve patient outcomes (Campbell et al., 2012).

6.6. Pathological myopia

Myopia is of significant global public health concern due to its increasing prevalence and earlier age-of-onset (Leo and Young, 2011). In western populations, the prevalence of myopia is low in children compared to the significantly higher prevalence rates in Asian populations where a prevalence of 6% in 6 year olds rising to a staggering 70% by the age of 15 has been reported (Kaneko et al., 2014; Leo and Young, 2011). Pathological myopia causes several characteristic changes including an increased axial length of the eye and peripheral retinal thinning. Retinal lesions associated with pathological myopia include: myopic choroidal neovascularisation (Avila et al., 1984), myopic maculopathy, myopic optic neuropathy and myopic chorioretinal atrophy; these have all been detected already using traditional imaging techniques (Kaneko et al., 2014). A relatively small study of highly myopic eyes examined the retinal vasculature using UWFI and found numerous abnormalities of the retinal vasculature in the far periphery such as retinal capillary telangiectasia and retinal capillary microaneurysms. None of the eyes analysed developed retinal neovascularisation. Further research is required to examine if peripheral changes occur before posterior changes as this could lead to quicker diagnosis, prognosis and treatment of pathological myopia (Kaneko et al., 2014).

6.7. Cytomegalovirus retinitis

Cytomegalovirus (CMV) retinitis is a retinal inflammation that can ultimately lead to blindness. It is primarily seen in patients whose immune system is compromised. Lesions associated with CMV may appear in the central and peripheral retina, these include: white granular zones of retinal necrosis, associated haemorrhages and low-grade iritis and vitritis (Heinemann, 1992). A relatively small study compared Optomap imaging with standard fundus imaging in CMV retinitis patients and found that 48.3% more retinal area and 40% more retinitis were captured and found with UWFI. In two cases the standard fundus photography missed peripheral CMV lesions, this could have had disastrous consequences for the eye and the patient and so they concluded that Optomap imaging CMV patients is of benefit (Mudvari et al., 2010).

6.8. Ocular markers of disease in the peripheral retina

Due to the ease of examination and the possibilities in imaging the eye, it is sometimes referred to as the "window to the soul"(Foster and Khaw, 2009). The ability to non-invasively image both the retinal vasculature and neural layers provides the opportunity to develop early markers of systemic diseases. Such markers have been extensively studied for systemic diseases such as cardiovascular disease and diabetes, while OCT imaging led to interest in markers of neurological diseases such as multiple sclerosis and Alzheimer's disease (AD). As UWFI technology developed, markers in the retinal periphery are also being sought and comparisons between presentation in the macular and periphery undertaken. For some conditions, the initial assumption that evaluation in the macula is sufficient is gradually being undermined as data accumulate from wide-field imaging from a variety of systemic disorders.

6.8.1. Diabetes mellitus

It is understood that the worldwide prevalence of diabetes mellitus

(DM) was approximately 366 million in 2011, predicted to rise to 552 million people by 2030 (Whiting et al., 2011). DM is one of the leading systemic diseases affecting people's vision. A variety of ocular diseases is associated directly with DM; DR, Diabetic Macular Oedema (DMO), cataracts, anterior ischemic optic neuropathy (AION), diabetic papillopathy and ocular movement disorders (Jeganathan et al., 2008). Of these, DR is the most commonly diagnosed ocular complication and is the leading cause of legal blindness in working age adults around the world, but not in parts of the UK anymore (Liew et al., 2014). Previously, the bulk of DR research concentrated on retinal vascular changes such as microaneurysms, vascular abnormality and increased vascular permeability, however more recently degenerative changes are being recognised as well (Barber, 2003). Our detailed and systematic understanding of features of DR started in 1968, when the Airlie House Symposium evaluated knowledge and understanding of DR. The main outcome of this meeting was a standardized DR classification (Goldberg and Jampol, 1987). Over the years, DR classification underwent changes, such as in 2003, when Wilkinson et al. produced a more simplified classification system (Wilkinson et al., 2003): 1) No apparent retinopathy; 2) Mild non-proliferative DR; 3) Moderate non-proliferative DR; 4) Severe non-proliferative DR; 5) Proliferative DR.

Recently several research studies concentrated on UWFA and its reliability in DR evaluation compared to traditional techniques. UWFA produces a wider view and has been shown to have better reproducibility than standard FA methods for classifying DR (Friberg et al., 2008). Wessel et al. compared UWFA (Optomap Panoramic 200A) and conventional 7SF angiography and found that Optomap captured more non-perfusion, neovascularisation and panretinal photocoagulation than 7SF imaging (Wessel et al., 2012b). These findings were largely replicated by UPMC Eye Centre, Pittsburgh, showing that retinal ischemia was better detected using Optomap (Friberg et al., 2008), confirming that Optomap captured and revealed significantly more pathology in the diabetic eye than the conventional 7SF imaging.

In 2015, three studies evaluated the effect different imaging modalities have on detecting DR related retinal abnormalities. Talks et al. (2015) examined identifications of retinal new vessels comparing the use of the Optomap, the UK's DR screening two field imaging and 7SF photography and showed that 30% more new vessels were detected on Optomap than on 7SF imaging (Talks et al., 2015). Price et al. found substantial agreement (0.8) between the severity of DR based on Optomap and 7SF but noted that a minority of patients were diagnosed with more severe DR using Optomap. (Price et al., 2015). Manjunath et al. compared OCT and Optomap imaging to clinical examination of DR on a large sample of 2040 eyes and showed that UWFI was more sensitive when compared to clinical examination. They recommended that using both UWFI and OCT deciding on DR severity would lead to enhanced quality of assessment (Manjunath et al., 2015).

Kong et al. carried out a pilot study for evaluating DR by the use of UWFA. UWFI were obtained from 59 patients with diabetes (118 eyes); 11 eyes with no DR, 71 eyes with non-proliferative DR (NPDR) and 36 with proliferative DR (PDR). Findings showed that on UWFI microaneurysms were seen in more than half (54.5%) of those patients with no apparent DR on conventional imaging; with this percentage progressively increasing with NPDR (84.2%) and PDR (100%) patients. In NPDR and PDR patients new vessels in the periphery and ischemia were detected using the Optomap FA (Kong et al., 2012). This group concluded UWFA had significant advantages in detecting and evaluating peripheral retinal lesions due to its wider field of view and this was found to be especially advantageous in cases where detectable pathology was seen on the periphery before any pathology was seen on the posterior pole.

The relationship between peripheral retinal ischemia and the presence of diabetic macular oedema (DMO) is a topic currently being investigated by several studies. Wessel found that on UWFA, out of the 122 treatment-naïve eyes of 70 subjects with DMO, 66 eyes (62%) displayed areas of retinal peripheral ischemia, ($p < 0.001$). These findings suggested that UWFI may provide useful information in assessing peripheral retinal changes associated with DMO (Wessel et al., 2012b). In analysis of subjects in the Efficacy and Safety Trial of Intravitreal Injections Combined with Panretinal Photocoagulation for Clinically Significant Macular Oedema Secondary to Diabetes Mellitus (DAVE) clinical trial, Fan and colleagues observed that the severity of ischemia in eyes with DMO appeared to increase with increasing distance from the fovea (Fan et al., 2017). Non-perfusion in the mid-periphery, but not in other regions, was associated with severity of DMO.

A target pattern scan laser (Pascal) retinal photocoagulation (TRP) was designed to treat areas of retinal capillary non-perfusion and intermediate retinal ischemia regions in PDR. UWFI was used to detect areas of peripheral retinal ischemia and neovascularisation in order to guide TRP laser to the four quadrants of the retina. The researchers found that UWFI-guided laser treatment was a promising procedure for treatment of PDR as it destroyed less normal retinal tissue than traditional methods yet obtained favourable disease regression rates at 3–6 months (Muqit et al., 2013).

In 2013 Silva et al. assessed DR lesions identified by UWFI and compared these to ETDRS 7SF. The lesions identified included haemorrhages and/or microaneurysms, venous beading, intraretinal microvascular abnormality and new vessels elsewhere. UWFI demonstrated substantial agreement with ETDRS film photographs in determining DR severity. Additional lesions identified by UWFI suggested a more severe assessment of DR in 10% of eyes than suggested by lesions found within the ETDRS view (Silva et al., 2013). However, the implications of peripheral lesions on DR are unknown and further studies will need to be carried out to evaluate this. More recently, Silva et al. (2015) reported that the presence and increasing extent of peripheral lesions were associated with increased risk of DR progression over 4 years, suggesting that detailed peripheral retinal evaluation provides important information necessary to assess risk of DR progression (Silva et al., 2015). Currently, there are studies ongoing to test the clinical significance of peripheral DR lesions in relation to the development, diagnosis, progression and choice of DR treatment modalities. Once these studies report their results, a re-classification of DR might be required in order to incorporate the peripheral lesion in the clinical pathway.

Most studies exploring visual loss in DR focused on visual acuity; however, numerous studies using perimetry showed DR's detrimental effects on peripheral visual function and field (Duh et al., 2017; Nentwich and Ulbig, 2015; Shrestha and Kaiti, 2014). Importantly, these studies noted that using perimetry for tracking peripheral visual function captures early diabetes related pathologies better than traditional fundoscopy or visual acuity testing (Greite et al., 1981; Guy, 2012; Henricsson and Heijl, 1994; Jackson and Gardner, 2014).

A perimetry study dating back to the 1980s illustrated deficits in peripheral visual functioning before central visual changes could be noted in DR patients. Such visual impairments include visual dysfunction in dim light and difficulty in recognizing contour of objects in low contrast conditions even when visual acuity is unaffected (Hyvarinen et al., 1983). However, most research emphasizes central acuity loss over peripheral visual field monitoring due to DMO related visual loss' immediate impact on social functioning. (Duh et al., 2017; Lee et al., 2015). Early perimetry studies illustrated that these peripheral field deficits and smaller isopter areas could be observed even in DR patients where neovascularisation, haemorrhage, or microaneurysm weren't observed (Wisznia et al., 1971).

Recent studies utilizing automated perimetry support these early findings; additional studies have also shown a decreased ability in diabetics with DR to recognize objects with low spatial frequency in the periphery, similar to studies performed on AD and AMD referenced in this review. These effects were seen in patients with type 2 diabetes who were diagnosed for ten years or less and before any vasculopathies could be visualized in the peripheral retina by imaging (Bell et al., 2010). In agreement, a study from 2008 found that an automated

Humphrey Perimetry program found reduced peripheral visual functioning in those with type 1 diabetes before vascular changes were noted in both peripheral and central retina. It should be noted though that this study only studied as far out to 30 degrees of visual functioning (Parravano et al., 2008).

A 2013 study on patients with type 1 diabetes illustrated that peripheral visual dysfunction could be seen in the early stages of DR before images could capture vascular changes. Disease onset was so early in patients with diabetes that deficits in perimetric testing of the peripheral visual fields weren't significant; however, those with diabetes showed poorer performance and significantly higher variability in total performance. Even without visualization of peripheral retinal pathologies, perimetry is still highly sensitive at detecting the onset and progression of DR (Isabel Pinilla et al., 2013).

Recently, perimetric studies sought to correlate these peripheral visual deficits with the onset of retinal pathologies. Some claimed that deficits noted on perimetric monitoring of vision might predict future vasculopathies, but lately it seems that visual peripheral deficits are associated with areas of lowered autofluorescence, outside the macula of course (which is protected by an accumulation of luteal pigments). One 2011 study was able to correlate visual deficits, as tracked by Humphrey perimetry, with areas of lowered FAF in DR patients. Although the AF images were taken by traditional fundoscopy (at 40°), they were visualized outside the macula. The study showed that while no vasculopathies or lesions could be visualized in these areas, the visual dysfunction corresponded to areas of lowered AF, presuming these areas were vulnerable to ischemia or retinal cell dysfunction (Midena and Vujosevic, 2011).

Many of these studies suggest that the visual deficits perceived in the setting of early DR are due to vascular insufficiency and that these can be imaged early if the correct imaging methods are used. However, if we were better able to screen for onset and subsequently determine the progression of DR, it might aid us in treating the disease early and maintaining visual function for longer in patients with diabetes.

6.8.2. Alzheimer's disease and cognitive decline

50 million people living with dementia worldwide and this number will be 152 by 2050 (Alzheimer's Disease International, 2018). AD is the most common type of senile dementia in aging adults amounting to 10% of people aged 65 or over being affected. AD affects 24.3 million individuals worldwide, with around 4.6 million new cases reported each year (Reitz and Mayeux, 2014). AD clinically manifests by progressive loss of memory, changes in behaviour, mood and thinking processes (McKhann et al., 1984). Diagnosing AD is based on clinical presentation and therefore is difficult in any given patient. Definite diagnosis can only be made pathologically by examination of the brain tissue at autopsy (Braak and Braak, 1997). In the early stages of disease assessments relies on psychological assessments and costly and highly invasive clinical tests (Neugroschl and Wang, 2011). Therefore, there is a need to find biomarkers that is objective, could be used repeatedly, could be used for early detection and monitoring progression and a procedure that patients are comfortable with and can comply with it easily even at a more advanced stage of disease.

The retina is part of the central nervous system; it shares embryological origin and anatomical characteristics with the brain (Byerly and Blackshaw, 2009; Risau, 1997). As such, it has been proposed that changes in the retina may reflect changes in the brain and provide accessible biomarkers for AD (Colligris et al., 2018; Dehghani et al., 2018; Frost, 2010; Ikram et al., 2012; Liao et al., 2018; Lim et al., 2016). In general, imaging of the retina is non-invasive, well tolerated and readily repeatable in follow up studies. Using OCT/OCTA in AD, several studies report thinning of RNFL, macular volume loss and altered retinal vasculature, implying that similar changes take place in the retina than in the brain (Coppola et al., 2015; Cunha et al., 2016; den Haan et al., 2018; den Haan et al., 2017; Doustar et al., 2017; O'Bryhim et al., 2018; Wang et al., 2018). Quantitative and qualitative changes in retinal microvasculature using conventional fundus photographs showed an association between cognitive decline/AD and retinal vascular characteristics (McGrory et al., 2017). Further studies suggested that there is increased arterial reaction time in people with AD (Mroczkowska et al., 2015) and there is an overall increase in vessel calibres when peripapillary B-scans are evaluated (Csincsik et al., 2016). However, all these measurements were carried out on the posterior pole of the eye without consideration for the peripheral retina.

Based on observations on flat mounted retinas of cadaveric eyes (Lengyel et al., 2004; Ukalovic et al., 2018) it was proposed that monitoring the development and progression of pathology in the peripheral regions might serve as a valuable tool in detecting and monitoring the progression in age-related diseases such as AMD and AD. It has been shown that UWFI is comparable to normal fundus imaging (Csutak et al., 2010) and can detect pathological abnormalities at the peripheral retina (Csincsik et al., 2018; Lengyel et al., 2015). Recent pilot study revealed an association between AD and peripheral hard drusen formation and changes to the vasculature beyond the posterior pole using UWFI (Csincsik et al., 2018). Similar results were found in an independent study that showed patient with moderate AD has higher burden of peripheral retinal deposits compared to aged matched controls or mild cognitive impairment (MCI) (Whitson et al., 2016). Retinal amyloid deposits also been detected in mid-peripheral region of the retina using modified ophthalmoscope after oral administration of curcumin (Koronyo et al., 2017). Based on these findings, it is feasible to speculate that imaging not only the central but the peripheral retina too has potentials to be used as biomarkers for progression of disease. To test the validity of retinal imaging as biomarkers several ongoing dementia studies include retinal imaging components. These will examine drusen deposition, vascular and RPE changes and look for additional pathological changes in the eye that may not have been identified before, especially at the peripheral regions.

Retinal functional changes also have been reported in AD. Studies have shown that AD patients have difficulty processing and recognizing environmental scenes, especially those with low spatial frequency or a lack of details. It is worth noting, however, that visual acuity and colour recognition in AD is generally comparable to age-matched controls (Lee et al., 2015; Wood et al., 1997). This suggests a preservation of aspects associated with central vision in AD. Other studies correlated AD with an increased incidence of traffic accidents and implicated deficits in peripheral visual functioning over the degree of cognitive impairment in the occurrence of these accidents. Motion processing, contrast sensitivity, and depth perception, attributes associated with the peripheral vision, have also been shown to be poor in AD patients (Lakshminarayanan et al., 1996; Mendez et al., 1990; Neargarder et al., 2003; Schlotterer et al., 1984).

The observed effects of AD above focus on a characteristic of vision itself because these studies are neurological and approach the visual loss as a result of cortical dysfunction. However, very few studies sought to localize or quantify a loss in the visual field of AD patients. In the 1980s (Nissen et al., 1985), there were a few case studies where Goldmann Perimetry showed dramatic inferior hemifield losses in AD patients. These results were echoed in a 1995 Humphrey Perimetry study which again found inferotemporal and inferonasal losses prevalent in AD patients (Ceccaldi, 1996; Trick et al., 1995). These studies, though sparse, both agreed that the peripheral inferior visual field was greatly upset in the onset and progression of AD (Ceccaldi, 1996; Nissen et al., 1985; Trick et al., 1995).

A 1996 study tried to correlate these perimetric findings in AD patients by looking at the visual cortices. By measuring the thickness of the cuneal and lingual cortex in AD patients, the study hoped to illustrate the pathway of visual loss through cortical atrophy. The study found thinning of the lingual over the cuneal, vice versa, and equal thinning in its AD patients but did not find a direct relationship or a direct trend (Armstrong, 1996). The presence of cortical thinning in AD patients was not as surprising as the fact that this study could not point

to a definite trend in the visual association cortices despite such similar attributes observed in peripheral visual functioning in AD. Why AD is associated with the inferonasal and inferotemporal hemifield losses in perimetry? Why is AD associated with attributes of peripheral visual function over central visual function?

Very little new research has been carried out since then in quantifying or localizing peripheral visual loss. In contrast, our understanding of retinal nerve ganglion health increased (Berisha et al., 2007; Liu et al., 2015; Marziani et al., 2013). In 2013, frequency-doubling technology (FDT), a form of perimetry that studies flicker sensitivity (an attribute of the retinal nerve ganglion cells) found that AD patients had poor results in their inferior visual fields and concluded that the retinal nerve ganglion cells of the superior retina must be pathologic or must endure the greatest insult in AD. These results might suggest the aetiology of the peripheral visual function and observed visual field losses could directly be due to insult in the retina (Valenti, 2013).

One last attribute to discuss about AD is the presence of hallucinations (Chapman et al., 1999). Two different commonly reported findings in AD that are of interest to the peripheral vision are “illusions” and “misperceptions.” Illusions involve a patient not being able to distinguish between two objects in their environment. Another type is called “misperception,” and this emerges when a subject does not recognize something and makes a best guess as to what it could be. Most research understands and views these illusions and misperceptions as a manifestation of damage to the visual cycle occurring in the brain. It is worth noting that similar delusions are seen in AMD and correlated to the degree of vision loss in the central retina. This phenomenon is called Charles Bonnet Syndrome (CBS), and it is understood as a manifestation of how the brain copes with vision loss, especially in AMD patients (Berrios and Brook, 1982). CBS also occurs in patients with cataract, glaucoma, and DR. Some studies suggest that up to 60% of people who have dramatic sight loss experience it (RNIB, 2016). It could be perhaps that hallucinations seen with AD have a similar source to those experienced in patients with other retinal pathologies. These documented visual disturbances in AD indicate that more understanding into the relationship between peripheral vision and the progression of AD is necessary.

7. Future directions & conclusions

In summary, it is evident that the peripheral retina has great importance for the prognosis and overall outcome of systemic diseases affecting large number of patients. The significance of the appropriate imaging and analysis of the peripheral retina is being shown in this review by depicting the various imaging and investigative techniques clinicians and researcher now have at their disposal. Currently ophthalmic imaging is undergoing a major revolution due to the availability and utilization of technologies from other discipline. Combining these technological advances with a more complete understanding of retinal morphology, better molecular understanding of diseases led to an increased need for examining the peripheral retina in clinical setting. The need for continued research for the use of UWFI has been highlighted by the successes of new studies on diabetic retinopathy. Once the results of the ongoing studies are fully understood and implemented in clinical practice, these should result in more complete evaluation, earlier diagnosis, better prognostication and more appropriate care of patients. Implementation of UWFI systems into clinical practice will have to be balanced against with increased costs of such systems, though as is the case for most technologies, one might anticipate that costs will come down with time. Consensus on imaging and grading protocols will be needed for easier comparison of different studies. Ultimately, clinically relevant methods to test functional changes associated with UWFI abnormalities will be required; these will need to fuel wider societal changes leading to better environmental and town planning taking into account the changes in peripheral vision.

Competing financial interest of the authors

SriniVas R. Sadda is a consultant for Optos, Carl Zeiss Meditec, Centervue, Heidelberg Engineering, Allergan, Roche, Novartis, Iconic, Thrombogenics and receives research support from Optos, Carl Zeiss Meditec, Allergan, Genentech. Christine Curcio receives research support from Heidelberg Engineering and Hoffman LaRoche. Imre Lengyel receives unrestricted research support from Optos Plc. Tunde Peto is a consultant for Optos Plc, Bayer, Novartis and received unrestricted grant from Allergan and Alimera. Szilard Kiss has served on the speaker's bureau of Optos, PLC and a consultant for Allergan. Other authors do not have any competing financial interest.

Acknowledgements

The research was supported by the Bill Brown Charitable Trust, Moorfields Eye Hospital Special Trustees, Mercer Fund from Fight for Sight (I.L). Special thank for The Joint Library of Ophthalmology, Moorfields Eye Hospital & UCL Institute of Ophthalmology for the retinal drawings. Lajos Csincsik is supported by an unrestricted PhD studentship from Optos Plc. The work was part-supported by the EyeRisk project funded from the European Union’s Horizon 2020 research and innovation programme under grant agreement No 634479 (I.L and T.P).

Appendix A. Supplementary data

Supplementary data to this article can be found online at https://doi.org/10.1016/j.preteyeres.2018.10.001.

References

Ablonczy, Z., Higbee, D., Anderson, D.M., Dahrouj, M., Grey, A.C., Gutierrez, D., Koutalos, Y., Schey, K.L., Hanneken, A., Crouch, R.K., 2013. Lack of correlation between the spatial distribution of A2E and lipofuscin fluorescence in the human retinal pigment EpitheliumLocalization of A2E in the human RPE. Investig. Ophthalmol. Vis. Sci. 54, 5535–5542.

Ach, T., Huisingh, C., McGwin, G., Messinger, J.D., Zhang, T., Bentley, M.J., Gutierrez, D.B., Ablonczy, Z., Smith, R.T., Sloan, K.R., Curcio, C.A., 2014. Quantitative autofluorescence and cell density maps of the human retinal pigment epithelium. Investig. Ophthalmol. Vis. Sci. 55, 4832–4841.

Adler, L.t., Boyer, N.P., Anderson, D.M., Spraggins, J.M., Schey, K.L., Hanneken, A., Ablonczy, Z., Crouch, R.K., Koutalos, Y., 2015. Determination of N-retinylidene-N-retinylethanolamine (A2E) levels in central and peripheral areas of human retinal pigment epithelium. Photochem. Photobiol. Sci.: Off. J. Eur. Photochem. Assoc. Eur. Soc. Photobiol. 14, 1983–1990.

Agarwal, A., Fan, S., Invernizzi, A., Do, D.V., Nguyen, Q.D., Harms, N.V., Sepah, Y.J., 2015. Characterization of retinal structure and diagnosis of peripheral acquired retinoschisis using high-resolution ultrasound B-scan. Graefe’s Arch. Clin. Exp. Ophthalmol. 1–7.

Age-Related Eye Disease Study 2 Research Group, 2013. Lutein + zeaxanthin and omega-3 fatty acids for age-related macular degeneration: the Age-Related Eye Disease Study 2 (AREDS2) randomized clinical trial. Jama 309, 2005–2015.

Agrawal, A., Biswas, J., 2011. Unilateral vogt-koyanagi-harada disease: report of two cases. Middle East Afr. J. Ophthalmol. 18, 82–84.

AIDS Clinical Trials Group, 1992. Studies of ocular complications of AIDS foscarnet-ganciclovir cytomegalovirus retinitis trial: 1. Rationale, design, and methods. AIDS clinical trials group (ACTG). Contr. Clin. Trials 13, 22–39.

Al-Hussaini, H., Kilarkaje, N., Shahabi, G., Al-Mulla, F., 2016. Proliferation and migration of peripheral retinal pigment epithelial cells are associated with the upregulation of wingless-related integration and bone morphogenetic protein signaling in dark Agouti rats. Med. Princ. Pract.: Int. J. Kuwait Univ. Health Science Centre 25, 408–416.

Alzheimer's Disease International, 2018. The State of the Art of Dementia Research: New Frontiers. World Alzheimer Report 2018.

Ament, C.S., Zacks, D.N., Lane, A.M., Krzystolik, M., D'Amico, D.J., Mukai, S., Young, L.H., Loewenstein, J., Arroyo, J., Miller, J.W., 2006. Predictors of visual outcome and choroidal neovascular membrane formation after traumatic choroidal rupture. Arch. Ophthalmol. 124, 957–966.

Anderson, D.M.G., Ablonczy, Z., Koutalos, Y., Hanneken, A.M., Spraggins, J.M., Calcutt, M.W., Crouch, R.K., Caprioli, R.M., Schey, K.L., 2017. Bis(monoacylglycero)phosphate lipids in the retinal pigment epithelium implicate lysosomal/endosomal dysfunction in a model of Stargardt disease and human retinas. Sci. Rep. 7, 17352.

Anderson, D.M.G., Ablonczy, Z., Koutalos, Y., Spraggins, J., Crouch, R.K., Caprioli, R.M., Schey, K.L., 2014. High resolution MALDI imaging mass spectrometry of retinal tissue lipids. J. Am. Soc. Mass Spectrom. 25, 1394–1403.

Appold, K., 2017. New product applications: widening the imaging field. Retin. Physician 14 (59), 61.
Arepalli, S., Kaliki, S., Shields, C.L., 2015. Choroidal metastases: origin, features, and therapy. Indian J. Ophthalmol. 63, 122–127.
Armstrong, J.D., Meyer, D., Xu, S., Elfervig, J.L., 1998. Long-term follow-up of stargardt's disease and fundus flavimaculatus1. Ophthalmology 105, 448–457.
Armstrong, R.A., 1996. Visual field defects in Alzheimer's disease patients may reflect differential pathology in the primary visual cortex. Optom. Vis. Sci. 73, 677–682.
Aslam, A., Peto, T., Barzegar-Befroei, N., Gregory, S., Morrison, G., Ritchie, C., Lengyel, I., 2014. Assessing peripheral retinal drusen progression in Alzheimer's dementia: a pilot study using ultra-wide field imaging. Investig. Ophthalmol. Vis. Sci. 55 659-659.
Avila, M.P., Weiter, J.J., Jalkh, A.E., Trempe, C.L., Pruett, R.C., Schepens, C.L., 1984. Natural history of choroidal neovascularization in degenerative myopia. Ophthalmology 91, 1573–1581.
Boycott, B.B., Dowling, J.E., 1969. Organization of the primate retina: light microscopy, with an appendix: a second type of midget bipolar cell in the primate retina. Philos. Trans. R. Soc. Lond. Ser. B Biol. Sci. 255, 109–184.
Barber, A.J., 2003. A new view of diabetic retinopathy: a neurodegenerative disease of the eye. Prog. Neuro-Psychopharmacol. Biol. Psychiat. 27, 283–290.
Barnard, S., Shneor, E., Brauner, J., Millodot, M., Gordon-Shaag, A., 2012. Bilateral chorioretinal coloboma discovered with ultra-wide field retinal imaging. J. optometry 5, 150–154.
Bartlett, H., Howells, O., Eperjesi, F., 2010. The role of macular pigment assessment in clinical practice: a review. Clin. Exp. Optom. 93, 300–308.
Bass, S.J., Sherman, J., Giovinazzo, V., 2011. Bilateral Coats' response in a female patient leads to diagnosis of facioscapulohumeral muscular dystrophy. Optometry. J. Am. Optom. Assoc. 82, 72–76.
Bastek, J.V., Siegel, E.B., Straatsma, B.R., Foos, R.Y., 1982. Chorioretinal juncture: pigmentary patterns of the peripheral fundus. Ophthalmology 89, 1455–1463.
Bell, A., James, A.C., Kolic, M., Essex, R.W., Maddess, T., 2010. Dichoptic multifocal pupillography reveals afferent visual field defects in early type 2 diabetes. Investig. Ophthalmol. Vis. Sci. 51, 602–608.
Berisha, F., Feke, G.T., Trempe, C.L., McMeel, J.W., Schepens, C.L., 2007. Retinal abnormalities in early Alzheimer's disease. Investig. Ophthalmol. Vis. Sci. 48, 2285–2289.
Bernstein, P.S., Delori, F.C., Richer, S., van Kuijk, F.J.M., Wenzel, A.J., 2010. The value of measurement of macular carotenoid pigment optical densities and distributions in age-related macular degeneration and other retinal disorders. Mechanisms in Macular Degeneration 50, 716–728.
Bernstein, P.S., Li, B., Vachali, P.P., Gorusupudi, A., Shyam, R., Henriksen, B.S., Nolan, J.M., 2016. Lutein, zeaxanthin, and meso-zeaxanthin: the basic and clinical science underlying carotenoid-based nutritional interventions against ocular disease. Prog. Retin. Eye Res. 50, 34–66.
Berrios, G.E., Brook, P., 1982. The Charles Bonnet syndrome and the problem of visual perceptual disorders in the elderly. Age Ageing 11, 17–23.
Bhosale, P., Serban, B., Bernstein, P.S., 2009. Retinal carotenoids can attenuate formation of A2E in the retinal pigment epithelium. Arch. Biochem. Biophys. 483, 175–181.
Black, A.A., Wood, J.M., Lovie-Kitchin, J.E., Newman, B.M., 2008. Visual impairment and postural sway among older adults with glaucoma. Optom. Vis. Sci. 85, 489–497.
Black, G.C.M., Perveen, R., Bonshek, R., Cahill, M., Clayton-Smith, J., Christopher Lloyd, I., McLeod, D., 1999. Coats' disease of the retina (unilateral retinal telangiectasis) caused by somatic mutation in the NDP gene: a role for Norrin in retinal angiogenesis. Hum. Mol. Genet. 8, 2031–2035.
Bone, R.A., Landrum, J.T., Mayne, S.T., Gomez, C.M., Tibor, S.E., Twaroska, E.E., 2001. Macular pigment in donor eyes with and without AMD: a case-control study. Investig. Ophthalmol. Vis. Sci. 42, 235–240.
Bonnay, G., Nguyen, F., Meunier, I., Ducasse, A., Hamel, C., Arndt, C., 2011. Screening for retinal detachment using wide-field retinal imaging. J. Fr. Ophtalmol. 34, 482–485.
Booij, J.C., Baas, D.C., Beisekeeva, J., Gorgels, T.G., Bergen, A.A., 2010. The dynamic nature of Bruch's membrane. Prog. Retin. Eye Res. 29, 1–18.
Boulton, M., Dayhaw-Barker, P., 2001. The role of the retinal pigment epithelium: topographical variation and ageing changes. Eye 15, 384–389 (London, England).
Bowling, B., 2015a. Choroidal Melanoma, Kanski's Clinical Ophthalmology: a Systematic Approach, eighth ed. Elsevier, pp. 487–492.
Bowling, B., 2015b. Diabetic Retinopathy, Kanski's Clinical Ophtalmology: a Systematic Approach, eighth ed. Elsevier, pp. 520–526.
Bowling, B., 2015c. Innocuous Peripheral Retinal Degenerations, Kanski's Clinical Ophthalmology: a Systematic Approach, eighth ed. Elsevier, pp. 682–684.
Bowling, B., 2015d. Neural Retinal Tumours: Retinoblastoma, Kanski's Clinical Ophthalmology: a Systematic Approach, eighth ed. Elsevier, pp. 497–504.
Bowling, B., 2015e. Peripheral Lesions Predisposing to Retinal Detachment, Kanski's Clinical Ophthalmology: a Systematic Approach, eighth ed. Elsevier, pp. 689–690.
Bowling, B., 2015f. Retinal Detachment, eighth ed. Elsevier, pp. 701–713.
Braak, H., Braak, E., 1997. Frequency of stages of Alzheimer-related lesions in different age categories. Neurobiol. Aging 18, 351–357.
Bringmann, A., Syrbe, S., Gorner, K., Kacza, J., Francke, M., Wiedemann, P., Reichenbach, A., 2018. The primate fovea: structure, function and development. Prog. Retin. Eye Res. 66, 49–84.
Brown, K., Sewell, J.M., Trempe, C., Peto, T., Travison, T.G., 2013. Comparison of image-assisted versus traditional fundus examination. Eye Brain 5, 1–8.
Burris, C., Klug, K., Ngo, I.T., Sterling, P., Schein, S., 2002. How Muller glial cells in macaque fovea coat and isolate the synaptic terminals of cone photoreceptors. J. Comp. Neurol. 453, 100–111.
Byerly, M.S., Blackshaw, S., 2009. Vertebrate Retina and Hypothalamus Development, vol. 1. Wiley interdisciplinary reviews. Systems biology and medicine, pp. 380–389.
Cai, H., Fields, M.A., Hoshino, R., Del Priore, L.V., 2012. Effects of aging and anatomic location on gene expression in human retina. Front. Aging Neurosci. 4.
Calkins, D.J., Schein, S.J., Tsukamoto, Y., Sterling, P., 1994. M and L cones in macaque fovea connect to midget ganglion cells by different numbers of excitatory synapses. Nature 371, 70–72.
Campbell, J.P., Leder, H.A., Sepah, Y.J., Gan, T., Dunn, J.P., Hatef, E., Cho, B., Ibrahim, M., Bittencourt, M., Channa, R., Do, D.V., Nguyen, Q.D., 2012. Wide-field retinal imaging in the management of noninfectious posterior uveitis. Am. J. Ophthalmol. 154, 908–911 e902.
Casteels, I., Cassiman, C., Van Calster, J., Allegaert, K., 2012. Educational paper: retinopathy of prematurity. Eur. J. Pediatr. 171, 887–893.
Ceccaldi, M., 1996. La vision dans la maladie d'Alzheimer. Rev. Neurol. 152, 441–446.
Chapman, F.M., Dickinson, J., McKeith, I., Ballard, C., 1999. Association among visual hallucinations, visual acuity, and specific eye pathologies in Alzheimer's disease: treatment implications. Am. J. Psychiatry 156, 1983–1985.
Chen, J., Smith, L.E.H., 2007. Retinopathy of prematurity. Angiogenesis 10, 133–140.
Cho, M., Aaker, G., D'Amico, D.J., Kiss, S., 2011. Peripheral vascular abnormalities in β-thalassemia major detected by ultra wide-field fundus imaging. Retin. Cases Brief Rep. 5, 339–342.
Choudhry, N., Golding, J., Manry, M.W., Rao, R.C., 2016. Ultra-widefield steering-based spectral-domain optical coherence tomography imaging of the retinal periphery. Ophthalmology 123, 1368–1374.
Christine, A., Curcio, M.J., 2012. Structure, Function, and Pathology of Bruch's Membrane, vol. 1. Elsevier Inc, pp. 465–481.
Chun, M.H., Grünert, U., Martin, P.R., Wässle, H., 1996. The synaptic complex of cones in the fovea and in the periphery of the macaque monkey retina. Vis. Res. 36, 3383–3395.
Coffee, R.E., Jain, A., McCannel, T.A., 2009. Ultra Wide-field Imaging of Choroidal Metastasis Secondary to Primary Breast Cancer, Seminars in Ophthalmology, 1 ed. Informa UK Ltd UK, pp. 34–36.
Colligris, P., Perez de Lara, M.J., Colligris, B., Pintor, J., 2018. Ocular manifestations of Alzheimer's and other neurodegenerative diseases: the prospect of the eye as a tool for the early diagnosis of Alzheimer's disease. J. Ophthalmol. 2018, 12.
Coppola, G., Di Renzo, A., Ziccardi, L., Martelli, F., Fadda, A., Manni, G., Barboni, P., Pierelli, F., Sadun, A.A., Parisi, V., 2015. Optical coherence tomography in Alzheimer's disease: a meta-analysis. PloS One 10, e0134750.
Croft, D.E., van Hemert, J., Wykoff, C.C., Clifton, D., Verhoek, M., Fleming, A., Brown, D.M., 2014. Precise montaging and metric quantification of retinal surface area from ultra-widefield fundus photography and fluorescein angiography. Ophthalmic Surg. Laser. Imag. 45, 312–317.
Csincsik, L., MacGillivray, T.J., Flynn, E., Pellegrini, E., Papanastasiou, G., Barzegar-Befroei, N., Csutak, A., Bird, A.C., Ritchie, C.W., Peto, T., Lengyel, I., 2018. Peripheral retinal imaging biomarkers for Alzheimer's disease: a pilot study. Ophthalmic Res. 59, 182–192.
Csincsik, L., Shakespeare, T., Quinn, N., Hogg, R.E., Crutch, S., Craigh, R., Peto, T., Lengyel, I., 2016. Retinal imaging in early and late Alzheimer's disease. Investig. Ophthalmol. Vis. Sci. 57 3373-3373.
Csutak, A., Lengyel, I., Jonasson, F., Leung, I., Geirsdottir, A., Xing, W., Peto, T., 2010. Agreement between image grading of conventional (45[deg]) and ultra wide-angle (200[deg]) digital images in the macula in the Reykjavik eye study. Eye 24, 1568–1575.
Cunha, L.P., Almeida, A.L.M., Costa-Cunha, L.V.F., Costa, C.F., Monteiro, M.L.R., 2016. The role of optical coherence tomography in Alzheimer's disease. Int. J. Retina and Vitreous 2, 24.
Curcio, C.A., 2018. Antecedents of soft drusen, the specific deposit of age-related macular degeneration, in the biology of human macula. Investig. Ophthalmol. Vis. Sci.
Curcio, C.A., Allen, K.A., 1990. Topography of ganglion cells in human retina. J. Comp. Neurol. 300, 5–25.
Curcio, C.A., Messinger, J.D., Sloan, K.R., McGwin, G., Medeiros, N.E., Spaide, R.F., 2013. Subretinal drusenoid deposits in non-neovascular age-related macular degeneration: morphology, prevalence, topography, and biogenesis model. Retina 33, 265–276 (Philadelphia, Pa.).
Curcio, C.A., Messinger, J.D., Sloan, K.R., Mitra, A., McGwin, G., Spaide, R.F., 2011. Human chorioretinal layer thicknesses measured in macula-wide, high-resolution histologic sections. Investig. Ophthalmol. Vis. Sci. 52, 3943–3954.
Curcio, C.A., Sloan, K.R., Kalina, R.E., Hendrickson, A.E., 1990. Human photoreceptor topography. J. Comp. Neurol. 292, 497–523.
Dacey, D.M., 1993. The mosaic of midget ganglion cells in the human retina. J. Neurosci. 13, 5334–5355.
Dacey, D.M., 2000. Parallel pathways for spectral coding in primate retina. Annu. Rev. Neurosci. 23, 743–775.
Dacey, D.M., Petersen, M.R., 1992. Dendritic field size and morphology of midget and parasol ganglion cells of the human retina. Proc. Natl. Acad. Sci. U. S. A. 89, 9666–9670.
Dai, S., Chow, K., Vincent, A., 2011. Efficacy of wide-field digital retinal imaging for retinopathy of prematurity screening. Clin. Exp. Ophthalmol. 39, 23–29.
Daruich, A., Matet, A., Dirani, A., Bousquet, E., Zhao, M., Farman, N., Jaisser, F., Behar-Cohen, F., 2015. Central serous chorioretinopathy: recent findings and new physiopathology hypothesis. Prog. Retin. Eye Res. 48, 82–118.
Dean, J.C., 2002. Management of marfan syndrome. Heart 88, 97–103.
Dehghani, C., Frost, S., Jayasena, R., L Masters, C., Kanagasingam, Y., 2018. Ocular Biomarkers of Alzheimer's Disease: the Role of Anterior Eye and Potential Future Directions.
Delori, F.C., Goger, D.G., Keilhauer, C., Salvetti, P., Staurenghi, G., 2006. Bimodal spatial distribution of macular pigment: evidence of a gender relationship. J Opt Soc Am A Opt Image Sci Vis 23, 521–538.
den Haan, J., Janssen, S.F., van de Kreeke, J.A., Scheltens, P., Verbraak, F.D., Bouwman,

F.H., 2018. Retinal thickness correlates with parietal cortical atrophy in early-onset Alzheimer's disease and controls. Alzheimer's Dementia 10, 49–55 (Amsterdam, Netherlands).
den Haan, J., Verbraak, F.D., Visser, P.J., Bouwman, F.H., 2017. Retinal thickness in Alzheimer's disease: a systematic review and meta-analysis. Alzheimer's Dementia: Diagnosis, Assessment & Disease Monitoring 6, 162–170.
Denniston, A.K.O., Murray, P.I., 2009. Oxford Handbook of Ophthalmology. Oxford University Press.
Desapriya, E., Harjee, R., Brubacher, J., Chan, H., Hewapathirane, D.S., Subzwari, S., Pike, I., 2014. Vision screening of older drivers for preventing road traffic injuries and fatalities. In: The Cochrane Database of Systematic Reviews, Cd006252.
Dhaliwal, C., Wright, E., Graham, C., McIntosh, N., Fleck, B.W., 2009. Wide-field digital retinal imaging versus binocular indirect ophthalmoscopy for retinopathy of prematurity screening: a two-observer prospective, randomised comparison. Br. J. Ophthalmol. 93, 355–359.
Dietzel, M., Zeimer, M., Heimes, B., Pauleikhoff, D., Hense, H.W., 2011. The ringlike structure of macular pigment in age-related maculopathy: results from the Muenster Aging and Retina Study (MARS). Investig. Ophthalmol. Vis. Sci. 52, 8016–8024.
Domalpally, A., Clemons, T.E., Danis, R.P., Sadda, S.R., Cukras, C.A., Toth, C.A., Friberg, T.R., Chew, E.Y., 2017. Peripheral retinal changes associated with age-related macular degeneration in the age-related eye disease study 2: age-related eye disease study 2 report number 12 by the age-related eye disease study 2 Optos PEripheral RetinA (OPERA) study research group. Ophthalmology 124, 479–487.
Doustar, J., Torbati, T., Black, K.L., Koronyo, Y., Koronyo-Hamaoui, M., 2017. Optical coherence tomography in Alzheimer's disease and other neurodegenerative diseases. Front. Neurol. 8, 701.
Drasdo, N., Millican, C.L., Katholi, C.R., Curcio, C.A., 2007. The length of Henle fibers in the human retina and a model of ganglion receptive field density in the visual field. Vis. Res. 47, 2901–2911.
Duh, E.J., Sun, J.K., Stitt, A.W., 2017. Diabetic retinopathy: current understanding, mechanisms, and treatment strategies. JCI insight 2, e93751.
Duke-Elder, S.W., 1961. System of Ophthalmologyvol11: the Anatomy of the Visual System.
Dvorak, L., Russell, S.R., 2011. Retinal drawing: a lost art of medicine. Perm. J. 15, 74–75.
Dysli, C., Wolf, S., Zinkernagel, M.S., 2016. Autofluorescence lifetimes in geographic atrophy in patients with age-related macular degeneration. Investig. Ophthalmol. Vis. Sci. 57, 2479–2487.
Early Treatment Diabetic Retinopathy Study Research Group, 1991a. Classification of diabetic retinopathy from fluorescein angiograms. ETDRS report number 11. Early treatment diabetic retinopathy study research group. Ophthalmology 98, 807–822.
Early Treatment Diabetic Retinopathy Study Research Group, 1991b. Grading diabetic retinopathy from stereoscopic color fundus photographs–an extension of the modified Airlie House classification. ETDRS report number 10. Early Treatment Diabetic Retinopathy Study Research Group. Ophthalmology 98, 786–806.
El-Dairi, M.A., Asrani, S.G., Enyedi, L.B., Freedman, S.F., 2009. Optical coherence tomography in the eyes of normal children. Arch. Ophthalmol. 127, 50–58.
Eldred, G.E., Lasky, M.R., 1993. Retinal age pigments generated by self-assembling lysosomotropic detergents. Nature 361, 724–726.
Erdman, J.W., Smith, J.W., Kuchan, M.J., Mohn, E.S., Johnson, E.J., Rubakhin, S.S., Wang, L., Sweedler, J.V., Neuringer, M., 2015. Lutein and brain function. Foods 4, 547–564.
Espina, M., Barteselli, G., Ma, F., Arcinue, C.A., Camacho, N., Freeman, W.R., Bartsch, D.-U.G., 2014. Noncontact ultra-wide field lens system by Heidelberg Spectralis. In: ARVO Meeting Abstracts, vol. 55. pp. 1615.
Ethen, C.M., Reilly, C., Feng, X., Olsen, T.W., Ferrington, D.A., 2006. The proteome of central and peripheral retina with progression of age-related macular degeneration. Investig. Ophthalmol. Vis. Sci. 47, 2280–2290.
Fan, W., Wang, K., Ghasemi Falavarjani, K., Sagong, M., Uji, A., Ip, M., Wykoff, C.C., Brown, D.M., van Hemert, J., Sadda, S.R., 2017. Distribution of nonperfusion area on ultra-widefield fluorescein angiography in eyes with diabetic macular edema: DAVE study. Am. J. Ophthalmol. 180, 110–116.
Feeney, L., 1978. Lipofuscin and melanin of human retinal pigment epithelium. Fluorescence, enzyme cytochemical, and ultrastructural studies. Investig. Ophthalmol. Vis. Sci. 17, 583–600.
Fisk, G.D., Mennemeier, M., 2006. Common neuropsychological deficits associated with stroke survivors' impaired performance on a useful field of view test. Percept. Mot. Skills 102, 387–394.
Fisk, G.D., Novack, T., Mennemeier, M., Roenker, D., 2002. Useful field of view after traumatic brain injury. J. Head Trauma Rehabil. 17, 16–25.
Flinn, J.M., Kakalec, P., Tappero, R., Jones, B., Lengyel, I., 2014. Correlations in distribution and concentration of calcium, copper and iron with zinc in isolated extracellular deposits associated with age-related macular degeneration. Metallomics 6, 1223–1228.
Foster, P., Khaw, K.-T., 2009. The eye: window to the soul or a mirror of systemic health? Heart 95, 348–349.
Friberg, T.R., Chew, E.Y., Domalpally, A., Sadda, S.R., Clemons, T.E., Danis, R.P., 2014. Peripheral retinal findings in color images in age-related macular degeneration-OPERA, an AREDS 2 Ancillary study. Investig. Ophthalmol. Vis. Sci. 55 4017-4017.
Friberg, T.R., Gupta, A., Yu, J., Huang, L., Suner, I., Puliafito, C.A., Schwartz, S.D., 2008. Ultrawide angle fluorescein angiographic imaging: a comparison to conventional digital acquisition systems. Ophthalmic Surg. Laser. Imag.: Off. J. Int. Soc. Imaging in the Eye 39, 304–311.
Friedman, E., van Buskirk, E.M., Fineberg, E., Messner, K., Schinazi, H., 1971. Pathogenesis of Senile Disciform Degeneration of the Macula, XXI Concilium Ophthalmologicum Mexico. Elsevier Inc, pp. 454–458.
Frost, S., 2010. Ocular biomarkers for early detection of Alzheimer's disease. J. Alzheim. Dis. 22, 1–16.
Fung, T.H., Muqit, M.M., Mordant, D.J., Smith, L.M., Patel, C.K., 2014. Noncontact high-resolution ultra-wide-field oral fluorescein angiography in premature infants with retinopathy of prematurity. JAMA ophthalmology 132, 108–110.
Gao, H., Hollyfield, J.G., 1992. Aging of the human retina. Differential loss of neurons and retinal pigment epithelial cells. Investig. Ophthalmol. Vis. Sci. 33, 1–17.
Gasch, A.T., Smith, J.A., Whitcup, S.M., 1999. Birdshot retinochoroidopathy. Br. J. Ophthalmol. 83, 241–249.
Gass, J.D., 1972. Drusen and disciform macular detachment and degeneration. Trans. Am. Ophthalmol. Soc. 70, 409–436.
Gilmour, D.F., 2015. Familial exudative vitreoretinopathy and related retinopathies. Eye 29, 1–14.
Goldberg, M.F., Jampol, L.M., 1987. Knowledge of diabetic retinopathy before and 18 years after the Airlie House Symposium on treatment of diabetic retinopathy. Ophthalmology 94, 741–746.
Gordon-Shaag, A., Barnard, S., Millodot, M., Gantz, L., Chiche, G., Vanessa, E., Ruth, W., Pinchasov, R., Gosman, Z., Simchi, M., Koslowe, K., Shneor, E., 2014. Prevalence of choroidal naevi using scanning laser ophthalmoscope. Ophthalmic Physiol. Optic. 34, 94–101.
Greite, J.H., Zumbansen, H.P., Adamczyk, R., 1981. Visual field in diabetic retinopathy (DR). In: Greve, E.L., Verriest, G. (Eds.), Fourth International Visual Field Symposium Bristol, April 13–16,1980. Springer Netherlands, Dordrecht, pp. 25–32.
Guduru, A., Fleischman, D., Shin, S., Zeng, D., Baldwin, J.B., Houghton, O.M., Say, E.A., 2017. Ultra-widefield fundus autofluorescence in age-related macular degeneration. PloS One 12, e0177207.
Guy, S., 2012. Perimetry identifies visual function changes in diabetic retinopathy. Medical Research News 1–2.
Hamel, C., 2006. Retinitis pigmentosa. Orphanet J. Rare Dis. 1, 40.
Hammond Jr., B.R., Wooten, B.R., Snodderly, D.M., 1997. Individual variations in the spatial profile of human macular pigment. J Opt Soc Am A Opt Image Sci Vis 14, 1187–1196.
Harman, A.M., Fleming, P.A., Hoskins, R.V., Moore, S.R., 1997. Development and aging of cell topography in the human retinal pigment epithelium. Investig. Ophthalmol. Vis. Sci. 38, 2016–2026.
Heiden, D., Ford, N., Wilson, D., Rodriguez, W.R., Margolis, T., Janssens, B., Bedelu, M., Tun, N., Goemaere, E., Saranchuk, P., Sabapathy, K., Smithuis, F., Luyirika, E., Drew, W.L., 2007. Cytomegalovirus retinitis: the neglected disease of the AIDS pandemic. PLoS Med. 4, e334.
Heinemann, M.-H., 1992. Characteristics of cytomegalovirus retinitis in patients with acquired immunodeficiency syndrome. Am. J. Med. 92, S12–S16.
Hendrickson, A., 2016. Development of retinal layers in prenatal human retina. Am. J. Ophthalmol. 161, 29–35 e21.
Hendrickson, A., Drucker, D., 1992. The development of parafoveal and mid-peripheral human retina. Behav. Brain Res. 49, 21–31.
Henricsson, M., Heijl, A., 1994. Visual fields at different stages of diabetic retinopathy. Acta Ophthalmol. 72, 560–569.
Heussen, F.M., Vasconcelos-Santos, D.V., Pappuru, R.R., Walsh, A.C., Rao, N.A., Sadda, S.R., 2011. Ultra-wide-field green-light (532-nm) autofluorescence imaging in chronic Vogt-Koyanagi-Harada disease. Ophthalmic Surg. Laser. Imag.: Off. J. Int. Soc. Imaging in the Eye 42, 272–277.
Hildebrand, G.D., Fielder, A.R., 2011. Anatomy and physiology of the retina. In: Reynolds, J., Olitsky, S. (Eds.), Pediatric Retina. Springer Berlin Heidelberg, Berlin, Heidelberg, pp. 39–65.
Hirsch, J., Curcio, C.A., 1989. The spatial resolution capacity of human foveal retina. Vis. Res. 29, 1095–1101.
Hogan, M.J., Alvarado, J.A., Weddell, J.E., 1971. Histology of the Human Eye. An Atlas and Textbook. W. B. Saunders, Philadelphia.
Holland, G.N., Buhles Jr., W.C., Mastre, B., Kaplan, H.J., 1989. A controlled retrospective study of ganciclovir treatment for cytomegalovirus retinopathy. Use of a standardized system for the assessment of disease outcome. UCLA CMV Retinopathy. Study Group. Arch. Ophthalmol. 107, 1759–1766.
Huang, D., Swanson, E.A., Lin, C.P., Schuman, J.S., Stinson, W.G., Chang, W., Hee, M.R., Flotte, T., Gregory, K., Puliafito, C.A., 1991. Optical coherence tomography. Science 254, 1178–1181 (New York, N.Y.).
Huestegge, L., Bockler, A., 2016. Out of the corner of the driver's eye: peripheral processing of hazards in static traffic scenes. J. Vis. 16, 11.
Hughes, A., 1977. The topography of vision in mammals of contrasting life style: comparative optics and retinal organisation. In: Crescitelli, F. (Ed.), Handbook of Sensory Physiology. Springer-Verlag, Berlin 613-756.
Humphrey, W.T., Carlson, R.E., Valone Jr., J.A., 1984. Senile reticular pigmentary degeneration. Am. J. Ophthalmol. 98, 717–722.
Huurneman, B., Cox, R.F.A., Vlaskamp, B.N.S., Boonstra, F.N., 2014. Crowded visual search in children with normal vision and children with visual impairment. Vis. Res. 96, 65–74.
Hyvarinen, L., Laurinen, P., Rovamo, J., 1983. Contrast sensitivity in evaluation of visual impairment due to macular degeneration and optic nerve lesions. Acta Ophthalmol. 61, 161–170.
Ikram, M.K., Cheung, C.Y., Wong, T.Y., Chen, C.P., 2012. Retinal pathology as biomarker for cognitive impairment and Alzheimer's disease. J. Neurol. Neurosurg. Psychiatry 83, 917–922.
Isabel Pinilla, A.F., Idoipe, Miriam, Sanchez-Cano, Ana I., Perez-Garcia, Diana, Herrera, Laura X., Pinilla, Maria J., Abecia, Emilio, 2013. Changes in frequency-doubling perimetry in patients with type I diabetes prior to retinopathy. BioMed Res. Int 7 pages.
Ishibashi, K., Tian, J., Handa, J.T., 2004. Similarity of mRNA phenotypes of morphologically normal macular and peripheral retinal pigment epithelial cells in older human

eyes. Investig. Ophthalmol. Vis. Sci. 45, 3291–3301.
Jackman WT, W.J., 1886. On photographing the retina of the living human eye. Phila Photogr 23, 275–276.
Jackson, G.R., Gardner, T.W., 2014. Visual fields refine understanding of diabetic retinopathy progression. Diabetes 63, 2909–2910.
Jayadev, C., Jain, N., Sachdev, S., Mohan, A., Yadav, N.K., 2016. Utility of noninvasive imaging modalities in a retina practice. Indian J. Ophthalmol. 64, 940–943.
Jeganathan, V.S., Wang, J.J., Wong, T.Y., 2008. Ocular associations of diabetes other than diabetic retinopathy. Diabetes Care 31, 1905–1912.
Jesberg, D.O., Schepens, C.L., 1961. Retinal detachment associated with coloboma of the choroid. Arch. Ophthalmol. 65, 163–173 (Chicago, Ill.: 1960).
Johnson, M., Dabholkar, A., Huang, J.-D., Presley, J.B., Chimento, M.F., Curcio, C.A., 2007. Comparison of morphology of human macular and peripheral Bruch's membrane in older eyes. Curr. Eye Res. 32, 791–799.
Jones, B.W., Pfeiffer, R.L., Ferrell, W.D., Watt, C.B., Marmor, M., Marc, R.E., 2016. Retinal remodeling in human retinitis pigmentosa. Exp. Eye Res. 150, 149–165.
Kador, P.F., Wyman, M., 2008. Asteroid hyalosis: pathogenesis and prospects for prevention. Eye 22, 1278–1285 (London, England).
Kaiser-Kupfer Mi, C.R.C.V.D., 2002. Gyrate atrophy of the choroid and retina: further experience with long-term reduction of ornithine levels in children. Arch. Ophthalmol. 120, 146–153.
Kaneko, Y., Moriyama, M., Hirahara, S., Ogura, Y., Ohno-Matsui, K., 2014. Areas of nonperfusion in peripheral retina of eyes with pathologic myopia detected by ultra-widefield fluorescein AngiographyRetinal vasculature in periphery in pathologic myopia. Investig. Ophthalmol. Vis. Sci. 55, 1432–1439.
Karia, N., 2010. Retinal vein occlusion: pathophysiology and treatment options. Clin. Ophthalmol. 4, 809–816 (Auckland, N.Z.).
Kaufman, M., Medina-Mendez, C., Friberg, T., Eller, A., 2013. Evaluation of peripheral retinal vasculitis in retinitis pigmentosa using wide-field fluorescein angiography. Investigative Ophtalmol. Visual Sci. 54, 4018.
Keeler, C.R., 2002. The ophthalmoscope in the lifetime of Hermann von Helmholtz. Arch. Ophthalmol. 120, 194–201.
Kernt, M., Schaller, U.C., Stumpf, C., Ulbig, M.W., Kampik, A., Neubauer, A.S., 2010. Choroidal pigmented lesions imaged by ultra-wide-field scanning laser ophthalmoscopy with two laser wavelengths (Optomap). Clin. Ophthalmol. 4, 829–836 (Auckland, N.Z.).
Kim, D.Y., Kim, J.G., Kim, Y.J., Joe, S.G., Lee, J.Y., 2014. Ultra-widefield fluorescein angiographic findings in patients with recurrent vitreous hemorrhage after diabetic vitrectomy. Investig. Ophthalmol. Vis. Sci. 55, 7040–7046.
Kitchens, J., Stone, T., Westhouse, S., Sommerville, D., Isernhagen, R., Wood, W., 2009. Ultra-widefield Fluorescein Angiography Prompted and Guided Treatment for Uveitis.
Klein, R., Davis, M.D., Magli, Y.L., Segal, P., Klein, B.E., Hubbard, L., 1991. The Wisconsin age-related maculopathy grading system. Ophthalmology 98, 1128–1134.
Klein, R., Klein, B.E., Linton, K.L., 1992. Prevalence of age-related maculopathy. The beaver dam eye study. Ophthalmology 99, 933–943.
Kociok, N., Joussen, A.M., 2007. Varied expression of functionally important genes of RPE and choroid in the macula and in the periphery of normal human eyes. Graefe's Arch. Clin. Exp. Ophthalmol. 245, 101–113.
Kolb, H., 1995. Simple anatomy of the retina. In: Kolb, H., Fernandez, E., Nelson, R. (Eds.), Webvision: the Organization of the Retina and Visual System, Salt Lake City (UT).
Kolb, H., 2005. Simple Anatomy of the Retina. Webvision: The Organization of the Retina and Visual System.
Kong, M., Lee, M.Y., Ham, D.-I., 2012. Ultrawide-field fluorescein angiography for evaluation of diabetic retinopathy. Kor. J. Ophthalmol. 26, 428–431.
Kornberg, D.L., Klufas, M.A., Yannuzzi, N.A., Orlin, A., D'Amico, D.J., Kiss, S., 2016. Clinical utility of ultra-widefield imaging with the Optos Optomap compared with indirect ophthalmoscopy in the setting of non-traumatic rhegmatogenous retinal detachment. Semin. Ophthalmol. 31, 505–512.
Koronyo, Y., Biggs, D., Barron, E., Boyer, D.S., Pearlman, J.A., Au, W.J., Kile, S.J., Blanco, A., Fuchs, D.T., Ashfaq, A., Frautschy, S., Cole, G.M., Miller, C.A., Hinton, D.R., Verdooner, S.R., Black, K.L., Koronyo-Hamaoui, M., 2017. Retinal amyloid pathology and proof-of-concept imaging trial in Alzheimer's disease. JCI insight 2.
Kothari, A., Narendran, V., Saravanan, V.R., 2012. In vivo sectional imaging of the retinal periphery using conventional optical coherence tomography systems. Indian J. Ophthalmol. 60, 235–239.
Kumar, P., Courtney, R., Baynes, K., Lowder, C., Ehlers, J., Rennebohm, R., Srivastava, S., 2013. Novel angiographic findings in Susac syndrome identified by ultra-widefield imaging technology. Investig. Ophthalmol. Vis. Sci. 54 5853-5853.
Lakshminarayanan, V., Lagrave, J., Kean, M.L., Dick, M., Shankle, R., 1996. Vision in dementia: contrast effects. Neurol. Res. 18, 9–15.
Larson, A.M., Loschky, L.C., 2009. The contributions of central versus peripheral vision to scene gist recognition. J. Vis. 9 6-6.
Lee, R., Wong, T.Y., Sabanayagam, C., 2015. Epidemiology of diabetic retinopathy, diabetic macular edema and related vision loss. Eye and Vision 2, 17.
Leicht, S.F., Kernt, M., Neubauer, A., Wolf, A., Oliveira, C.M., Ulbig, M., Haritoglou, C., 2014. Microaneurysm turnover in diabetic retinopathy assessed by automated RetmarkerDR image analysis–potential role as biomarker of response to ranibizumab treatment. Ophthalmologica.Journal international d'ophtalmologie.International journal of ophthalmology.Zeitschrift fur Augenheilkunde 231, 198–203.
Lengyel, I., Csutak, A., Florea, D., Leung, I., Bird, A.C., Jonasson, F., Peto, T., 2015. A population-based ultra-widefield digital image grading study for age-related macular degeneration-like lesions at the peripheral retina. Ophthalmology 22, 1340–1347.
Lengyel, I., Tufail, A., Hosaini, H.A., Luthert, P., Bird, A.C., Jeffery, G., 2004. Association of drusen deposition with choroidal intercapillary pillars in the aging human eye. Investig. Ophthalmol. Vis. Sci. 45, 2886–2892.
Leo, S.-W., Young, T.L., 2011. An evidence-based update on myopia and interventions to retard its progression. J. Am. Assoc. Pediatr. Ophthalmol. Strabismus 15, 181–189.
Lewis, H., Straatsma, B.R., Foos, R.Y., 1986a. Chorioretinal juncture. Multiple extramacular drusen. Ophthalmology 93, 1098–1112.
Lewis, H., Straatsma, B.R., Foos, R.Y., 1986b. The prevalence of macular drusen in postmortem eyes. Am. J. Ophthalmol. 102, 801–803.
Lewis, H., Straatsma, B.R., Foos, R.Y., Lightfoot, D.O., 1985. Reticular degeneration of the pigment epithelium. Ophthalmology 92, 1485–1495.
Li, M., Huisingh, C., Messinger, J., Dolz-Marco, R., Ferrara, D., Freund, K.B., Curcio, C.A., 2018. HISTOLOGY OF geographic atrophy secondary to AGE-RELATED macular degeneration: a multilayer approach. Retina 38, 1937–1953 (Philadelphia, Pa.).
Li, M., Jia, C., Kazmierkiewicz, K.L., Bowman, A.S., Tian, L., Liu, Y., Gupta, N.A., Gudiseva, H.V., Yee, S.S., Kim, M., Dentchev, T., Kimble, J.A., Parker, J.S., Messinger, J.D., Hakonarson, H., Curcio, C.A., Stambolian, D., 2014. Comprehensive analysis of gene expression in human retina and supporting tissues. Hum. Mol. Genet. 23, 4001–4014.
Li, M., Zauhar, R.J., Grazal, C., Curcio, C.A., DeAngelis, M.M., Stambolian, D., 2017. RNA expression in human retina. Hum. Mol. Genet. 26, R68–r74.
Li, Z.Y., Possin, D.E., Milam, A.H., 1995. Histopathology of bone spicule pigmentation in retinitis pigmentosa. Ophthalmology 102, 805–816.
Liao, H., Zhu, Z., Peng, Y., 2018. Potential utility of retinal imaging for Alzheimer's disease: a review. Front. Aging Neurosci. 10.
Liegl, R., Liegl, K., Ceklic, L., Haritoglou, C., Kampik, A., Ulbig, M.W., Kernt, M., Neubauer, A.S., 2014. Nonmydriatic ultra-wide-field scanning laser ophthalmoscopy (Optomap) versus two-field fundus photography in diabetic retinopathy. Ophthalmologica.Journal international d'ophtalmologie.International journal of ophthalmology.Zeitschrift fur Augenheilkunde 231, 31–36.
Liew, G., Michaelides, M., Bunce, C., 2014. A comparison of the causes of blindness certifications in England and Wales in working age adults (16-64 years), 1999-2000 with 2009-2010. BMJ open 4, e004015.
Lim, J.K.H., Li, Q.-X., He, Z., Vingrys, A.J., Wong, V.H.Y., Currier, N., Mullen, J., Bui, B.V., Nguyen, C.T.O., 2016. The eye as a biomarker for Alzheimer's disease. Front. Neurosci. 10.
Liu, D., Zhang, L., Li, Z., Zhang, X., Wu, Y., Yang, H., Min, B., Zhang, X., Ma, D., Lu, Y., 2015. Thinner changes of the retinal nerve fiber layer in patients with mild cognitive impairment and Alzheimer's disease. BMC Neurol. 15, 14.
Loane, E., Kelliher, C., Beatty, S., Nolan, J.M., 2008. The rationale and evidence base for a protective role of macular pigment in age-related maculopathy. Br. J. Ophthalmol. 92, 1163–1168.
Lotmar, W., 1977. A fixation lamp for panoramic fundus pictures (author's transl. Klinische Monatsblatter fur Augenheilkunde 170, 767–774.
Ludwig, C.J.H., Davies, J.R., Eckstein, M.P., 2014. Foveal analysis and peripheral selection during active visual sampling. Proc. Natl. Acad. Sci. U. S. A. 111, E291–E299.
Ly, A., Nivison-Smith, L., Hennessy, M., Kalloniatis, M., 2015. Pigmented Lesions of the Retinal Pigment Epithelium, vol. 92. Optometry and vision science: official publication of the American Academy of Optometry, pp. 844–857.
Manjunath, V., Papastavrou, V., Steel, D.H., Menon, G., Taylor, R., Peto, T., Talks, J., 2015. Wide-field imaging and OCT vs clinical evaluation of patients referred from diabetic retinopathy screening. Eye 29, 416–423 (London, England).
Manuchehri, K., Kirkby, G., 2003. Vitreous haemorrhage in elderly patients: management and prevention. Drugs Aging 20, 655–661.
Marigold, D.S., 2008. Role of peripheral visual cues in online visual guidance of locomotion. Exerc. Sport Sci. Rev. 36, 145–151.
Martin, P.R., Grunert, U., 1992. Spatial density and immunoreactivity of bipolar cells in the macaque monkey retina. J. Comp. Neurol. 323, 269–287.
Marziani, E., Pomati, S., Ramolfo, P., Cigada, M., Giani, A., Mariani, C., Staurenghi, G., 2013. Evaluation of retinal nerve fiber layer and ganglion cell layer thickness in Alzheimer's disease using spectral-domain optical coherence tomography. Investig. Ophthalmol. Vis. Sci. 54, 5953–5958.
McGrory, S., Cameron, J.R., Pellegrini, E., Warren, C., Doubal, F.N., Deary, I.J., Dhillon, B., Wardlaw, J.M., Trucco, E., MacGillivray, T.J., 2017. The application of retinal fundus camera imaging in dementia: a systematic review. Alzheimer's Dementia 6, 91–107 (Amsterdam, Netherlands).
McKhann, G., Drachman, D., Folstein, M., Katzman, R., Price, D., Stadlan, E.M., 1984. Clinical diagnosis of Alzheimer's disease: report of the NINCDS-ADRDA work group* under the auspices of department of health and human services task force on Alzheimer's disease. Neurology 34, 939.
McNabb, R.P., Grewal, D.S., Mehta, R., Schuman, S.G., Izatt, J.A., Mahmoud, T.H., Jaffe, G.J., Mruthyunjaya, P., Kuo, A.N., 2016. Wide field of view swept-source optical coherence tomography for peripheral retinal disease. Br. J. Ophthalmol. 100, 1377–1382.
Melo, M.B.d., 2014. An eye on sickle cell retinopathy. Rev. Bras. Hematol. Hemoter. 36, 319–321.
Mendez, M.F., Tomsak, R.L., Remler, B., 1990. Disorders of the visual system in Alzheimer's disease. J. Clin. Neuro Ophthalmol. 10, 62–69.
Meyer, C.H., Saxena, S., 2010. Non-mydriatic imaging of a giant retinal tear with the Optos Optomap Panoramic 200MA. Clin. Exp. Ophthalmol. 38 427-427.
Midena, E., Vujosevic, S., 2011. Microperimetry in diabetic retinopathy. Saudi Journal of Ophthalmology 25, 131–135.
Mitchell, P., Smith, W., Attebo, K., Wang, J.J., 1995. Prevalence of age-related maculopathy in Australia. The blue mountains eye study. Ophthalmology 102, 1450–1460.
Mohn, E.S., Erdman Jr., J.W., Kuchan, M.J., Neuringer, M., Johnson, E.J., 2017. Lutein accumulates in subcellular membranes of brain regions in adult rhesus macaques: relationship to DHA oxidation products. PloS One 12, e0186767.
Mollon, J.D., Regan, B.C., Bowmaker, J.K., 1998. What is the function of the cone-rich rim

of the retina? Eye 12 (Pt 3b), 548–552 (Lond).
Morgan, J.I.W., Han, G., Maguire, A.M., Bennett, J., 2014. Retinal structure-function comparison through adaptive optics imaging reveals disease pathogenesis in choroideremia. Investig. Ophthalmol. Vis. Sci. 55 1653-1653.
Mrejen, S., Gallego-Pinazo, R., Wald, K.J., Freund, K.B., 2013. Acute posterior multifocal placoid pigment epitheliopathy as a choroidopathy: what we learned from adaptive optics imaging. JAMA ophthalmology 131, 1363–1364.
Mroczkowska, S., Benavente-Perez, A., Patel, S.R., Negi, A., Sung, V., Bentham, P., Gherghel, D., 2015. Retinal microvascular dysfunction occurs similarly in Alzheimer's disease and primary open angle glaucoma patients. Investig. Ophthalmol. Vis. Sci. 56, 2763.
Mudvari, S.S., Virasch, V.V., Singa, R.M., MacCumber, M.W., 2010. Ultra-wide-field imaging for cytomegalovirus retinitis. Ophthalmic Surg. Laser. Imag. 41, 311.
Munch, I.C., Ek, J., Kessel, L., Sander, B., Almind, G.J., Brondum-Nielsen, K., Linneberg, A., Larsen, M., 2010. Small, hard macular drusen and peripheral drusen: associations with AMD genotypes in the Inter99 Eye Study. Investig. Ophthalmol. Vis. Sci. 51, 2317–2321.
Muqit, M.M.K., Marcellino, G.R., Henson, D.B., Young, L.B., Patton, N., Charles, S.J., Turner, G.S., Stanga, P.E., 2013. Optos-guided pattern scan laser (Pascal)-targeted retinal photocoagulation in proliferative diabetic retinopathy. Acta Ophthalmol. 91, 251–258.
Musel, B., Bordier, C., Dojat, M., Pichat, C., Chokron, S., Le Bas, J.F., Peyrin, C., 2013. Retinotopic and lateralized processing of spatial frequencies in human visual cortex during scene categorization. J. Cognit. Neurosci. 25, 1315–1331.
Musel, B., Hera, R., Chokron, S., Alleysson, D., Chiquet, C., Romanet, J.P., Guyader, N., Peyrin, C., 2011. Residual abilities in age-related macular degeneration to process spatial frequencies during natural scene categorization. Vis. Neurosci. 28, 529–541.
Nakagawa, T.A., Skrinska, R., 2001. Improved documentation of retinal hemorrhages using a wide-field digital ophthalmic camera in patients who experienced abusive head trauma. Arch. Pediatr. Adolesc. Med. 155, 1149–1152.
Nakayama, K., 1985. Biological image motion processing: a review. Vis. Res. 25, 625–660.
Nam, K.T., Yun, C.M., Kim, J.T., Yang, K.S., Kim, H.J., Kim, S.W., Oh, J., Huh, K., 2015. Central serous chorioretinopathy fundus autofluorescence comparison with two different confocal scanning laser ophthalmoscopes. In: Graefe's archive for clinical and experimental ophthalmology = Albrecht von Graefes Archiv Fur klinische und experimentelle Ophthalmologie.
Natarajan, S., 2011. Retinitis pigmentosa: a brief overview. Indian J. Ophthalmol. 59, 343–346.
Nazari, F., Azimi, A., Abdi, S., 2014. What is Susac syndrome?-A brief review of articles. Iran. J. Neurol. 13, 209.
Neargarder, S.A., Stone, E.R., Cronin-Golomb, A., Oross 3rd, S., 2003. The impact of acuity on performance of four clinical measures of contrast sensitivity in Alzheimer's disease. J. Gerontol. B Psychol. Sci. Soc. Sci. 58, P54–P62.
Nentwich, M.M., Ulbig, M.W., 2015. Diabetic retinopathy - ocular complications of diabetes mellitus. World J. Diabetes 6, 489–499.
Neugroschl, J., Wang, S., 2011. Alzheimer's disease: diagnosis and treatment across the spectrum of disease severity. MSJM (Mt. Sinai J. Med.) 78, 596–612 New York.
Nissen, M.J., Corkin, S., Buonanno, F.S., Growdon, J.H., Wray, S.H., Bauer, J., 1985. Spatial vision in Alzheimer's disease. General findings and a case report. Arch. Neurol. 42, 667–671.
Nolan, J.M., Loughman, J., Akkali, M.C., Stack, J., Scanlon, G., Davison, P., Beatty, S., 2011. The impact of macular pigment augmentation on visual performance in normal subjects: COMPASS. Vis. Res. 51, 459–469.
Nolan, J.M., Power, R., Stringham, J., Dennison, J., Stack, J., Kelly, D., Moran, R., Akuffo, K.O., Corcoran, L., Beatty, S., 2016. Enrichment of macular pigment enhances contrast sensitivity in subjects free of retinal disease: central retinal enrichment supplementation trials - report 1. Investig. Ophthalmol. Vis. Sci. 57, 3429–3439.
O'Bryhim, B., Apte, R.S., Kung, N., Coble, D., Van Stavern, G.P., 2018. Association of preclinical alzheimer disease with optical coherence tomographic angiography findings. JAMA Ophthalmology.
Obana, A., Sasano, H., Okazaki, S., Otsuki, Y., Seto, T., Gohto, Y., 2017. Evidence of carotenoid in surgically removed lamellar hole-associated epiretinal proliferation. Investig. Ophthalmol. Vis. Sci. 58, 5157–5163.
Oellers, P., Lains, I., Mach, S., Garas, S., Kim, I.K., Vavvas, D.G., Miller, J.W., Husain, D., Miller, J.B., 2017. Novel grid combined with peripheral distortion correction for ultra-widefield image grading of age-related macular degeneration. Clin. Ophthalmol. 11, 1967–1974.
Ogino, K., Murakami, T., Yoshimura, N., 2014. Photocoagulation guided by wide-field fundus autofluorescence in eyes with asteroid hyalosis. Eye 28, 634–635 (London, England).
Ogura, S., Yasukawa, T., Kato, A., Usui, H., Hirano, Y., Yoshida, M., Ogura, Y., 2014. Wide-field fundus autofluorescence imaging to evaluate retinal function in patients with retinitis pigmentosa. Am. J. Ophthalmol. 158, 1093–1098 e1093.
Okamoto, H., Umeda, S., Nozawa, T., Suzuki, M.T., Yoshikawa, Y., Matsuura, E.T., Iwata, T., 2010. Comparative proteomic analyses of macular and peripheral retina of cynomolgus monkeys (Macaca fascicularis). Exp. Anim. 59, 171–182.
Orlin, A., Fatoo, A., Ehrlich, J., D'Amico, D.J., Chan, R.P., Kiss, S., 2013. Ultra-widefield fluorescein angiography of white without pressure. Clin. Ophthalmol. 7, 959–964.
Osterberg, G., 1935. Topography of the Layer of Rods and Cones in the Human Retina. Copenhagen [Levin & Munksgaard].
Østerberg, G.A., 1937. Topography of the layer of rods and cones in the human retina. J. Am. Med. Assoc. 108 232-232.
Owsley, C., McGwin, G., 2010. Vision and driving. Vis. Res. 50, 2348–2361.
Oyster, C.W., 1999. The Human Eye. Sinauer, Sunderland, MA.
Paciuc-Beja, M., Salcedo, G., Smith, J.M., Harasawa, M., Velez-Montoya, R., Olson, J.L., Oliver, S.C., Mandava, N., Quiroz-Mercado, H., 2014. Measurement of progression of gyrate atrophy using ultra-wide field fundus photography. Investig. Ophthalmol. Vis. Sci. 55 265-265.
Pallitto, P., Ablonczy, Z., Jones, E.E., Drake, R.R., Koutalos, Y., Crouch, R.K., Donello, J., Herrmann, J., 2015. A2E and lipofuscin distributions in macaque retinal pigment epithelium are similar to human. Photochem. Photobiol. Sci.: Off. J. Eur. Photochem. Assoc. Eur. Soc. Photobiol. 14, 1888–1895.
Pang, C.E., Maberley, D.A., Freund, K.B., White, V.A., Rasmussen, S., To, E., Matsubara, J.A., 2016. Lamellar hole-associated epiretinal proliferation: a clinicopathologic correlation. Retina 36, 1408–1412 (Philadelphia, Pa.).
Parravano, M., Oddone, F., Mineo, D., Centofanti, M., Borboni, P., Lauro, R., Tanga, L., Manni, G., 2008. The role of Humphrey Matrix testing in the early diagnosis of retinopathy in type 1 diabetes. Br. J. Ophthalmol. 92, 1656–1660.
Patel, C.K., Fung, T.H., Muqit, M.M., Mordant, D.J., Brett, J., Smith, L., Adams, E., 2013. Non-contact ultra-widefield imaging of retinopathy of prematurity using the Optos dual wavelength scanning laser ophthalmoscope. Eye 27, 589–596 (London, England).
Peli, E., Apfelbaum, H., Berson, E.L., Goldstein, R.B., 2016. The risk of pedestrian collisions with peripheral visual field loss. J. Vis. 16 5-5.
Perry, V.H., Cowey, A., 1988. The lengths of the fibres of Henle in the retina of macaque monkeys: implications for vision. Neuroscience 25, 225–236.
Piffer, A.L., Boissonnot, M., Gobert, F., Zenger, A., Wolf, S., Wolf, U., Korobelnik, J.F., Rougier, M.B., 2014. Relevance of wide-field autofluorescence imaging in Birdshot retinochoroidopathy: descriptive analysis of 76 eyes. Acta Ophthalmol. 92, e463–469.
Polyak, S.L., 1941. The Retina. The University of Chicago Press.
Polyak, S.L., 1957. The Vertebrate Visual System. University of Chicago, Chicago.
Pomerantzeff, O., 1975. Equator-plus camera. Invest. Ophthalmol. 14, 401–406.
Postel, E.A., Agarwal, A., Schmidt, S., Fan, Y.T., Scott, W.K., Gilbert, J.R., Haines, J.L., Pericak-Vance, M.A., 2005. Comparing age-related macular degeneration phenotype in probands from singleton and multiplex families. Am. J. Ophthalmol. 139, 820–825.
Powner, M.B., Gillies, M.C., Tretiach, M., Scott, A., Guymer, R.H., Hageman, G.S., Fruttiger, M., 2010. Perifoveal muller cell depletion in a case of macular telangiectasia type 2. Ophthalmology 117, 2407–2416.
Powner, M.B., Gillies, M.C., Zhu, M., Vevis, K., Hunyor, A.P., Fruttiger, M., 2013. Loss of Muller's cells and photoreceptors in macular telangiectasia type 2. Ophthalmology 120, 2344–2352.
Prasad, P.S., Oliver, S.C.N., Coffee, R.E., Hubschman, J.-P., Schwartz, S.D., 2010. Ultra wide-field angiographic characteristics of branch retinal and hemicentral retinal vein occlusion. Ophthalmology 117, 780–784.
Price, L.D., Au, S., Chong, N.V., 2015. Optomap ultrawide field imaging identifies additional retinal abnormalities in patients with diabetic retinopathy. Clin. Ophthalmol. 9, 527–531 (Auckland, N.Z.).
Provis, J.M., 2001. Development of the primate retinal vasculature. Prog. Retin. Eye Res. 20, 799–821.
Provis, J.M., Dubis, A.M., Maddess, T., Carroll, J., 2013. Adaptation of the central retina for high acuity vision: cones, the fovea and the avascular zone. Prog. Retin. Eye Res. 35, 63–81.
Provis, J.M., Penfold, P.L., Cornish, E.E., Sandercoe, T.M., Madigan, M.C., 2005. Anatomy and development of the macula: specialisation and the vulnerability to macular degeneration. Clin. Exp. Optom. 88, 269–281.
Quinn, N.B., Wright, D., Peto, T., Cruise, S.M., Young, I., Kee, F., Chakravarthy, U., Hogg, R.E., 2017. Prevalence and characteristics of peripheral retinal lesions in an ageing population. Investig. Ophthalmol. Vis. Sci. 58 1497-1497.
Rahmani, S., Fawzi, A., Lyon, A., Maumenee, I., Mets, M., 2013. Ultra-widefield retinal imaging documentation and analysis of peripheral retinal disease in Marfan syndrome: from the Marfan Eye Consortium of Chicago. Investig. Ophthalmol. Vis. Sci. 54 5845-5845.
Ramanoel, S., Kauffmann, L., Cousin, E., Dojat, M., Peyrin, C., 2015. Age-related differences in spatial frequency processing during scene categorization. PloS One 10, e0134554.
Reitz, C., Mayeux, R., 2014. Alzheimer disease: epidemiology, diagnostic criteria, risk factors and biomarkers. Biochem. Pharmacol. 88, 640–651.
Renzi, L.M., Hammond Jr., B.R., 2010. The relation between the macular carotenoids, lutein and zeaxanthin, and temporal vision. Ophthalmic Physiol. Optic. 30, 351–357.
Reznicek, L., Wasfy, T., Stumpf, C., Kampik, A., Ulbig, M., Neubauer, A.S., Kernt, M., 2012. Peripheral fundus autofluorescence is increased in age-related macular degeneration. Investig. Ophthalmol. Vis. Sci. 53, 2193–2198.
Risau, W., 1997. Mechanisms of angiogenesis. Nature 386, 671–674.
RNIB, 2016. Charles Bonnet Syndrome (CBS)—visual Hallucinations Associated with Poor Vision.
Rosenholtz, R., 2016. Capabilities and limitations of peripheral vision. Annual review of vision science 2, 437–457.
Rousseau, A., de Monchy, I., Barreau, E., Yahiaoui, Y., M'Garrech, M., Kaswin, G., Labetoulle, M., 2013. Retinal emboli in cholesterol crystal embolism. Case reports in ophthalmological medicine 2013, 421352.
Rudolf, M., Clark, M.E., Chimento, M.F., Li, C.M., Medeiros, N.E., Curcio, C.A., 2008a. Prevalence and morphology of druse types in the macula and periphery of eyes with age-related maculopathy. Investig. Ophthalmol. Vis. Sci. 49, 1200–1209.
Rudolf, M., Malek, G., Messinger, J.D., Clark, M.E., Wang, L., Curcio, C.A., 2008b. Subretinal drusenoid deposits in human retina: organization and composition. Exp. Eye Res. 87, 402–408.
Rutnin, U., Schepens, C.L., 1967. Fundus appearance in normal eyes. II. The standard peripheral fundus and developmental variations. Am. J. Ophthalmol. 64, 840–852.
Sagong, M., van Hemert, J., Olmos de Koo, L.C., Barnett, C., Sadda, S.R., 2015.

Assessment of accuracy and precision of quantification of ultra-widefield images. Ophthalmology 122, 864–866.
Sala-Puigdollers, A., Caputo, S., Jaberansari, H., Gray, J., D'Souza, Y., Charles, S., Young, L., Henson, D., McLeod, D., Stanga, P., 2013. New software to assess retinal non-perfusion on Optomap® wide-field fundus fluorescein angiography in diabetic macular oedema. Investig. Ophthalmol. Vis. Sci. 54 2410-2410.
Salcedo-Villanueva, G., Paciuc-Beja, M., Villanueva-Mendoza, C., Harasawa, M., Smith, J.M., Velez-Montoya, R., Olson, J.L., Oliver, S.C., Mandava, N., Quiroz-Mercado, H., 2015. Progression of gyrate atrophy measured with ultra-wide-field imaging. Int. Ophthalmol. 36, 111–120.
Santini, B., 2017. Controlling Myopia in Children.
Sarks, J.P., Sarks, S.H., Killingsworth, M.C., 1994. Evolution of soft drusen in age-related macular degeneration. Eye 8 (Pt 3), 269–283.
Sarks, S.H., Van Driel, D., Maxwell, L., Killingsworth, M., 1980. Softening of drusen and subretinal neovascularization. Trans. Ophthalmol. Soc. U. K. 100, 414–422.
Sarks, S.H., Arnold, J.J., Sarks, J.P., Gilles, M.C., Walter, C.J., 1996. Prophylactic perifoveal laser treatment of soft drusen. Aust. N. Z. J. Ophthalmol. 24, 15–26.
Sauer, L., Klemm, M., Peters, S., Schweitzer, D., Schmidt, J., Kreilkamp, L., Ramm, L., Meller, D., Hammer, M., 2018. Monitoring foveal sparing in geographic atrophy with fluorescence lifetime imaging ophthalmoscopy - a novel approach. Acta Ophthalmol. 96, 257–266.
Schepens, C.L., Bahn, G.C., 1950. Examination of the ora serrata. Its importance in retinal detachment. A.M.A.archives of ophthalmology 44, 677–690.
Schlotterer, G., Moscovitch, M., Crapper-Mclachlan, D., 1984. Visual processing deficits as assessed by spatial frequency contrast sensitivity and backward masking in normal ageing and alzheimer's disease. Brain: J. Neurol. 107, 309–324.
Sebag, J., Yee, K.M., Wa, C.A., Huang, L.C., Sadun, A.A., 2014. Vitrectomy for floaters: prospective efficacy analyses and retrospective safety profile. Retina 34, 1062–1068 (Philadelphia, Pa.).
Seddon, J.M., Reynolds, R., Rosner, B., 2009. Peripheral retinal drusen and reticular pigment: association with CFHY402H and CFHrs1410996 genotypes in family and twin studies. Investig. Ophthalmol. Vis. Sci. 50, 586–591.
Selaru, D., Ocian, R., Stingu, C., Dragomir, M., Mitulescu, D., 2000. Retinoschisis–the clinical associations and therapeutic possibilities. Oftalmologia 51, 83–86 (Bucharest, Romania: 1990).
Sharon, D., Blackshaw, S., Cepko, C.L., Dryja, T.P., 2002. Profile of the genes expressed in the human peripheral retina, macula, and retinal pigment epithelium determined through serial analysis of gene expression (SAGE). Proc. Natl. Acad. Sci. U. S. A. 99, 315–320.
Shifera, A.S., Pennesi, M.E., Yang, P., Lin, P., 2017. Ultra-wide-field fundus autofluorescence findings in patients with acute zonal occult outer retinopathy. Retina 37, 1104–1119 (Philadelphia, Pa.).
Shin, S.K., O'Brien, K.M., 2009. Progenitor cells of the rod-free area centralis originate in the anterior dorsal optic vesicle. BMC Dev. Biol. 9 57-213X-219-257.
Shinohara, K., Tanaka, N., Jonas, J.B., Shimada, N., Moriyama, M., Yoshida, T., Ohno-Matsui, K., 2018. Ultrawide-field OCT to investigate relationships between myopic macular retinoschisis and posterior staphyloma. Ophthalmology 125, 1575–1586.
Shneor, E., Millodot, M., Barnard, S., Gantz, L., Koslowe, K., Gordon-Shaag, A., 2014. Prevalence of congenital hypertrophy of the retinal pigment epithelium (CHRPE) in Israel. Ophthalmic Physiol. Optic.: J. Brit. Col. Ophthalmic Opticians (Optometrists) 34, 385.
Shrestha, G.S., Kaiti, R., 2014. Visual functions and disability in diabetic retinopathy patients. J. Optom. 7, 37–43.
Shuler Jr., R.K., Schmidt, S., Gallins, P., Hauser, M.A., Scott, W.K., Caldwell, J., Agarwal, A., Haines, J.L., Pericak-Vance, M.A., Postel, E.A., 2008a. Peripheral reticular pigmentary change is associated with complement factor H polymorphism (Y402H) in age-related macular degeneration. Ophthalmology 115, 520–524.
Shuler Jr., R.K., Schmidt, S., Gallins, P., Hauser, M.A., Scott, W.K., Caldwell, J., Agarwal, A., Haines, J.L., Pericak-Vance, M.A., Postel, E.A., 2008b. Phenotype analysis of patients with the risk variant LOC387715 (A69S) in age-related macular degeneration. Am. J. Ophthalmol. 145, 303–307.
Shunmugam, M., Ang, G.S., Lois, N., 2014. Giant retinal tears. Surv. Ophthalmol. 59, 192–216.
Silva, P.S., Cavallerano, J.D., Haddad, N.M.N., Kwak, H., Dyer, K.H., Omar, A.F., Shikari, H., Aiello, L.M., Sun, J.K., Aiello, L.P., 2015. Peripheral lesions identified on ultrawide field imaging predict increased risk of diabetic retinopathy progression over 4 years. Ophthalmology 122, 949–956.
Silva, P.S., Cavallerano, J.D., Sun, J.K., Soliman, A.Z., Aiello, L.M., Aiello, L.P., 2013. Peripheral lesions identified by mydriatic ultrawide field imaging: distribution and potential impact on diabetic retinopathy severity. Ophthalmology 120, 2587–2595.
Silva, P.S., Cavallerano, J.D., Tolls, D., Omar, A., Thakore, K., Patel, B., Sehizadeh, M., Tolson, A.M., Sun, J.K., Aiello, L.M., Aiello, L.P., 2014. Potential efficiency benefits of nonmydriatic ultrawide field retinal imaging in an ocular telehealth diabetic retinopathy program. Diabetes Care 37, 50–55.
Simpson, M.J., 2017. Mini-review: far peripheral vision. Vis. Res. 140, 96–105.
Singer, M., Tan, C.S., Bell, D., Sadda, S.R., 2014. Area of peripheral retinal nonperfusion and treatment response in branch and central retinal vein occlusion. Retina 34, 1736–1742 (Philadelphia, Pa.).
Smith, B.F., Ripps, H., Goodman, G., 1959. Retinitis punctata albescens; a functional and diagnostic evaluation. A.M.A.archives of ophthalmology 61, 93–101.
Snodderly, D.M., Auran, J.D., Delori, F.C., 1984. The macular pigment. II. Spatial distribution in primate retinas. Investig. Ophthalmol. Vis. Sci. 25, 674–685.
Snodderly, D.M., Sandstrom, M.M., Leung, I.Y.F., Zucker, C.L., Neuringer, M., 2002. Retinal pigment epithelial cell distribution in central retina of rhesus monkeys. Investig. Ophthalmol. Vis. Sci. 43, 2815–2818.
Spaide, R.F., 2011. Peripheral areas of nonperfusion in treated central retinal vein occlusion as imaged by wide-field fluorescein angiography. Retina 31, 829–837 (Philadelphia, Pa.).
Sparrow, J.R., Zhou, J., Ben-Shabat, S., Vollmer, H., Itagaki, Y., Nakanishi, K., 2002. Involvement of oxidative mechanisms in blue-light-induced damage to A2E-laden RPE. Investig. Ophthalmol. Vis. Sci. 43, 1222–1227.
Stringham, J.M., Garcia, P.V., Smith, P.A., Hiers, P.L., McLin, L.N., Kuyk, T.K., Foutch, B.K., 2015. Macular pigment and visual performance in low-light conditions. Investig. Ophthalmol. Vis. Sci. 56, 2459–2468.
Sung, K.R., Wollstein, G., Kim, N.R., Na, J.H., Nevins, J.E., Kim, C.Y., Schuman, J.S., 2012. Macular assessment using optical coherence tomography for glaucoma diagnosis. Br. J. Ophthalmol. 96, 1452–1455.
Sunness, J.S., Bressler, N.M., Tian, Y., Alexander, J., Applegate, C.A., 1999. Measuring geographic atrophy in advanced age-related macular degeneration. Investig. Ophthalmol. Vis. Sci. 40, 1761–1769.
Tadin, D., Nyquist, J.B., Lusk, K.E., Corn, A.L., Lappin, J.S., 2012. Peripheral vision of youths with low vision: motion perception, crowding, and visual search. Investig. Ophthalmol. Vis. Sci. 53, 5860–5868.
Talks, S.J., Manjunath, V., Steel, D.H., Peto, T., Taylor, R., 2015. New vessels detected on wide-field imaging compared to two-field and seven-field imaging: implications for diabetic retinopathy screening image analysis. Br. J. Ophthalmol. 99, 1606–1609.
Tan, C.S., Heussen, F., Sadda, S.R., 2013. Peripheral autofluorescence and clinical findings in neovascular and non-neovascular age-related macular degeneration. Ophthalmology 120, 1271–1277.
Tasman, W., 1974. Peripheral retinal changes following blunt trauma. Mod. Probl. Ophthalmol. 12, 446–450.
Theelen, T., Berendschot, T.T., Klevering, B.J., Fuijkschot, J., Hoyng, C.B., Willemsen, M.A., 2014. Multimodal imaging of the macula in hereditary and acquired lack of macular pigment. Acta Ophthalmol. 92, 138–142.
Theodoropoulou, S., Ainsworth, S., Blaikie, A., 2013. Ultra-wide field imaging of retinopathy of prematurity (ROP) using Optomap-200TX. BMJ Case Rep 2013, bcr-2013-200734.
Thompson, R.B., Reffatto, V., Bundy, J.G., Kortvely, E., Flinn, J.M., Lanzirotti, A., Jones, E.A., McPhail, D.S., Fearn, S., Boldt, K., Ueffing, M., Ratu, S.G., Pauleikhoff, L., Bird, A.C., Lengyel, I., 2015. Identification of hydroxyapatite spherules provides new insight into subretinal pigment epithelial deposit formation in the aging eye. Proc. Natl. Acad. Sci. U. S. A. 112, 1565–1570.
Thomson, K.L., Yeo, J.M., Waddell, B., Cameron, J.R., Pal, S., 2015. A systematic review and meta-analysis of retinal nerve fiber layer change in dementia, using optical coherence tomography. Alzheimer's Dementia: Diagnosis, Assessment & Disease Monitoring 1, 136–143.
Tian, L., Kazmierkiewicz, K.L., Bowman, A.S., Li, M., Curcio, C.A., Stambolian, D.E., 2015. Transcriptome of the human retina, retinal pigmented epithelium and choroid. Genomics 105, 253–264.
To, M.P.S., Regan, B.C., Wood, D., Mollon, J.D., 2011. Vision out of the corner of the eye. Vis. Res. 51, 203–214.
Tokoro, T., SpringerLink, 1998. Atlas of Posterior Fundus Changes in Pathologic Myopia, 1 ed. Springer Japan, Tokyo.
Trantas, A., 1900. Moyens d'explorer par l'ophtalmoscope—et par translucidite—La partie anterieure du fond oculaire, le cercle ciliaire y compris. Arch.Ophtal.(Paris) 20, 314–326.
Trese, M.T., Kashani, A.H., Capone Jr., A., Drenser, K.A., 2012. Wide field angiography in diagnosis and management of familial exudative vitreoretinopathy (FEVR). Investig. Ophthalmol. Vis. Sci. 53 4161-4161.
Trick, G.L., Trick, L.R., Morris, P., Wolf, M., 1995. Visual field loss in senile dementia of the Alzheimer's type. Neurology 45, 68–74.
Tripathy, K., Chawla, R., Venkatesh, P., Vohra, R., Sharma, Y.R., Gogia, V., Jain, S., Behera, A., 2016. Ultra-wide field fluorescein angiography in retinitis pigmentosa with intermediate uveitis. J. Ophthalmic Vis. Res. 11, 237.
Turgut, B., 2015. Congenital hypertrophy of the retinal pigment epithelium in two different presentations. EC Ophthal-mology 2, 42–46.
Ukalovic, K., Cao, S., Lee, S., Tang, Q., Beg, M.F., Sarunic, M.V., Hsiung, G.R., Mackenzie, I.R., Hirsch-Reinshagen, V., Cui, J.Z., Matsubara, J.A., 2018. Drusen in the peripheral retina of the Alzheimer's eye. Curr. Alzheimer Res. 15, 743–750.
Umeda, S., Ayyagari, R., Suzuki, M.T., Ono, F., Iwata, F., Fujiki, K., Kanai, A., Takada, Y., Yoshikawa, Y., Tanaka, Y., Iwata, T., 2003. Molecular Cloning of ELOVL4 Gene from Cynomolgus Monkey (Macaca fascicularis), vol. 52. Experimental animals/Japanese Association for Laboratory Animal Science, pp. 129–135.
Valenti, D.A., 2013. Alzheimer's disease: screening biomarkers using frequency doubling technology visual field. ISRN Neurology 2013, 989583.
van der Veen, R.L., Fuijkschot, J., Willemsen, M.A., Cruysberg, J.R., Berendschot, T.T., Theelen, T., 2010. Patients with Sjogren-Larsson syndrome lack macular pigment. Ophthalmology 117, 966–971.
Vaney, D.I., 1980. A quantitative comparison between the ganglion cell populations and axonal outflows of the visual streak and periphery of the rabbit retina. J. Comp. Neurol. 189, 215–233.
Vargas-Martin, F., Peli, E., 2006. Eye movements of patients with tunnel vision while walking. Investig. Ophthalmol. Vis. Sci. 47, 5295–5302.
Venters, S.J., Mikawa, T., Hyer, J., 2013. Central and peripheral retina arise through distinct developmental paths. PloS One 8, e61422.
Venters, S.J., Mikawa, T., Hyer, J., 2015. Early Divergence of Central and Peripheral Neural Retina Precursors during Vertebrate Eye Development, vol. 244. Developmental dynamics: an official publication of the American Association of Anatomists, pp. 266–276.
Vingerling, J.R., Dielemans, I., Hofman, A., Grobbee, D.E., Hijmering, M., Kramer, C.F., de Jong, P.T., 1995. The prevalence of age-related maculopathy in the Rotterdam Study. Ophthalmology 102, 205–210.

Walls, G.L., 1963. The Vertebrate Eye and its Adaptive Radiation. Hafner Publishing Company.
Wang, L., Murphy, O., Caldito, N.G., Calabresi, P.A., Saidha, S., 2018. Emerging applications of optical coherence tomography angiography (OCTA) in neurological research. Eye and Vision 5, 11.
Wassle, H., Boycott, B.B., 1991. Functional architecture of the mammalian retina. Physiol. Rev. 71, 447–480.
Wassle, H., Dacey, D.M., Haun, T., Haverkamp, S., Grunert, U., Boycott, B.B., 2000. The mosaic of horizontal cells in the macaque monkey retina: with a comment on biplexiform ganglion cells. Vis. Neurosci. 17, 591–608.
Wassle, H., Grunert, U., Chun, M.H., Boycott, B.B., 1995. The rod pathway of the macaque monkey retina: identification of AII-amacrine cells with antibodies against calretinin. J. Comp. Neurol. 361, 537–551.
Wassle, H., Grunert, U., Martin, P.R., Boycott, B.B., 1994. Immunocytochemical characterization and spatial distribution of midget bipolar cells in the macaque monkey retina. Vis. Res. 34, 561–579.
Wassle, H., Grunert, U., Rohrenbeck, J., Boycott, B.B., 1989. Cortical magnification factor and the ganglion cell density of the primate retina. Nature 341, 643–646.
Watson, A.B., 2014. A formula for human retinal ganglion cell receptive field density as a function of visual field location. J. Vis. 14.
Wessel, M.M., Aaker, G.D., Parlitsis, G., Cho, M., D'Amico, D.J., Kiss, S., 2012a. Ultra-wide-field Angiography Improves the Detection and Classification of Diabetic Retinopathy, vol. 32. Retina, Philadelphia, Pa, pp. 785–791.
Wessel, M.M., Nair, N., Aaker, G.D., Ehrlich, J.R., D'Amico, D.J., Kiss, S., 2012b. Peripheral retinal ischaemia, as evaluated by ultra-widefield fluorescein angiography, is associated with diabetic macular oedema. Br. J. Ophthalmol. 96, 694–698.
Whiting, D.R., Guariguata, L., Weil, C., Shaw, J., 2011. IDF Diabetes Atlas: global estimates of the prevalence of diabetes for 2011 and 2030. Diabetes Res. Clin. Pract. 94, 311–321.
Whitson, H., Farsiu, S., Stinnett, S.S., Kwark, L., Potter, G., Burke, J., Cousins, S.W., Lad, E.M., 2016. Retinal biomarkers of Alzheimer's disease. Investig. Ophthalmol. Vis. Sci. 57 3372-3372.
Wilkinson, C.P., Ferris 3rd, F.L., Klein, R.E., Lee, P.P., Agardh, C.D., Davis, M., Dills, D., Kampik, A., Pararajasegaram, R., Verdaguer, J.T., Global Diabetic Retinopathy Project, G., 2003. Proposed international clinical diabetic retinopathy and diabetic macular edema disease severity scales. Ophthalmology 110, 1677–1682.
Wing, G.L., Blanchard, G.C., Weiter, J.J., 1978. The topography and age relationship of lipofuscin concentration in the retinal pigment epithelium. Investig. Ophthalmol. Vis. Sci. 17, 601–607.
Wisznia, K.I., Lieberman, T.W., Leopold, I.H., 1971. Visual fields in diabetic retinopathy. Br. J. Ophthalmol. 55, 183–188.
Witmer, M.T., Kiss, S., 2013. Wide-field imaging of the retina. Surv. Ophthalmol. 58, 143–154.
Witmer, M.T., Parlitsis, G., Patel, S., Kiss, S., 2013. Comparison of ultra-widefield fluorescein angiography with the Heidelberg Spectralis((R)) noncontact ultra-widefield module versus the Optos((R)) Optomap((R)). Clin. Ophthalmol. 7, 389–394.
Wolfe, B., Dobres, J., Rosenholtz, R., Reimer, B., 2017. More than the useful field: considering peripheral vision in driving. Appl. Ergon. 65, 316–325.
Wood, S., Mortel, K.F., Hiscock, M., Breitmeyer, B.G., Caroselli, J.S., 1997. Adaptive and maladaptive utilization of color cues by patients with mild to moderate Alzheimer's Disease. Arch. Clin. Neuropsychol. 12, 483–489.
Wu, Y., Yanase, E., Feng, X., Siegel, M.M., Sparrow, J.R., 2010. Structural characterization of bisretinoid A2E photocleavage products and implications for age-related macular degeneration. Proc. Natl. Acad. Sci. U. S. A. 107, 7275–7280.
Yamada, E., 1969. Some structural features of the fovea centralis in the human retina. Arch. Ophthalmol. 82, 151–159.
Youhnovska, P., Toffoli, D., Gauthier, D., 2013. Congenital hypertrophy of the retinal pigment epithelium complicated by a choroidal neovascular membrane. Digit. J. Ophthalmol.: DJO/sponsored by Massachusetts Eye and Ear Infirmary 19, 24–27.
Zein, W.M., Brooks, B.P., 2012. Peripheral color and fundus autofluorescence imaging in patients with stargardt disease and fundus flavimaculatus. Investig. Ophthalmol. Vis. Sci. 53 2068-2068.
Zemski Berry, K.A., Gordon, W.C., Murphy, R.C., Bazan, N.G., 2014. Spatial organization of lipids in the human retina and optic nerve by MALDI imaging mass spectrometry. J. Lipid Res. 55, 504–515.
Zhang, P., Dufresne, C., Turner, R., Ferri, S., Venkatraman, V., Karani, R., Lutty, G.A., Van Eyk, J.E., Semba, R.D., 2015. The proteome of human retina. Proteomics 15, 836–840.
Zhang, P., Kirby, D., Dufresne, C., Chen, Y., Turner, R., Ferri, S., Edward, D.P., Eyk, J.E., Semba, R.D., 2016. Defining the proteome of human iris, ciliary body, retinal pigment epithelium, and choroid. Proteomics 16, 1146–1153.